PREPARATION OF PEDESTRIAN EVACUATION TIME MAPS FOR SOUTHERN COASTS OF BODRUM PENINSULA, TURKEY

A THESIS SUBMITTED TO
THE GRADUATE SCHOOL OF NATURAL AND APPLIED SCIENCES
OF
MIDDLE EAST TECHNICAL UNIVERSITY

BY

BÜŞRA ÇELİKBAŞ

IN PARTIAL FULFILLMENT OF THE REQUIREMENTS
FOR
THE DEGREE OF MASTER OF SCIENCE
IN
GEOLOGICAL ENGINEERING

JANUARY 2022

Approval of the thesis:

PREPARATION OF PEDESTRIAN EVACUATION TIME MAPS FOR SOUTHERN COASTS OF BODRUM PENINSULA, TURKEY

submitted by **BÜŞRA ÇELİKBAŞ** in partial fulfillment of the requirements for the degree of **Master of Science** i**n Geological Engineering, Middle East Technical University** by,

Prof. Dr. Halil Kalıpçılar
Dean, Graduate School of **Natural and Applied Sciences** _____

Prof. Dr. Erdin Bozkurt
Head of the Department, **Geological Engineering** _____

Prof. Dr. Mehmet Lütfi Süzen
Supervisor, **Geological Engineering, METU** _____

Prof. Dr. Ahmet Cevdet Yalçıner
Co-Supervisor, **Civil Engineering, METU** _____

Examining Committee Members:

Prof. Dr. Zuhal Akyürek
Civil Engineering, METU _____

Prof. Dr. Mehmet Lütfi Süzen
Geological Engineering, METU _____

Prof. Dr. Ahmet Cevdet Yalçıner
Civil Engineering, METU _____

Prof. Dr. Bekir Taner San
Geological Engineering, Akdeniz Uni. _____

Assoc. Prof. Dr. Koray Kamil Yılmaz
Geological Engineering, METU _____

Date: 28.01.2022

I hereby declare that all information in this document has been obtained and presented in accordance with academic rules and ethical conduct. I also declare that, as required by these rules and conduct, I have fully cited and referenced all material and results that are not original to this work.

Name Last name : Büşra Çelikbaş

Signature :

ABSTRACT

PREPARATION OF PEDESTRIAN EVACUATION TIME MAPS FOR SOUTHERN COASTS OF BODRUM PENINSULA, TURKEY

Çelikbaş, Büşra
Master of Science, Geological Engineering
Supervisor: Prof. Dr. Mehmet Lütfi Süzen
Co-Supervisor: Prof. Dr. Ahmet Cevdet Yalçıner

January 2022, 91 pages

Historical records reveal that Turkey coasts faced with a considerable number of tsunamis in its past. Although the tsunamis in the seas surrounding Turkey are not as catastrophic as the ones in Pacific Ocean, still they may cause substantial damage to the highly populated touristic coastal places. Eastern Mediterranean Sea and Aegean Sea are in the seismically active region of Turkey. Therefore, numerous earthquakes and associated tsunamis are threatening the western coasts of Turkey. Recently, two important tsunami events recorded and damaged the coastal areas of Turkey, which are Bodrum-Kos tsunami on 21 July 2017 and Izmir-Samos tsunami on 30 October 2020. These events reminded that the Turkey coasts should be prepared for a tsunami threat.

Numerical simulations based on critical worst-case tsunami scenarios are performed with NAMI DANCE numerical model. According to the simulation results, 1956-Amorgos seismic scenario and Gökova seismic and Gökova-North-Datça landslide scenario are selected as critical worst-case scenarios. In this study, evacuation walk time maps are prepared for the highly populated settlements of Bodrum Peninsula by using Pedestrian Evacuation Analyst Tool (PEAT) based on the selected critical

scenarios mentioned above. PEAT is a least-cost distance (LCD) evacuation model that estimates evacuation times throughout hazard zone based on elevation, land cover, walking speed and direction of movement. The resultant pedestrian evacuation maps revealed that the evacuation time needed for pedestrian is 8, 6, 5, 4, 3 minutes located in Central Bodrum, Yahşi, Akyarlar-Karaincir-Aspat Bays, Bitez, and Gümbet bays, respectively. The resultant evacuation times are tested and validated by on-site measurements.

Keywords: Tsunami evacuation, Least-cost distance (LCD) model, Pedestrian evacuation, Walk time maps, Pedestrian Evacuation Analysis Tool (PEAT)

ÖZ

BODRUM YARIMADASI GÜNEY KIYILARI İÇİN YAYA TAHLİYESİ SÜRE HARİTALARININ HAZIRLANMASI

Çelikbaş, Büşra
Yüksek Lisans, Jeoloji Mühendisliği
Tez Yöneticisi: Prof. Dr. Mehmet Lütfi Süzen
Ortak Tez Yöneticisi: Prof. Dr. Ahmet Cevdet Yalçıner

Ocak 2022, 91 sayfa

Tarihsel kayıtlar, Türkiye kıyılarının geçmişte önemli sayıda tsunami ile karşı karşıya kaldığını ortaya koymaktadır. Türkiye'yi çevreleyen denizlerde oluşan tsunamiler, Pasifik Okyanusu'ndakiler kadar felaket olmasa da, yine de Nüfusu yoğun olan turistik kıyılarda önemli hasarlara neden olabilir. Doğu Akdeniz ve Ege Denizi, Türkiye'nin sismik olarak aktif bölgelerindenir. Bu nedenle çok sayıda deprem ve buna bağlı tsunamiler Türkiye'nin batı kıyılarını tehdit etmektedir. Türkiye kıyılarında son zamanlarda, 21 Temmuz 2017'de Bodrum-Kos ve 30 Ekim 2020'de İzmir-Samos olmak üzere iki önemli tsunami olayı kaydedilmiş ve hasar meydana gelmiştir. Bu olaylar, Türkiye kıyılarının bir tsunami tehdidine karşı hazırlıklı olması gerektiğini hatırlatmıştır.

Kritik en kötü durum tsunami senaryolarına dayalı sayısal simülasyonlar, NAMI DANCE sayısal modeli ile gerçekleştirilmiştir. Simülasyon sonuçlarına göre kritik en kötü senaryo olarak 1956-Amorgos sismik senaryosu ve Gökova sismik ve Gökova-Kuzey-Datça heyelan senaryosu seçilmiştir. Bu çalışma kapsamında Yaya Tahliye Analiz Aracı (PEAT) kullanılarak, Bodrumun güney kıyılarındaki yerleşim

alanları için, yukarıda bahsedilen olan kritik senaryolara göre yaya tahliyesi haritaları hazırlanmıştır.

PEAT, risk bölgesi boyunca yükseklik, arazi örtüsü, yürüme hızı ve hareket yönüne dayalı olarak tahliye sürelerini tahmin eden bir en-kısa mesafe (LCD) tahliye modelidir. Elde edilen tahliye haritalarına göre yaya için gereken tahliye süresinin sırasıyla Bodrum Merkez, Yahşi, Akyarlar-Karaincir-Aspat Koyları, Bitez ve Gümbet koylarında yer alan 8, 6, 5, 4, 3 dakikadır. Ortaya çıkan tahliye süreleri daha sonra yerinde ölçümlerle test edilmiş ve doğrulanmıştır.

Anahtar Kelimeler: Tsunami Tahliyesi, En-kısa Mesafe (LCD) Modeli, Yaya Tahliyesi, Yürüyüş Süresi Haritaları, Yaya Tahliye Analiz Aracı (PEAT)

To those who always believed in me…

ACKNOWLEDGMENTS

I would like to express my deepest gratitude to my supervisor Prof. Dr. M. Lütfi Süzen and co-supervisor Prof. Dr. Ahmet Cevdet Yalçıner for their guidance, advice, criticism, encouragements, and insight throughout the research. I would also like to give special thanks to Dr. Çağıl Kolat and Duygu Tüfekçi-Enginar and Gözde Güney Doğan for their endless support throughout the research, without their help I couldn't have done. I would also like to thank my committee members for letting my defense be an enjoyable moment, and for your brilliant comments and suggestions, thanks to you.

My most sincere thanks go to my sisters Kübra Yılmaz, Emine Çelikbaş and my parents who were always there for me while writing this thesis, who believed in me and supported me even in the worst moments of my life. I also thank to my precious friends Hüseyin Bayrakdar, Büşra Uysal, Sevilay Şengül and Yunus Arslan, who encourage and support me every time as if I am failing.

Last but not least, I would like to thank also my brother Ahmet Efe Çelikbaş, for his patience at home during my research.

This study was partly supported by Turkey Tsunami Last Mile Project Analyses JRC/IPR/2018/E.1/0013/NC with contract number 936314-IPR-2018. The data used in this thesis is provided by Bodrum Municipality, therefore, I express my gratitude to them.

TABLE OF CONTENTS

LIST OF TABLES

TABLES

LIST OF FIGURES

FIGURES

CHAPTER 1

INTRODUCTION

1.1 Problem Definition

"Tsunami" is a Japanese word consisting of two meaningful words "tsu" (means giant) and "nami" (means wave). Tsunami word is known and used commonly in other languages after huge damage and destruction of Great Meiji Tsunami occurred in 1896. Tsunami is a series of giant and destructive waves formed by the sudden displacement of a large volume of water due to undersea motion caused by earthquakes, large volcanic eruptions, and submarine landslides large volume of land slump into the ocean or meteorite impact in the ocean. According to the available tsunami catalogs, tsunamis are mostly generated by large submarine earthquakes, less frequently by volcanic activities and landslides (CIESM, 2011).

The generated energy is transmitted and propagated via long waves from the source location towards coastal regions, causing huge fatalities and destruction. After the 2004 Indian Ocean tsunami event, which is one of the deadliest (killed approximately 230.000 people from 14 countries) and largest natural hazards in human history, tsunami risk reduction became a crucial phenomenon worldwide (Lovholt et al., 2014). Since 2004, many destructive tsunamis have occurred in Indonesia, Samoa, Solomon Islands, Chile, Japan in 2006, 2007, 2009, 2010, 2011, 2013, 2014, and 2018. Among them, "Great East Japan Earthquake" is the most powerful earthquake recorded in Japan that happened and caused giant tsunami waves that hit Tohoku's coasts in 2011. The tsunami caused thousands of death/injuries, structural damages on buildings, roads, railways, and nuclear explosions in the Fukushima Daiichi Nuclear Power Plant Complex. According to the World Bank's estimations, it is the costliest natural disaster in the world, with a total economic loss of US$ 235 billion.

Although most tsunamis occur in the Pacific Ocean, there are many tsunami records on Earth's smaller seas. Evidences of paleotsunamis and paleoseismological investigations affirm that the Eastern Mediterranean and its connected seas, including the Aegean, Marmara, and Black seas, are prone to tsunami hazards (Necmioglu, 2014). As it is declared by the Disaster and Emergency Management Presidency of Turkey (AFAD) that the Aegean and Eastern Mediterranean seas are tectonically active regions. Hence, numerous catastrophic tsunami events occurred and have the potential to occur in the future. Within the last decade, two recent tsunami events occurred in the eastern Mediterranean Sea. One is Bodrum-Kos tsunami event occurred on 21 July 2017, damaging the southern coastline of Bodrum Peninsula and Kos island. The other one is the 30 October 2020 Izmir - Samos earthquake and tsunami event affecting the Aegean coast of Turkey from Cesme Alacati to the Gumuldur. (Dogan et al., 2021). Both events indicated that Turkey should be prepared for possible tsunami hazards to reduce disaster results, which are possible loss of life and destruction of structural facilities with economic losses. Identifying possible tsunami scenarios is the primary step for the tsunami risk mitigation and preparation operations that mainly defines immensity and decreases the damage of the tsunami for the vulnerable coastal areas (Tinti et al., 2005).

The Mediterranean and its connected seas are small compared with large oceans like the Pacific Ocean. Hence, the distances that tsunami waves will propagate in the Mediterranean Sea is short, yielding in rapid arrival times of tsunami waves, resulting in less times for people to evacuate towards safer places. Among tsunami preparedness and mitigation strategies, evacuation is a significant impact on saving lives (NTHMP, 2001). Therefore, vulnerable coastal settlements must have a tsunami evacuation plan, conveying people away from the hazard zone. According to the Intergovernmental Oceanographic Commission of UNESCO (2009), tsunami evacuation routes must guide people towards either beyond the inundation zone of tsunami waves or to the assembly areas and emergency shelters in the time between the alarm and first arrival wave. As in the tsunamis occurred after Bodrum-Kos and

Izmir-Samos earthquakes, many people living in the hazard zone are affected and panic due to the absence of tsunami evacuation routes.

1.2 Purpose and Scope

This thesis aims to prepare evacuation walk time maps for highly populated coastal settlements of Bodrum Peninsula's southern coastline by using the Pedestrian Evacuation Analyst Tool (PEAT) based on selected critical tsunami scenarios. Evacuation walk maps show a detailed view of the time needed for coastal residents and visitors to evacuate on foot via available routes from the tsunami inundation zone. The produced resultant maps provide a base for emergency managers, planners, and local decision-makers in preparing emergency response plans for the region.

This thesis was studied as part of the Tsunami Last Mile Project. The Tsunami Last Mile Project was conceived and organized by the JRC with funding from the European Commission department for civil protection and humanitarian aid operations (DG ECHO). The project was conducted by the joint team at the Remote Sensing and GIS Laboratory in the Geological Engineering Department and Coastal and Ocean Engineering Laboratory in the Civil Engineering Department of Middle East Technical University. All the studies related to NAMI DANCE simulation were performed by the Coastal and Ocean Engineering Laboratory. Whereas the studies associated with the calculation of pedestrian evacuation time were done by the Remote Sensing and GIS Laboratory.

1.3 Description of Study Area

Bodrum peninsula is one of the important touristic places in Turkey. Therefore, the population of Bodrum varies due to the seasonal nature of tourism. It has a population of 181.541 (TUIK, 2020) that creep up as high as 1 million during summer months (Erdogan 2016). Bodrum's climate is warm and temperate, with an

average temperature of 28.0 °C in July, the warmest month, 11.1 °C in January, the coldest month. The annual rainfall is 765 mm; precipitation falls mostly in winter.

Bodrum Peninsula is a district of Muğla Province in the southwest of the Aegean Region of Turkey. It is located on the northern side of the Gulf of Gökova that has experienced hazardous earthquakes in history (Gurer et al. 2013). According to the historical reports and geological investigations, earthquakes, submarine landslides, volcanic eruptions, and tsunamis were common in the Mediterranean Sea for many years. Therefore, Bodrum district's coastline is vulnerable to any disaster coming from the sea, such as storms and tsunami waves, covered with hotels, hostels, and beaches that are densely populated areas of the region, especially in summer. In this thesis, the study area is selected as the southern coastline of Bodrum district, shown in Figure 1.1. In this thesis, only the mainland of Bodrum Peninsula is considered as the study area. Therefore, during the analysis the surrounding uninhabited islands are not considered.

Figure 1.1 Location of the study region

CHAPTER 2

LITERATURE REVIEW

2.1 Tsunami Potential in Eastern Mediterranean and Bodrum Peninsula

Historical and pre-historical tsunamis occurred in the Mediterranean Sea, associated with mainly earthquakes, massive submarine landslides, or volcanic activities (Lorito et al., 2008). Some of the important tsunami events that occurred before 2005 in the Eastern Mediterranean Sea affected the Turkey coasts listed in Table 2.1. In order to clarify possible tsunami catalogs affecting the coasts of the Eastern Mediterranean Sea several studies were conducted (Galanopoulos, 1960; Guidoboni et al., 1994; Yalciner et al., 1995; Tinti and Maramai, 1996; Cita and Rimoldi, 1997; Minoura et al., 2000; Dawson et al., 2003; Tinti et al., 2004; Papadopoulos and Fokaefs, 2005; Yolsal et al., 2007; Lorito et al., 2008; Shaw et al., 2008; Beisel et al., 2009; Okal et al., 2009; Altinok, 2009; 2011).

According to GPS velocities, the Aegean Sea is one of the most rapidly deforming continental rifting zones (Karasözen et al., 2008). It is the seismically active part of the Alpine-Himalayan belt; hence it has experienced large earthquakes and volcanic eruptions. Some of them caused destructive tsunamis throughout history which are studied by Galanopoulos (1960), Ambraseys (1962), Kuran and Yalciner (1993), Minoura et al., (2000), Ambraseys and Synolakis (2010), Papadopoulos et al., (2012), England et al., (2015), Howell et al., (2015), Papadopoulos (2016).

Table 2.1 Tsunami events occurred in the Eastern Mediterranean Sea and affected the Turkey coasts selected from Papadopoulos et al., (2005).

No.	Year	Month	Day	Region	*k*	*K*	*h* (m)
1	66			South Crete	3	4	
2	142/144			Rhodes Island, South-East Aegean Sea	4	7	
3	365	07	21	Crete Island	5	10	
4	556			Cos Island, South-East Aegean Sea	4	8	
5	1303	08	08	Crete Island	5	10	
6	1481	05	03	Rhodes Island, South-East Aegean Sea	4	7	
7	1494	07	01	Crete Island	3	4	
8	1609	04		Rhodes Island, South-East Aegean Sea	5	8	
9	1612	11	08	Crete Island	4	8	
10	1630	03	09	Kythira Island, South-East Aegean Sea	3	5	
11	1650	10	11	Thera Island, South Aegean Sea	6	10	20
12	1741	01	31	Rhodes Island, South-East Aegean Sea	5	8	
13	1947	10	06	South Ionian Sea	2	3	
14	1948	02	09	Karpathos Island, South-East Aegean Sea	4	7	4
15	1956	07	09	Cyclades, South Aegean Sea	5	8	15
16	1991	01	04	Ikaria Island, East Aegean Sea	2	3	
17	1991	05	07	Leros Island, East Aegean Sea	3	4	0.5
18	2000	04	05	Heraklion, North Crete Island	2	3	0.5
19	2002	26	03	Rhodes Island, East Aegean Sea	3	5	2

Key: *k* = tsunami intensity in the Sieberg-Ambraseys 6-point scale; *K* = tsunami intensity determined in this paper according to the Papadopoulos-Imamura 12-point scale; *h* = maximum wave height (amplitude) in the coast

Lorito et al. (2008) investigated tsunamis in the Mediterranean Sea associated with large earthquakes in several subduction zones shown in Figure 2.1. They examined earthquakes in Hellenic Arc, including the 365 AD earthquake mentioned as the maximum credible earthquake (MCE). Guidoboni et al. (1994) and Papazachos and Papazachou (1997) mentioned that it is the most impressive earthquake that caused tsunami affecting coasts of the entire eastern Mediterranean. They estimated the earthquake magnitude as M_w 8.4 by modeling the fault dislocation and depth as 5 and 60 km. Shaw et al. (2008) also studied the AD 365 earthquake-related tsunami hazard which inundated throughout coastal sites in the Mediterranean Sea. They

suggest that the earthquake did not occur on the subduction interface beneath Crete but on a fault within the overriding plate based on radiocarbon data and field observations. They state that other faults in the region between the coast of Crete and Mediterranean Ridge may be active according to the distribution of shallow earthquakes.

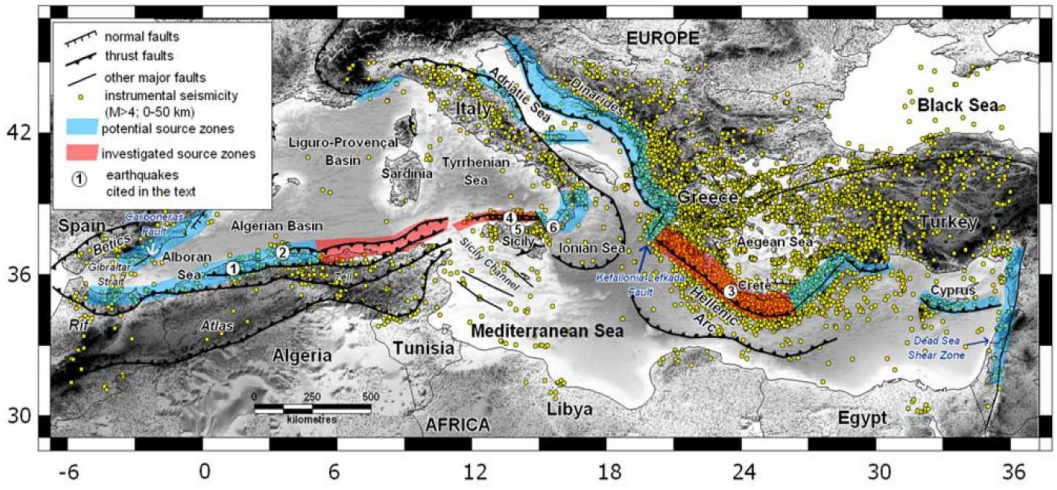

Figure 2.1 Tectonic map of the Mediterranean Sea. Yellow dots are taken from ISC, 2004, showing instrumental seismicity (M > 4; depth 0–50 km). Blue and red colored ribbons show main zones capable of generating tsunamis and causing a significant hazard to Mediterranean shore-facing settlements. Circles showing selected earthquakes 1) El Asnam, 1980; 2) Boumerdes, 2003; 3) Crete, 365 AD; 4) Palermo, 2002; 5) Northern Sicily, 1823; 6) Messina Straits, 1908. (Source: Lorito et al., 2008)

Okal et al. (2009) investigated Amorgos, Greece earthquake and tsunami that occurred on 09 July 1956. They state it is the largest tsunami in the 20th century, so several studies have been done such as Galanopoulos (1957), Papadopoulos and Pavlides (1992), Yalciner et al., (1995), Beisel et al., (2009). Rupture area is measured as 75 × 40 km from systematic relocation of mainshock associated with 34 events. The earthquake occurred in a plane dipping towards the southeast in a normal faulting mechanism in the back-arc behind the Hellenic subduction zone. Seismic moment is given as 3.9 × 1027 dyn cm, the largest measure in the Mediterranean Basin in the past 100 years.

The tsunami events occurred in the smaller domain of the study area located at the Gulf of Gökova that is formed by the North-South directed extensional tectonic regime of Western Anatolia. 20 July 2017 Bodrum-Kos tsunami event revealed that investigating Gulf of Gökova region is vital for the tsunami hazards that inundate and affect mostly southern coast of Bodrum Peninsula. The Gulf of Gökova is located in between Bodrum Peninsula (North), Datça Peninsula (South), and the island of Kos (West). Seismicity of Gulf of Gökova is studied by several people, including Dewey & Şengor (1979), Jackson & McKenzie (1984), McKenzie (1972), Sengor (1987), Aktug et al., (2009, 2010), Dogru et al., (2014), McClusky et al., (2000), Ozener et al., (2013), Reilinger et al., (2006), Tiryakioglu et al., (2013, 2018).

Tiryakioglu et al. (2018) stated that Gökova Fault zone (GFZ) lies in the north of the Gulf that is the most active fault in Southwest Anatolia. In order to comprehend fault systems in this region, several geophysical surveys have been performed (Iscan et al., 2013; Kurt et al., 1999; Tur et al., 2015; Ulug et al., 2005). In light of these studies, the GFZ extends in the E-W direction from Akyaka to Ören, where it bends towards the left and continues west-southwestward, separated into several second orders submarine faults (Tiryakioglu et al., 2018). Hence, GFZ has more complex patterns than single line characters within the Gulf of Gökova (Figure 2.2). They stated that interactions between shallow-seated normal faults and deep-seated strike slip faults cause the complexity of the GFZ within the Gulf. Gürer et al. (2013) indicate that GFZ formed from south dipping with 70°–85° normal faults.

The extensional regime in the Gulf of Gökova is also investigated by Ocakoğlu et al. (2018). They found a good correlation between the region's general seismicity and the focal mechanism solutions of Bodrum-Kos earthquake that occurred on 20 July 2017.

According to studies conducted by Şaroğlu et al., 1995; Görür et al., (1995); Eyidoğan et al., (1996); Kurt et al., (1999) and Uluğ et al., (2005), there are active normal faults in the Gulf of Gökova based on focal mechanism solutions, marine seismic reflection, surface morphology, and seismicity data.

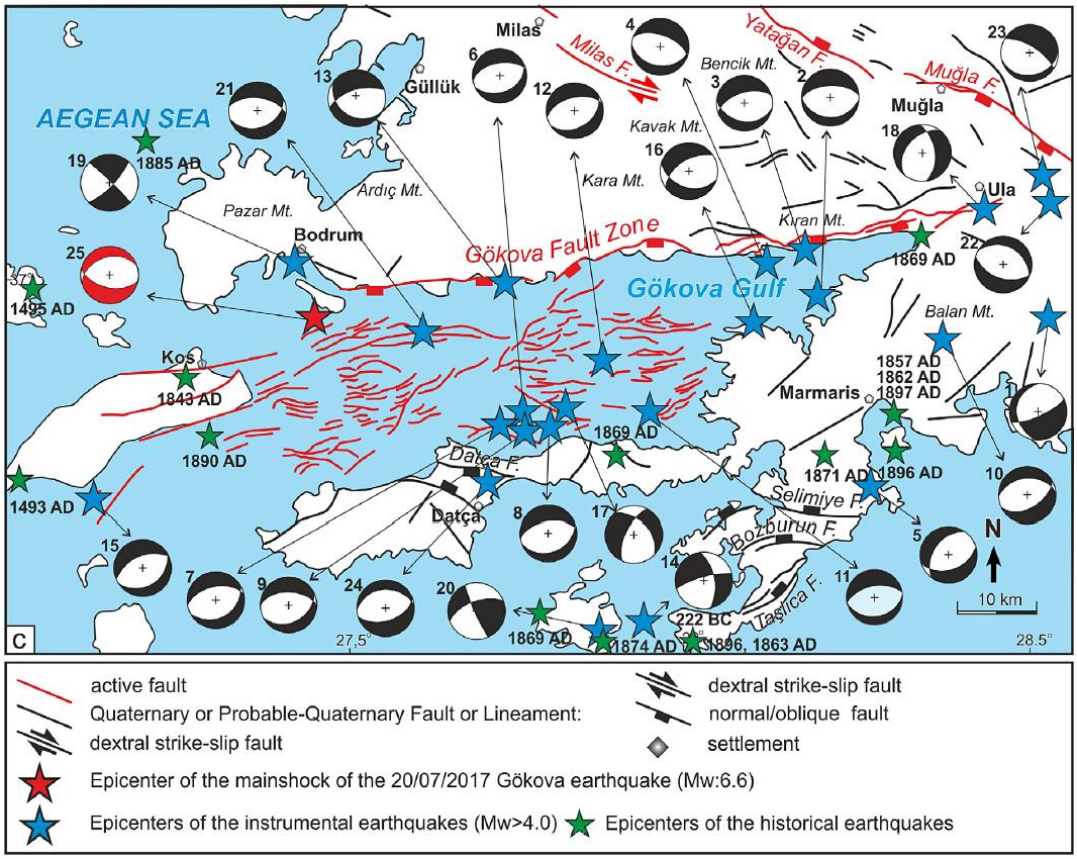

Figure 2.2 Seismotectonic map of the Gulf of Gökova which displays instrumental a historical earthquakes epicenter, focal mechanism solutions and epicenters are taken from McKenzie (1972); Yolsal et al., (2014) (Source: Tiryakioglu et al., 2018)

Kalafat and Horasan (2012) also studied seismogram characteristics of the earthquake in the Gulf of Gökova between 2004 and 2006. Earthquake swarms occurred in the Gökova for seven months within the two years, at which 1558 seismic events were recorded. The number of seismic events that occurred in the Gökova region for two years (2004-2006) is provided in Figure 2.3. Also, they stated that Muğla, Bodrum, and Gulf of Gökova are the most seismically active areas of western Turkey.

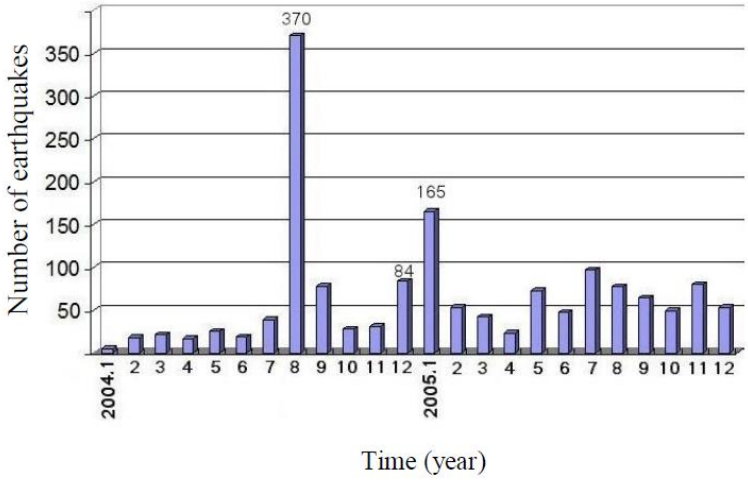

Figure 2.3 Histogram graph showing the number of events recorded between 2004 and 2006 in the Gulf of Gökova (Source: Kalafat and Horasan, 2012)

Papadopoulos et al. (2007) and Yalciner et al. (2008) documented the strong seismic events and tsunamis that occurred in the Eastern Mediterranean Sea. Yalciner et al. (2008), investigated the seismic tsunami sources that may create the tsunami hazard in Mediterranean and Aegean Sea. Acar (2015) extracted the available earthquake data, which may generate tsunamis affecting Güllük Bay. After an extreme statistical analysis, earthquake magnitudes (M_w) for the return periods of 100, 500, and 1000 years are detected as critical for Güllük Bay (Table 2.2).

Table 2.2 Calculated probable earthquake magnitudes for 100, 500- and 1000-years periods according to Poisson distribution (Source data is taken from Acar, 2015)

Rp (yr)	λ	Mw
100	0.01	6.5
500	0.002	7.6
1000	0.001	8.0

Sözbilir et al. (2017) investigated the geomorphology of the Gökova Fault Zone and historical earthquakes that occurred along this fault zone before 1900, after the Bodrum-Kos earthquake occurred on 20 July 2017. They state that earthquakes whose magnitudes (M_w) are five or larger in Gökova Fault Zone in the last century show that earthquake migration is based on energy transfer from east to west within the fault zone. Additionally, in the Ph.D. thesis of Necmioglu (2014), fault rupture in the Gökova region with a magnitude (M_w) of 7.2 and the 1303 Crete event are modified.

2.1.1 Non-seismic Tsunami Generic Sources in the Mediterranean Sea

Papazachos et al. (2005) studied active tectonics related to the southern Aegean volcanic arc. They presented strikes of five faults located at the five volcanic centers of the southern volcanic arc where epicenters of earthquakes clustered (Figure 2.4). Nomikou et al. (2013) investigated several submarine volcanos along the Aegean volcanic arc via swath bathymetric maps, air-gun profiles, underwater photos, and samples analysis which includes Methana, Milos, Santorini, and Nisyros islands. Acar (2015) mentioned the possibility of a tsunami due to the collapse of the caldera of Santorini and Columbus volcanos located along the southern Aegean volcanic arc. Rontogianni et al. (2011) stated a probable connection between the Gökova Transfer Fault (GTF) and the Fault of Kos. Because this is a 40° dipping fault buried under thick sediment deposits of about 2.5 km, there is a possibility of having a submarine landslide triggered by a large earthquake.

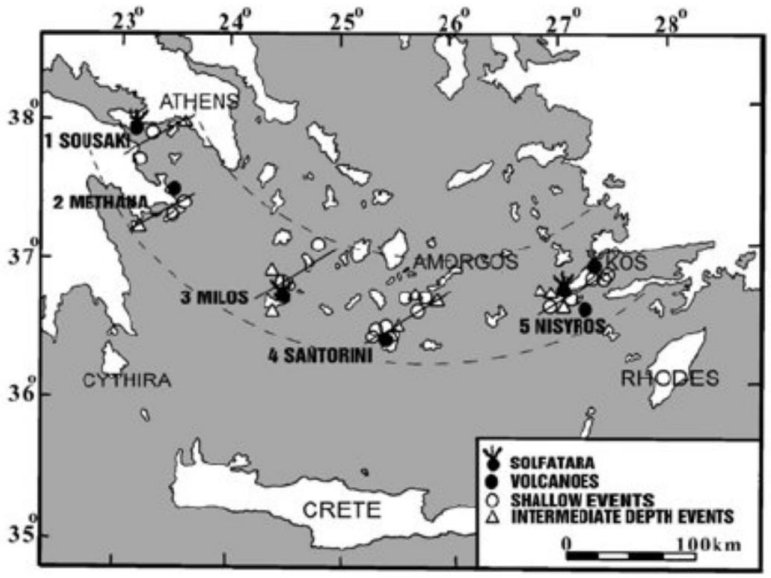

Figure 2.4 Seismovolcanic centers in the southern volcanic arc (Papazachos and Panagiotopoulos, 1993)

Okal et al. (2009) mentioned the formation of submarine landslides series triggered after mainshocks of the 1956-Amorgos earthquake. They presented that the landslide source is located approximately 10 km from the southwest of Amorgos island, shown in Figure 2.5.

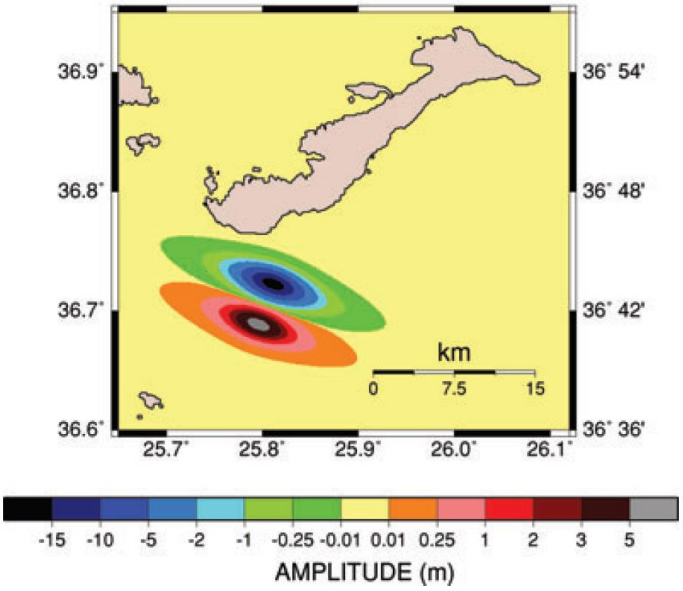

Figure 2.5 Initial state of the sea surface for Amorgos Landslide scenario (Source: Okal et al., 2009)

2.2 Literature Survey on Pedestrian Evacuation

Evacuation is one of the most effective ways to save lives from tsunami waves for people within the hazard zone (NTHMP, 2011). Pedestrian evacuation is the most efficient way, especially for tsunamis whose sources are close to the coast, meaning less time to evacuate. For this reason, there have been substantial efforts to model the pedestrian evacuation after losses of many lives during recent tsunami disasters (e.g., 2004 Sumatra, 2006 Java, 2010 Chile, 2011 Tohoku and 2018 Palu) (Wood and Schmidtlein, 2012). Examples include traffic simulation models (Franzese and Sorenson 2004; Marrero et al., 2010), egress simulations for building evacuations (Averill et al., 2005), agent-based models of movement along with road networks (Jonkmann et al., 2008; Yeh et al., 2009), and cost-distance models to incorporate landscape variability (Graehl 2009; Post et al., 2009; Wood and Schmidtlein 2012). In recent years, dynamic networks (simulation models), static algorithms (shortest path, minimum cost network flow, quickest path) have been used to capture the movement of evacuees over time (Hamacher and Tjandra, 2002).

Models for pedestrian evacuation may be classified as dynamic or static (Cheff et al., 2018). Firstly, dynamic network evacuation analysis considers the individual differences and decisions for selecting the evacuation routes during panic situations. However, human behavior is highly complex to model with mathematical equations, and it is the hardest part of dynamic evacuation modeling.

One of the most widely used dynamic methodologies to simulate tsunami evacuation is agent-based modeling (ABM), which allows individuals to evacuate according to user-defined rules (Mas et al., 2012). It is used widely in transportation platforms such as Multi-Agent Transport Simulation - MATSim (Lammel, 2011; Bakillah et al., 2013), TRansportation Analysis and SIMulation System - TRANSIMS (Zheng et al., 2013) and Open Activity–Mobility Simulator - OpenAMOS (Pendyala et al., 2005). However, some studies were conducted to understand people's behavior during tsunami evacuation by using Agent-based models such as Jonkmann et al., 2008. Agent-based models for tsunami evacuation include dynamic travel costs due

to route capacity, evacuee crowding, and congestion when determining the simulated evacuees' travel speed and locations (Jonkmann et al., 2008; Yeh et al., 2009). Detailed geospatial data of road networks, location of tsunami shelters, and population data are required in addition to the data of tsunami inundation processes. Furthermore, social information on how evacuee responds and interacts with other evacuees during panic situations is also required (Chu et al., 2017).

Mas et al. (2012) developed a dynamic model that considers tsunami inundation simulation and human behavior with different start times among the evacuees and the interaction between pedestrians and cars. Wang et al. (2017) implemented the Net logo modeling environment (Wilensky, 1999) to construct ABM in order to investigate the different behaviors of evacuees, such as different start times to evacuation, different moving speeds, and selection of different routes etc. The model also estimates the number of causalities who cannot evacuate.

Secondly, Geographic Information Systems (GIS) have been utilized in static evacuation analysis since the 90s by several authors with various contexts (Cova, 1999). De Silva et al. (1993) applied GIS to generate evacuation routes reaching out of hazard zone with an evacuation decision support system. Cova and Church (1997) proposed the critical cluster model (CCM) for assessing spatial evacuation vulnerability from a tsunami disaster. Cost distance weighting GIS approach named as least-cost distance analysis (LCD) is used widely to model pedestrian evacuation and eventually became a hot topic in the literature (Laghi and Cavalletti, 2004; Graehl and Dengler, 2009; Post et al., 2009; Wood and Schmidtlein, 2012, 2013; and Fraser et al., 2014).

Laghi and Cavalletti (2004) assembled Evacuation Routes Tools in the ArcGIS toolbox that is published as the manual of Coastal Risk Analysis of Tsunamis and Environmental Remediation (CRATER). They indicated that the fastest way to get out from the hazard zone may not always be the shortest one; there can be natural barriers, buildings, lakes, or very high slopes. For this reason, they calculated the

distance from every cell within the hazard zone to the assembly points by using geometric distance and cost, which is called Cost Weighted Distance (CWD)

The Cost Surface of each cell is calculated by using land-use information and slope data of the study area. The value of CWD is computed between each cell to the closest evacuation point. Land-use and slope data are created and then reclassified by the Reclassification tool that is a primary step for this analysis. Cost surface is created by using the Evacuation Speed Map tool that combines reclassified values of land-use and slope data with an average speed of pedestrian evacuation. The resultant map represents the cost that pedestrians must spend during walking. Finally, the Evacuation Time Map & Basins tool is used to obtain a CWD surface with the addition of shelters, assembly areas, and natural barriers.

Graehl (2008) investigated the changes in pedestrian walking times with (i) and without (ii) the additional predefined routes. Pedestrian evacuation walking times are calculated by using the least-cost path method, considering the quickest path to get out of the inundated area for both cases. In this study Evacuation Routes Toolbox of ArcGIS developed by Laghi and Cavalletti (2004) is used. For the analysis, land-use polygons of the study area were created, and slope were created from 5 m DEM. The generated land-use data were reclassified based on the type of surface that a pedestrian would walk over. Speed conservation values are assigned to each class after conducting fieldwork. All types of land-use data from fieldwork are normalized according to the walking speed over the flat pavement. Then, the slope is reclassified according to the speed conservation values of the Laghi and Cavalletti (2004) evaluation model. Inverse Evacuation Speed Map toolset was used to combine reclassified land-use and slope raster with an average walking speed of 1 meter per second. Finally, cost-weighted surfaces (CWS) were created for both cases, which are with (i) and without (ii) additional predefined routes by using The Evacuation Time Maps toolset. The final surfaces for both cases give the time that is required to reach the closest safe zone for the pedestrian located within the hazard zone. Graehl (2008) concluded that the addition of routes decreased the required time to reach a safe zone. Finally, the author discussed walking speed variations during evacuation

depending on evacuees' physical capabilities, given land-use and slope speed conservation values, and The Evacuation Time Maps toolset used to calculate pedestrian evacuation time maps.

Post et al. (2009) aim to quantify people's immediate response time after they get a tsunami warning. For that purpose, they conducted the following steps: quantification of the estimated minimum arrival time of tsunami (ETA), quantification of institutional reaction time including decision and notification time (ToNW), quantification of evacuation time that people need (ET), and finally quantification of the response time of population which is the time people actually have (RsT) (Figure 2.6). Institutional reaction time is assumed as 8 minutes (Institutional Decision Time (IDT) is set to 5 min. and Institutional Notification Time (INT) technical notification time to communicate is set to 3 min.). The reaction time of the population is the most unknown phenomenon to quantify, which may vary between 0 to ETA. Evacuation time (ET) is calculated based on the Cost Weighted Distance approach, least-cost distance analysis (ESRI, 2001) by considering extrinsic (land-use, slope, and population density) and intrinsic (age and gender) factors. Finally, the response time of the population is calculated by extracting "institutional reaction time (IDT + INT)" and population reaction time (RT) from the estimated time of arrival tsunami wave (ETA).

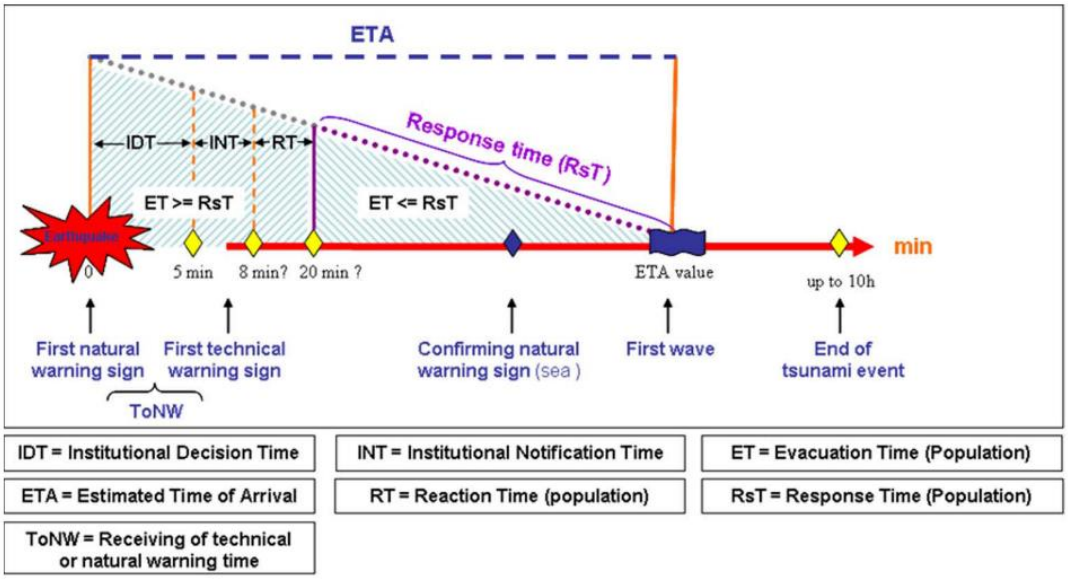

Figure 2.6 Time components of the assessment of human response capability to a tsunami warning (Post et al., 2009)

They classified human response capability as weak (evacuation time is higher than response time), moderate and good (evacuation time is lower than response time). Post et al. (2009) performed an uncertainty assessment in addition to the plausibility check. Results reveal that decision-makers at the local level may identify hotspots of weak response capabilities and suggest additional shelters for those areas. They also stressed the importance and necessity of early warning systems and disaster risk reduction strategies for saving lives from hazards.

Wood and Schmidtlein (2012) examined the sensitivity of the least-cost distance (LCD) model to variations in land-cover, directionality in slope (downhill and uphill travel costs are not the same), and data resolution. ESRI's ArcMap (10.1) Path Distance tool is used for travel speed assumptions. They examined four models, which are distance only, road-constrained, isotropic, and anisotropic approaches. Distance only model estimates travel times by calculating only the shortest path by using ArcMap's Cost Distance tool (ESRI, 2009a). The road-constrained model confines the road network and assumes pedestrians evacuate from the closest road until they reach the safe zone. This is done by adding cost distance from each location to the nearest road. The isotropic approach uses the cost distance model too, but also

includes remaining parts where pedestrians can also consider the influence of slope and land-cover type. Slope and land-cover layers are reclassified into speed conservation values (SCV) based on the maximum walking speed potential. The slope is reclassified according to Tobler's hiking function then speeds are converted into SCV regardless of uphill or downhill movement. The Cost Distance tool is used to create a cost surface, which is multiplied by the inverse of the assumed travel speed (1.1m/s). The anisotropic approach includes slope directionality. In this approach, travel distances are calculated by using the Path Distance tool (ESRI, 2009b) instead of the cost distance approach. As a result, an anisotropic approach is found as the most realistic model to estimate pedestrian travel times. It simplifies reality by a series of assumptions such as land-cover conditions and travel speed changes according to slope direction. Additionally, changes in the resolution of DEM and land-cover data have a more significant effect on the result of the study, so higher resolution data gives better results. Also, changes in travel speed assumptions have a greater effect on the population exposure estimates.

Wood and Schmidtlein (2013) studied the effect of community variations in population exposure to a tsunami in order to differentiate tsunami treats among multiple coastal communities. Travel times are estimated by using the anisotropic least-cost distance model described in Wood and Schmidtlein (2012). The resultant maps are merged with the population data, including residents, employees, public venues, and dependent-care facilities. This paper aims to identify hotspots of populations in tsunami-prone areas by coinciding with a population and a hazard zone. They generated the least evacuation time surfaces according to the model, and then, they developed a geospatial function that allows portraying the distribution of population as a function of minimum travel time. As a result, in some communities, fast walking speed may allow people to evacuate safe areas and divide the population into subgroups, allowing authorities to be more flexible in deciding the required time during evacuation.

Wood et al. (2014) examined the changing of post-disaster redevelopment's influence on the evacuation potential of population groups, mainly employee, customer, and tourist populations at Seward Alaska. They concluded that evacuation times to safety for most of the population are less than wave arrival times for possible future tectonic tsunamis; however, it is greater than wave arrival times for landslide-related tsunamis.

Fraser et al. (2014) improved the GIS-based least-cost distance evacuation model at which temporally variable exposure of population and variability in pedestrian travel speeds are considered. They created population time profiles to understand spatial exposure of each population groups for day, month or any time. According to the least-cost distance model, travel speed for all populations is assumed as only one value. However, the authors proposed that it does not represent the real case so that they try to collate travel speeds for different population groups based on age and mobility. They modeled multiple different scenarios by changing the spatial and temporal distribution of population groups and travel speeds, allowing an understanding of how evacuation time is affected. When they investigated the distribution of the mean difference between the base scenario and the Monte Carlo scenarios, the overall base model has good accuracy and precision to changes in landcover SCVs.

Schmidtlein and Wood (2015) investigated pedestrian evacuation time models' sensitivity to the assumptions made in the characterization of path movement and the land-cover surface. Descriptive statistics for the baseline model and normal direction model show that in almost every case baseline evacuation model tends to overestimate the evacuation times. The sensitivity of the anisotropic LCD model to changes of landcover SCVs is checked by using a Monte Carlo based uncertainty analysis. After GIS was used widely to model pedestrian evacuation, spatial constraints during selecting pedestrian evacuation routes were studied. This study focused on the path search problem implemented in the ArcCasper tool. In order to simulate pedestrian circulation, the Network Analyst extension of ArcGIS is used on which road vertices need to have slope and capacity attributes. Finally, they prepare

evacuation plan maps that show a need for vertical evacuation buildings to overcome congestion in evacuation routes and decrease evacuation time.

Trindade et al. (2018) also implemented one of the GIS tools named as ArcCasper for modeling evacuation tools based on the worst-credible scenario. The elements considered for the evacuation process include the worst-credible inundation scenario, number of people needed to evacuate, safe areas, roads, and finally the time needed for proper evacuation. By using the ArcCasper (Capacity-Aware Shortest Path Routing Evacuation), developed by Shahabi and Wilson (2014), evacuation simulation tool, an exposed population for four different times of day and the evacuation time is estimated. Road capacity with its length is combined to predict the speeds based on different traffic conditions and population density and size, or flow to generate evacuation routes. Basic travel speed is used as 0.7 m/s and 1.4 m/s which is taken as the average velocity of the entire population by ignoring the elderly, children, and people having disabilities. In this study, road capacities are considered the simulate traversal time and congestions. From the analysis of the simulation maps, it was concluded that the best solution to minimize the traversal times, vertical evacuation strategy could play an important role which must be discussed by the local decision-makers. The resultant maps show the optimal evacuation routes and the unfeasible routes depending on the inundated area according to the credible worst-case scenario. Some improvements needed for this study which earthquake impact on the roads such as blocking of the roads by collapsed buildings or accessibility of potential vertical evacuation shelters.

Sakata et al. (2019) conduct a study emphasizing the importance of selecting evacuation routes at the time of evacuation. They implemented a dynamic evacuation route guidance system based on a tsunami inundation database by using multiple tsunami sources, which shows evacuation routes with the lowest probability of encountering a tsunami. Tsunami inundation with the actual source of the tsunami wave is calculated via STOC. Based on the arrival time of the tsunami, corresponding to the tsunami source, they constructed the route selection method that avoids encountering tsunami during evacuation. The route selection simulator

developed by Arikawa and Ooie (2015), was incorporated to determine the death rate. The model selects the shortest distance route to the evacuation shelter by considering the topographical obstacles. Also, the evacuation speed is determined by considering the slope of the route by using Tobler's hiking function and inundation depth.

For the evacuees who started evacuation immediately before the first wave of the tsunami, the death rate was reduced by 6.8% in Otsuchi. Furthermore, in Nakatosa, it was reduced by 17% showing effectiveness of safe routes of the evacuation guidance. However, in this study, some important factors including human congestion and road blockage due to earthquakes are ignored. Evacuation behaviors at the time of the evacuation drill and actual evacuation route selection are compared. As a result, they found out that there was a difference that is necessary to examine for further analyses.

CHAPTER 3

TSUNAMI NUMERICAL MODELING

3.1 Capabilities of NAMI DANCE software

Numerical simulations of tsunami sources are performed via NAMI DANCE software that is developed by Zaytsev, Chernov, Yalciner, Pelinovsky, and Kurkin (Lynett et al. 2017; Yalciner and Zaytsev 2017; Yalciner et al. 2017). It is developed specifically for the modeling of a tsunami and tropical cyclone. NAMI DANCE developed in C++ solves nonlinear forms of long-wave equations with friction, including initial and boundary conditions. It estimates the major tsunami parameters: water surface elevation, flow depth, current velocities, momentum fluxes, and their direction and Froude number of selected study domains in either a Cartesian or spherical coordinate system. NAMI DANCE has been used and validated by several coastal scientists (e.g. Sozdinler et al., 2015; Dilmen et al., 2015; Aytore et al., 2016; Cankaya et al., 2016; Kian et al., 2016; Velioglu et al., 2016; Zaytsev et al., 2016; Lynett et al., 2017; Tufekci et al., 2018) to solve different specific benchmark problems some of which are introduced in International Workshops on Long-Wave Runup Models (Synolakis, 1991, Synolakis et al., 1995, 2004; Liu et al., 2008, Lynett et al., 2017).

3.2 Selected Tsunami Sources

In the light of studies mentioned in the literature survey section of the Eastern Mediterranean basin, large tsunamis occurred due to earthquakes, submarine landslides, and volcanic eruptions because of high seismicity throughout the region in the past 3000 years. In this study, tsunami hazards in the Gulf of Gökova and South Aegean Sea are investigated, mostly affecting the southern coasts of Bodrum Peninsula. Seismic and landslide tsunami sources are selected by the working groups of the Tsunami Last Mile Project. According to the project, the 365 and 1303 AD events occurred near Crete (Lorito et al., 2008; Shaw et al., 2008), 9 July 1956 Amorgos event (Galanopoulos, 1957, Papadopoulos and Pavlides, 1992; Yalciner et al., 1995; Beisel et al., 2009; Okal et al., 2009), and rupture in Gökova (Necmioglu, 2014) and Güllük Bay scenario (Acar, 2015) are selected as seismic scenarios of tsunami hazard in this study as they have large tsunami runup heights and inundation distances along southern coasts of Bodrum Peninsula. Based on the literature review mentioned above, seismic source parameters are given as compatible with the fault characteristics of each scenario according to the worst-case scenario (Table 3.1).

Table 3.1 Selected source parameters of seismic scenarios which are used in the numerical simulations

Selected Seismic Scenario	Lon. (º)	Lat. (º)	Length (km)	Width (km)	Strike (º)	Dip (º)	Rake (º)	Depth (km) (TOF)	Magnitude (Mw)	Slip (m)	Faulting Type
365-Crete	23.40	35.00	130	85	314	35	90	5	8.4	14	Trust
1303-Eastern Mediterranean	26.63	35.18	100	30	60	45	110	20	8.0	8	Trust
1956-Amorgos	26.00	36.90	75	40	39	25	246	5	7.8	7	Normal
Gökova	27.40	36.90	80	20	100	60	300	5	7.2	1.5	Normal
Güllük Bay	26.592	37.26	50	25	66	45	45	20*	7.6	8	-
											(* focal depth)

In addition to seismic sources, the Amorgos submarine landslide (Okal et al., 2009) is selected as the first landslide scenario. Another possible submarine landslide is assumed to be triggered by the seismic mechanism of the Gökova scenario named "Gökova-North-Datça". Parameters of two landslide sources needed for NAMI DANCE numerical simulations are provided in (Table 3.2).

Table 3.2 Selected source parameters of landslide scenarios which are used in the numerical simulations

Selected Landslide Scenario	Lon. (o)	Lat. (o)	Ellipse Dimensions (major axis x minor axis) (km)	Maximum Amplitude (m)
Amorgos	23.40	35.00	21ax5 18bx5	-18, +6
Gökova-North-Datça	27.5440	36.7853	6ax2 6bx2	-20, +20
				a subsidence-b uplift

Note: Each landslide scenario is assumed as a pair of elliptical shape subsidence and uplift areas of which the dimensions are provided in Table 3.2

3.3 Simulation of Selected Tsunami Sources

Modeling is one of the essential components of this study. It has several phases, including combining available earthquake data, obtaining bathymetric and topographic data with sufficient resolution, and selecting credible tsunami scenarios. Ocean Engineering Research Center of Middle East Technical University performs all the tsunami simulations within the scope of the Turkey Tsunami Last Mile Project. The resultant maps represent the inundation of tsunami used to define hazard zones during creating pedestrian evacuation maps.

Bathymetric and topographic data are gathered in order to be used during the numerical simulations of NAMI DANCE software. GEBCO with 30 arc-second grid resolution data is used as bathymetry. The bathymetry is enhanced with the national navigational charts of the Aegean coast of Turkey for the regions close to the southern coast of Bodrum. Additionally, the 5 m resolution Digital Elevation Model (DEM) is used as topographical data for the simulations. Then, bathymetry and topographical data are gathered to be compatible with each other. Simulation of tsunami is performed for three nested domains, which are Southern Aegean (Domain B), Bodrum Peninsula and Eastern Kos (Domain C), and a smaller area of Bodrum Peninsula and Eastern Kos (Domain D) that are shown in Figure 3.1. Coverage area, grid sizes, and boundary coordinates of all domains are provided in Table 3.3. During the numerical simulations via NAMI DANCE, the time step is selected as 0.05 s, and the friction coefficient is taken as 0.015.

For the critical parts throughout the southern coast of Bodrum Peninsula and northeast of Kos island, seven gauge points are selected, providing time histories of water surface during simulated tsunami (Figure 3.2). In this study, gauge points are either selected from places where flow depth values of the simulated tsunami are known as a result of field studies (Gümbet, Bitez, Karaincir and Kos-Port) after the 2017 Bodrum-Kos event in order to verify the simulation or from places where knowing time histories of the water surface via sea level stations (IDSL, IDSL* and

Bodrum-TG) is crucial for pedestrian evacuation. Coordinates of selected gauge points are listed in Table 3.4.

Table 3.3 Study domains used during numerical modeling with their grid size, boundary coordinates and coverage area

Domain Name	Grid Size (m)	Boundary Coordinates	Coverage area
B	150	22.500518° E – 28.499467° E 33.999078° N – 37.797605° N	Southern Aegean
C	30	27.200246° E – 27.699985° E 36.829972° N – 37.409784° N	Large area of Bodrum Peninsula and Eastern Kos
D	5	27.20999° E – 27.599991° E 36.839988° N – 37.209996° N	Smaller area of Bodrum Peninsula and Eastern Kos

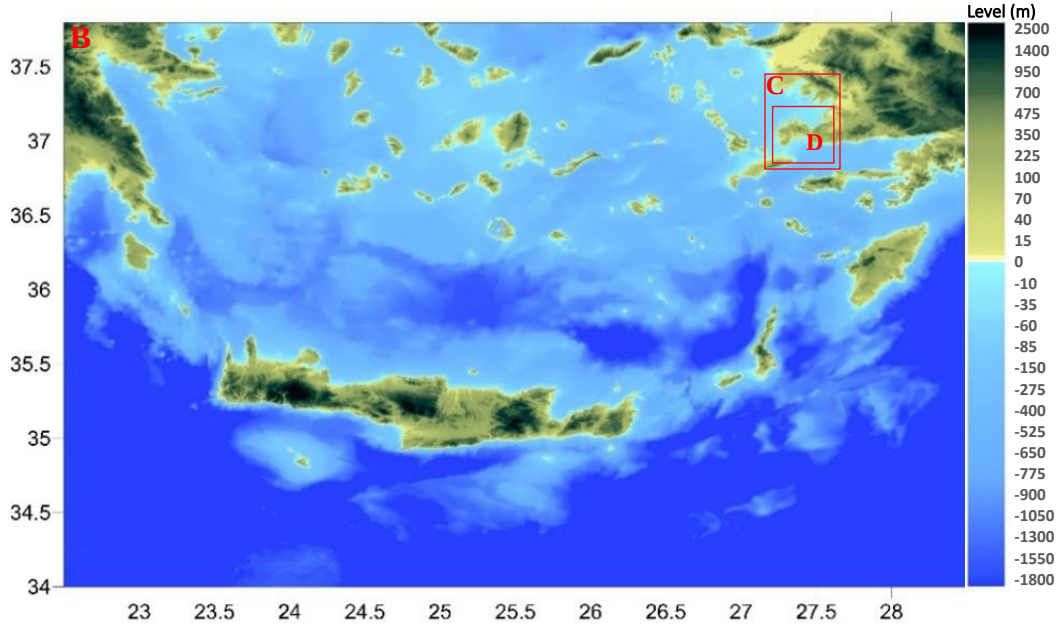

Figure 3.1 Bathymetric and topographic map showing three study Domains (B, C, and D) used for NAMI DANCE simulations

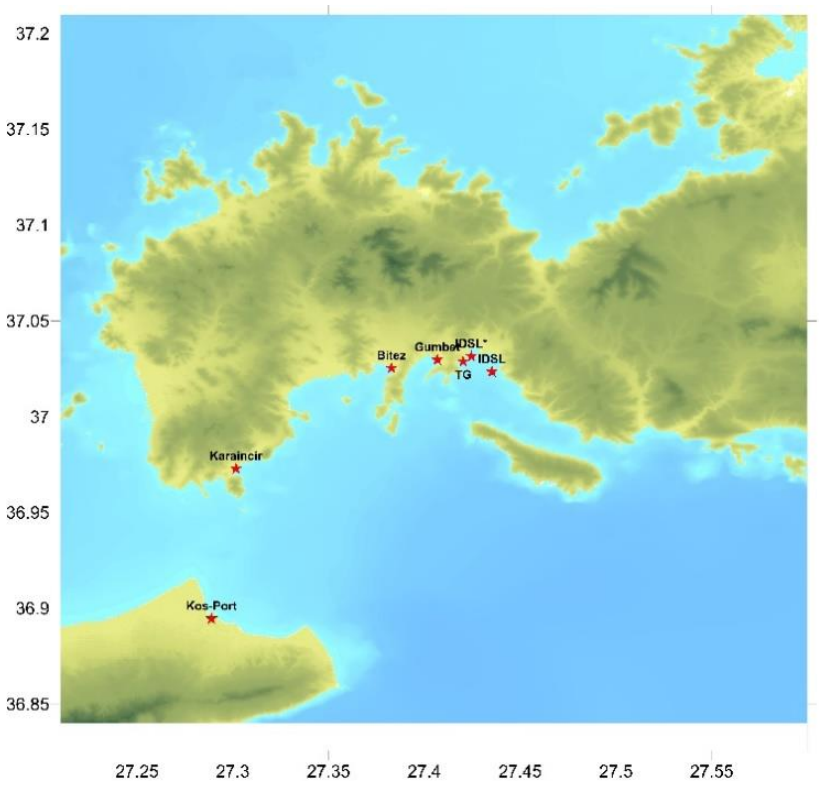

Figure 3.2 Showing all gauge points by red stars in study Domain D

Table 3.4 Properties of gauge points

Gauge Point Name	Longitude (ºE)	Latitude (ºN)
IDSL	27.424537	37.031483
IDSL*	27.435246	37.023434
Bodrum-TG	27.420310	37.028750
Gümbet	27.406760	37.029670
Bitez	27.382760	37.025304
Karaincir	27.301670	36.972844
Kos-Port	27.288852	36.894604

3.4 Results of Tsunami Scenarios

3.4.1 Results of Tsunami Scenarios Generated from Selected Seismic Sources

Tsunami nearshore parameters are computed and mapped for the smaller area (Domain D) for five selected seismic tsunami sources. For the 1956-Amorgos, Gökova, and Güllük Bay scenarios, the simulation duration is taken as 180 minutes. For the sources far away from Bodrum Peninsula, which are 365-Crete and 1303-Eastern Mediterranean, the duration is chosen as 240 minutes. Initial sea state conditions of selected seismic tsunami sources for Domain D are presented in Figure 3.3. Distributions of calculated maximum and minimum water levels for the selected seismic sources are given for Domain D (Appendix A1,2).

3.4.2 Results of Tsunami Scenarios Generated from Selected Landslide Sources

Two selected landslide sources, which are Amorgos Landslide and Gökova-North-Datça Landslide Scenarios, are simulated via NAMI DANCE software. Amorgos Landslide source consists of 18 m elliptical subsidence and 6 m uplift with dimensions of 21km×5km and 18km×5km, respectively. Gökova-North-Datça source is selected as possible landslide region that is the steepest coastal slope of Gulf of Gökova located in northern site of Datça Peninsula. It consists of 20 m elliptical subsidence and uplift with dimensions of 6km×2km. Initial sea states of two landslide sources are given in Figure 3.4. Simulation duration of Amorgos Landslide Scenario is selected as 240 min while it is taken as 180 min for Gökova-North-Datça Landslide Scenario. Maximum and minimum sea-level distributions of each landslide scenarios are given in Appendix B 1,2 respectively.

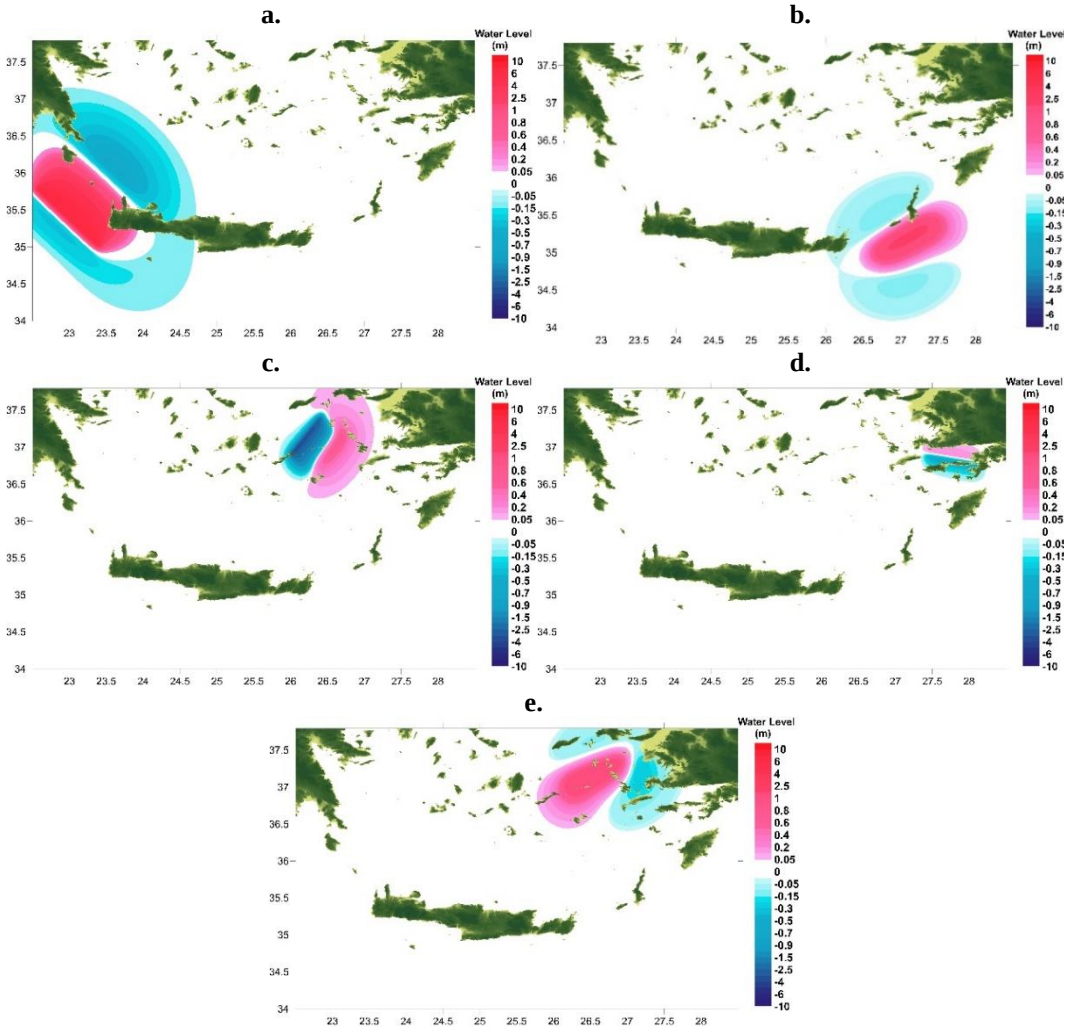

Figure 3.3 Initial Sea Surface Deformation of seismic tsunami scenarios of **a.** 365-Crete **b.** 1303-Eastern Mediterranean **c.** 1956-Amorgos **d.** Gökova **e.** Güllük Bay (label units in m)

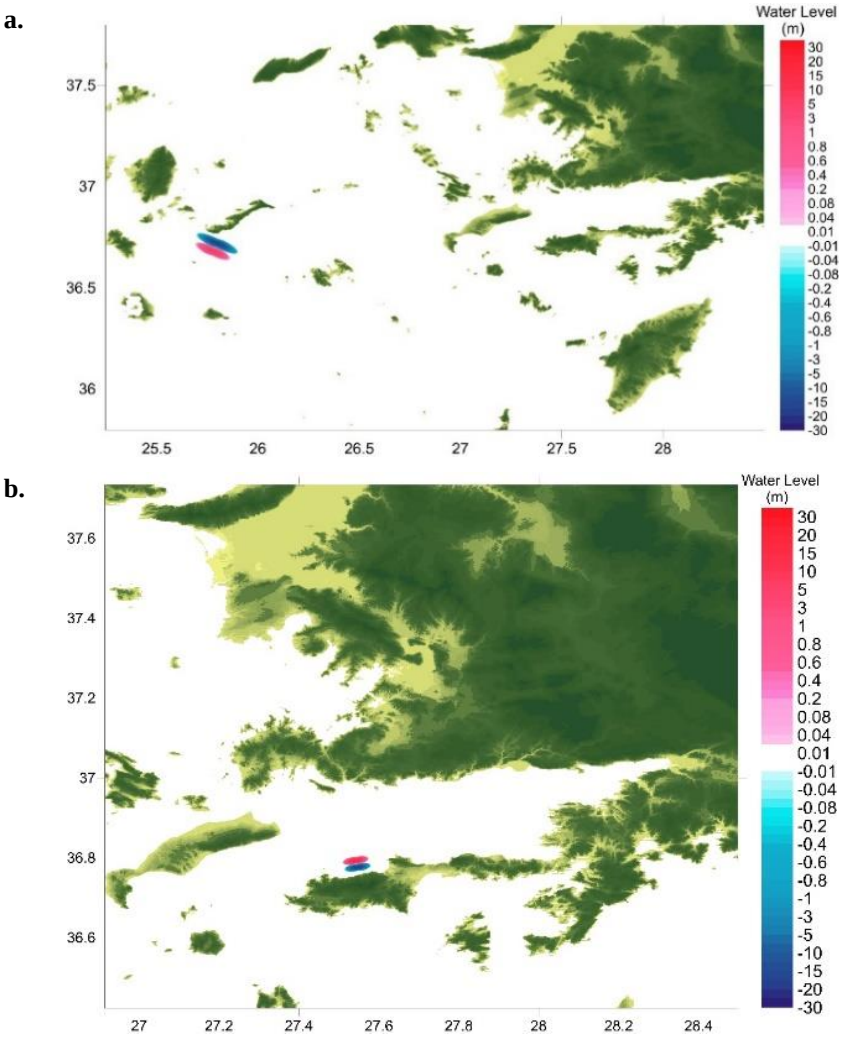

Figure 3.4 Initial Sea Surface Deformation of landslide tsunami scenarios in Domain B **a.** Amorgos Landslide Tsunami Scenario **b.** Gökova-North-Datça Landslide Tsunami Scenario

3.4.3 Results of Tsunami Scenarios Generated from Combined (Landslide and Seismic) Sources

Combined sources are generated by considering both landslide sources and their possible assumed triggering seismic mechanisms. In this study, two different combined seismic and landslide scenarios are determined that are Combined 1956-Amorgos Seismic + Amorgos Landslide Scenario and Combined Gökova Seismic + Gökova-North-Datça Landslide Scenario. Simulation duration of both combined scenarios is assigned as 180 min. Maximum and minimum water levels of combined landslide simulations for Domain D are given in Appendix C 1,2 respectively.

3.5 Selection of Critical Scenarios

According to the simulation results, 1956-Amorgos seismic scenario(i) gives maximum flow depth and inundation distance values among all seismic sources at selected gauge points in the southern coast of Bodrum Peninsula (Appendix D 1,2). On the other hand, Combined Gökova Seismic and Gökova-North-Datça Landslide scenario(ii) gives maximum levels at many locations among landslide and combined seismic + landslide scenarios. As a result, most critical scenarios are appeared as 1956-Amorgos seismic(i) and combined Gökova seismic and Gökova North Datça landslide(ii) scenarios for Bodrum Marina, Gümbet Bay, Bitez Bay which are the places where most of the settlements and touristic places are located. The first and maximum tsunami wave's arrival times to the gauge points are provided in Appendix D 3 and 4 respectively. The earliest arrival of the tsunami waves to the gauge points is about 10 minutes, considering all possible scenarios for Bodrum Peninsula. Maximum flow depth due to 1956-Amorgos seismic(i) and Combined Gökova seismic and Gökova-North Datça landslide(ii) scenario distribution of these places is given in Figures 3.5-7.

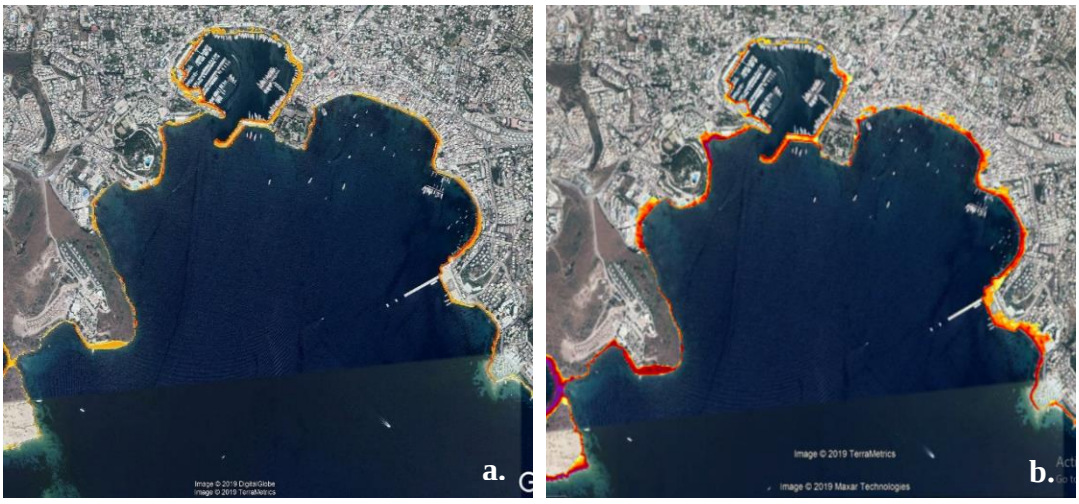

Figure 3.5 Distribution of maximum flow depth for Bodrum Marina and surroundings due to **a.** 1956-Amorgos Scenario **b.** Combined Gökova Seismic and Gökova-North-Datça Landslide Scenario

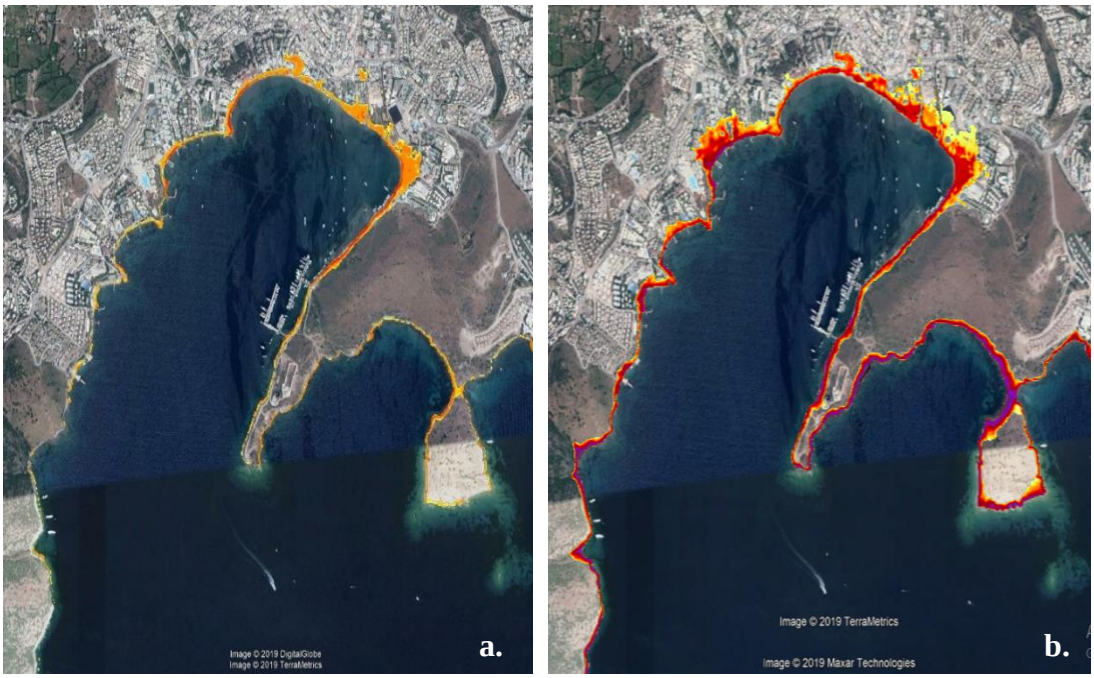

Figure 3.6 Distribution of maximum flow depth for Gümbet Bay due to **a.** 1956-Amorgos Scenario **b.** Combined Gökova Seismic and Gökova-North-Datça Landslide Scenario

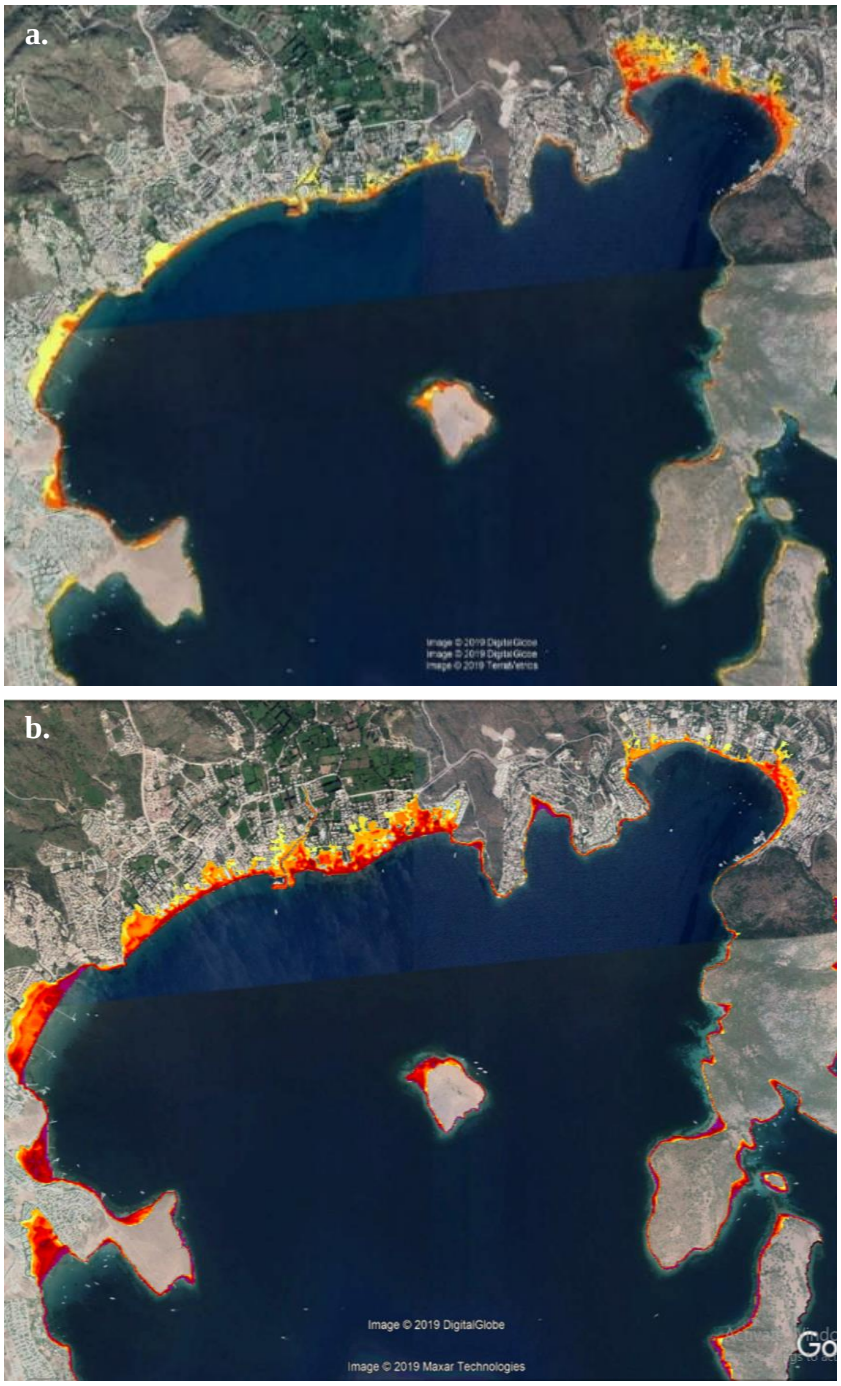

Figure 3.7 Distribution of maximum flow depth for Bitez and Karaincir Bays due to **a.** 1956-Amorgos Scenario **b.** Combined Gökova Seismic and Gökova-North-Datça Landslide Scenario

CHAPTER 4

PREPARATION OF PEDESTRIAN EVACUATION TIME MAPS BY USING PEAT

4.1 Concept and Methodology

Evacuation is the instant action of people moving from a hazardous location towards a place of greater safety. It is an important component of population protection analysis that is an element of community preparedness (Lindell and Perry 2007). Evacuation may significantly reduce the damage caused by hazards like the number of deaths and injuries (Lindell et al. 2006). Especially for the hazard-prone areas, self-initiated evacuation is the main way to save life as they have a few minutes to escape from the threat (Wood and Schmidtlein, 2012). For tsunamis, evacuation is possible by reaching out of the inundation zone towards the higher ground (horizontal evacuation) or evacuating to the higher floors like high buildings within the inundation zone (vertical evacuation) (Dewi, 2012). Evacuation maps should be created with the information of the direction to escape for pedestrian, available routes guiding people towards the nearest safe area, a number of people that will use the evacuation routes, minimum travel speeds of pedestrian, and the distance to the safe zone (Scheer et al., 2012).

In this study, the Pedestrian Evacuation Analyst Tool (PEAT) is used for producing evacuation walk time maps for the selected areas located on the southern coasts of Bodrum. PEAT is an extension of ArcGIS that scientists and emergency managers use for modeling pedestrian evacuation potential. It was developed by Jones et al. (2014) for the researchers studying self-initiated pedestrian evacuation from sudden-onset hazards such as local tsunamis, debris flows, lahars (volcanic mudflows), and flash floods.

In the literature, both static least-cost-distance (LCD) and dynamic agent-based models are used in order to assess pedestrian evacuation from sudden hazards. Among these evacuation models, GIS tools are used for LCD models to calculate the shortest path to the safe area from every place within the hazard zone. PEAT is one of the cost-distance models that include calculations based on static landscape properties such as slope, land-cover, and roads etc., within the hazard zone. Evacuation walk time maps are generated in PEAT by the main two steps: preprocessing of input data and creating evacuation surfaces and maps (Jones et al., 2014) (Figure 4.1). The first step of preprocessing of input data is the digital elevation model preprocessing at which the DEM raster and study area vector data are entered. Then, the tool clips the DEM according to the provided study areas. Also, PEAT calculates the slope that is derived from the digital elevation model (DEM). In this stage of PEAT, slope directionality is also considered during the calculation of travel cost based on Tobler's (1993) hiking function representing the relation between slope and walking speed (Wood and Schmidtlein, 2012). PEAT requires all input files in the same projection in order to have maximum accuracy. In this step, the analysis of cell size can also be defined; thus, the input DEM is either sampled or aggregated to match the defined cell size. According to Wood and Schmidtlein (2012), PEAT tended to underestimate evacuation travel times within the hazard zone when the DEM has a coarser resolution. The second step is the land-cover preprocessing at which PEAT considers the effect of different types of Earth's coverage on pedestrian evacuation by assigning different SCVs, representing the percentage of pedestrians' maximum travel speed (Wood and Schmidtlein, 2012). As a result of the land-cover preprocessing step, PEAT creates a cost-inverse raster, representing the inverse of the land-cover/land-use SCVs. In the hazard zone preprocessing step, the safe zone is created that is defined as the area out of the hazard zone within the study that should be verified manually to create a quality-assured safe zone in the safe zone validation step.

Preprocessed DEM, the cost-inverse raster and validated safe zone are taken as input to create the path distance surface representing the travel distance from every cell within the hazard zone towards the nearest safe zone. The path distance surface is multiplied by pedestrians' assumed travel speed during the evacuation that creates the evacuation surface representing the time required for pedestrians to get out from the hazard zone in minutes. The algorithm of path distance surface in ArcGIS is sensitive to the instant changes of elevation depending on the resolution of DEM input. It may calculate a very large distance for the sudden elevation changes between cells that causes very high time values in the evacuation surface. Therefore, the realistic maximum time value is identified manually, and by the time map tool all the values larger than the realistic are set to that value. Finally, the evacuation time map is created by reclassifying the evacuation surface into 1-minute increment integer bands.

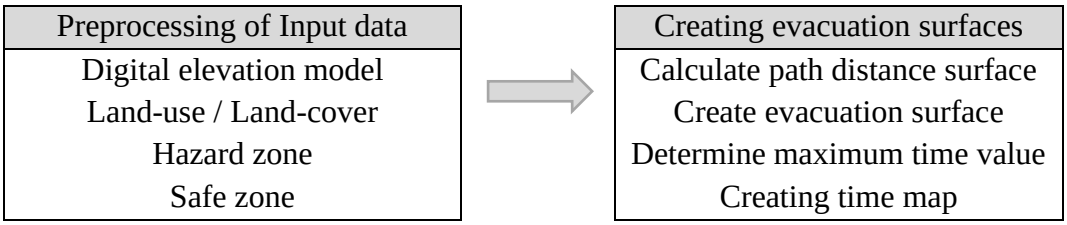

Figure 4.1 Two main processes of PEAT with their sub-processes (modified from Jones et al., 2014)

4.2 Selection of study areas for PEAT

Tsunami numerical simulations are performed with NAMI DANCE software as explained in Chapter 3, where 1956-Amorgos seismic scenario (i) and Combined Gökova Seismic and Gökova North Datça Landslide scenario (ii) are determined as critical scenarios. According to the results of numerical simulations, 1956-Amorgos seismic scenario (i) and Combined Gökova Seismic and Gökova North Datça Landslide scenario (ii) give higher inundation levels and flow depths among other scenarios at many locations along the southern coast of Bodrum where densely populated settlements and touristic places are located.

Study areas are selected for PEAT among the places having the highest inundation distances and ignoring the surrounding uninhabited islands which are out of the scope for this thesis, which are Central Bodrum, Gümbet Bay, Bitez Bay, Yahşi Bay, and Akyarlar-Karaincir-Aspat Bays shown in Figure 4.2. Evacuation walk time maps are prepared according to the worst-case scenario, meaning that the scenarios have the highest inundation at a location. It is observed that the Combined Gökova seismic and Gökova North Datça landslide scenario (ii) appears as the worst-case scenario for Central Bodrum, Gümbet Bay, Yahşi Bay, and Akyarlar-Karaincir-Aspat Bays. Consequently, as input for the evacuation walk time maps, the combined scenario (ii) is selected for those areas and shown in Figure 4.3-6. However, throughout Bitez Bay at some locations the 1956-Amorgos seismic scenario (i) gives the highest inundation distances, while at other locations of the Bay, the combined scenario (ii) gives the highest values (Figure 4.7). Therefore, these two critical scenarios are merged by taking the highest inundation values resulting from either of the two scenarios and used as input during preparing pedestrian evacuation walk time maps. The inundation maps are named as 'hazard zone' in the following chapters and used for further processes.

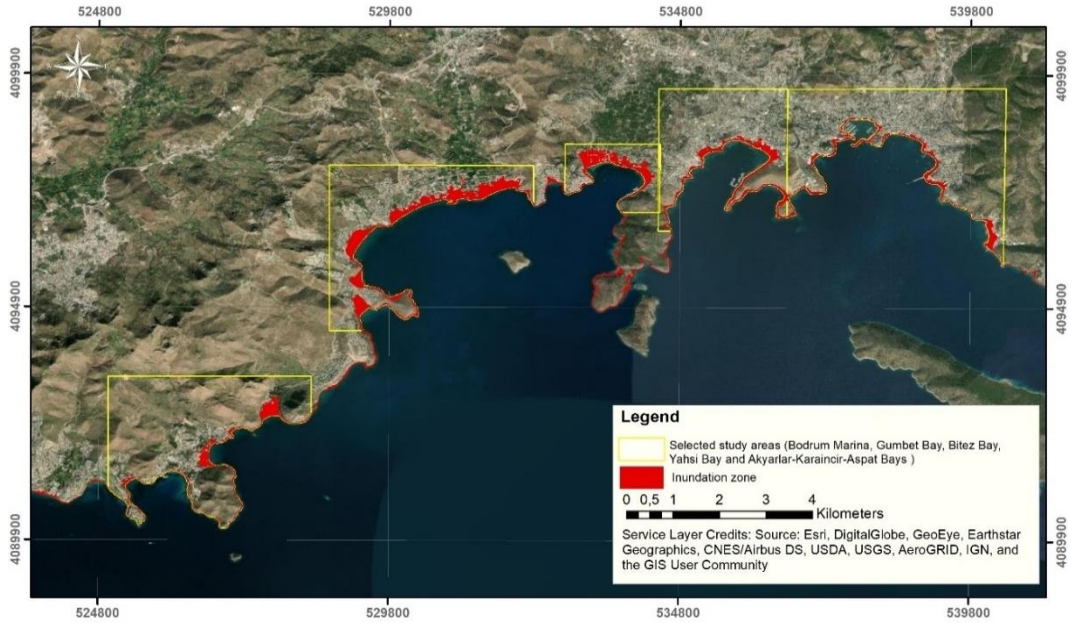

Figure 4.2 Resultant inundation zones and selected study areas for PEAT

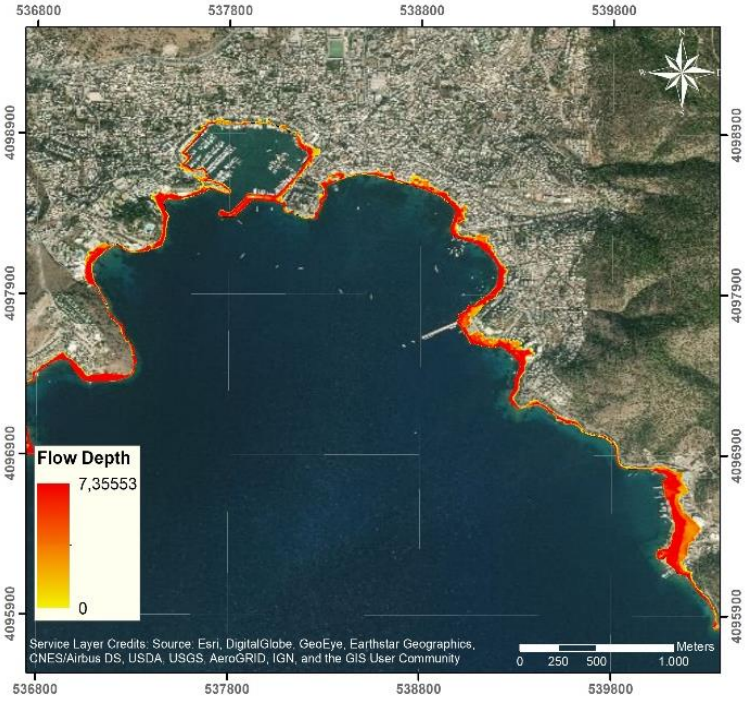

Figure 4.3 Maximum flow depth distribution due to Combined Gökova Seismic and Gökova-North-Datça Landslide Scenario (ii) in Central Bodrum

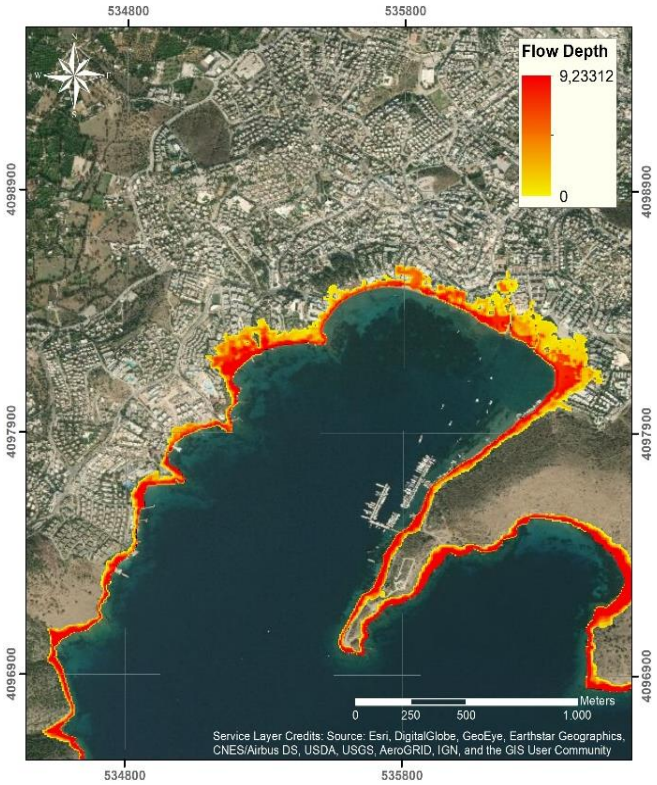

Figure 4.4 Maximum flow depth distribution due to Combined Gökova Seismic and Gökova-North-Datça Landslide Scenario (ii) in Gümbet Bay

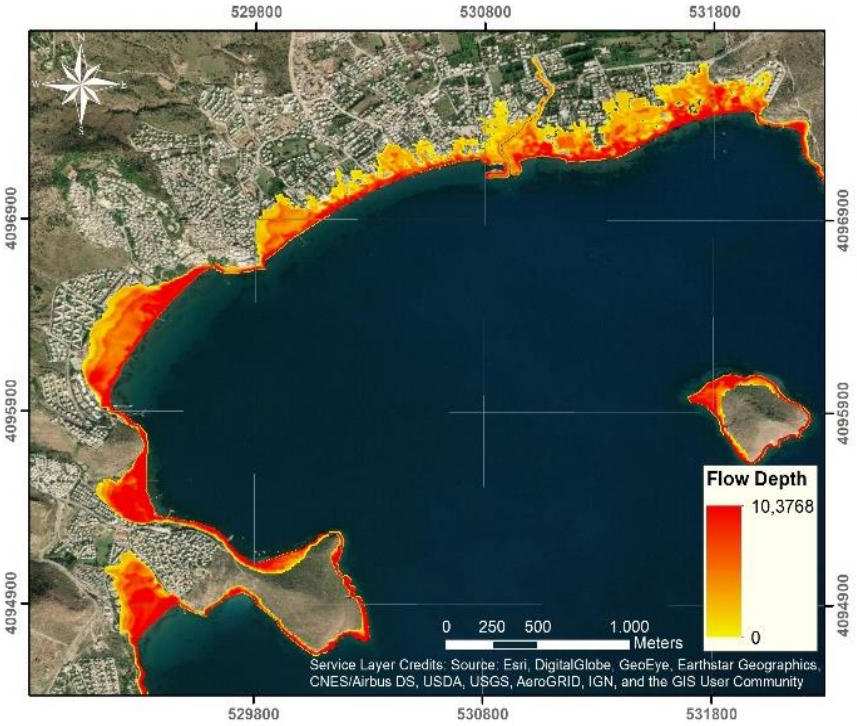

Figure 4.5 Maximum flow depth distribution due to Combined Gökova Seismic and Gökova-North-Datça Landslide Scenario (ii) in Yahşi Bay

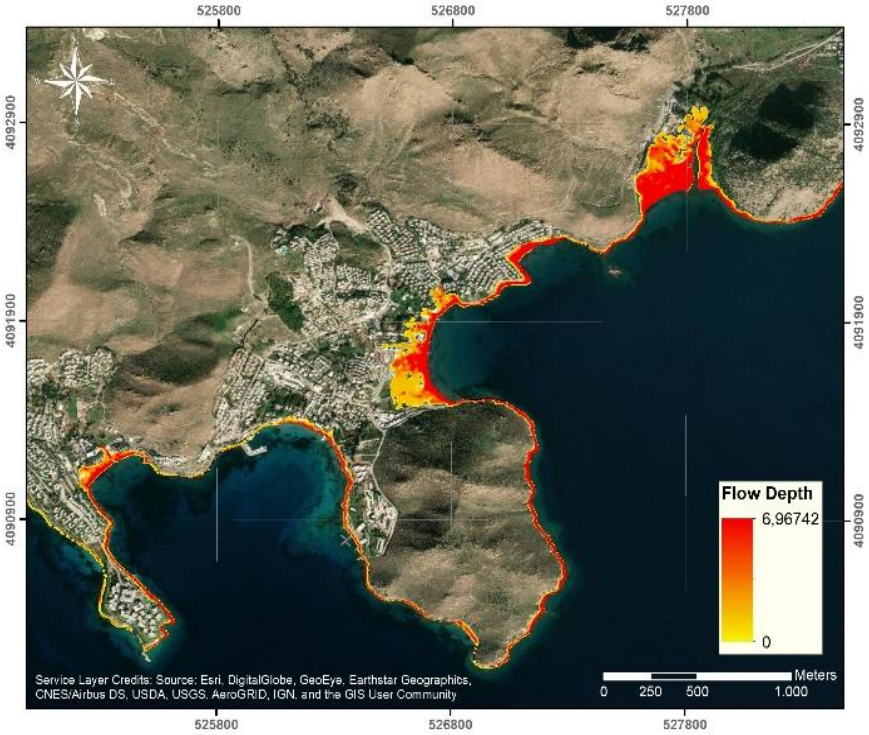

Figure 4.6 Maximum flow depth distribution due to Combined Gökova Seismic and Gökova-North-Datça Landslide Scenario (ii) in Akyarlar-Karaincir-Aspat Bays

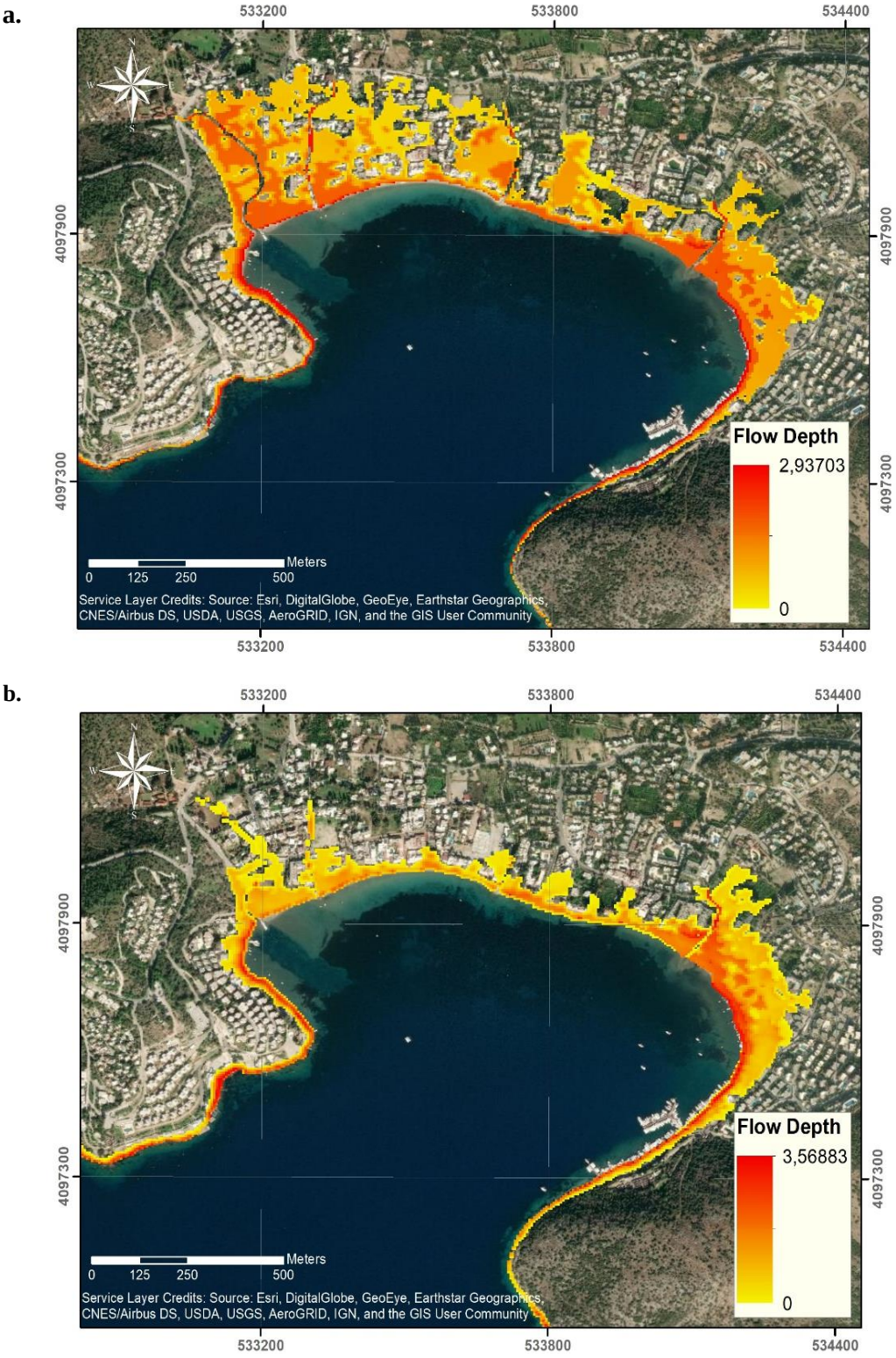

Figure 4.7 Maximum flow depth distribution of Bitez Bay due to a. 1956 Amorgos seismic scenario b. Combined Gökova Seismic and Gökova-North-Datça Landslide Scenario

4.3 Preprocessing of Data for PEAT

Data used in this part of the study is provided by Bodrum Municipality within the scope of the Last Mile project. Additionally, for the cases where the data have inconsistency or deficiency, open-source data are used, such as Google Earth Images and Open Street Map.

4.3.1 Digital elevation model (DEM)

In order to use for both numerical simulations of NAMI DANCE and PEAT, 5 m resolution Digital Elevation Model (DEM) is used. DEM also includes building heights. In the preprocessing step, DEM is clipped according to the selected five study areas within the scope of this study as explained in Chapter 4.2, which are covering Central Bodrum, Bitez Bay, Gümbet Bay, Yahşi Bay, and Akyarlar-Karaincir-Aspat Bays. The processed DEM of each study area is shown in Figures 4.8-12.

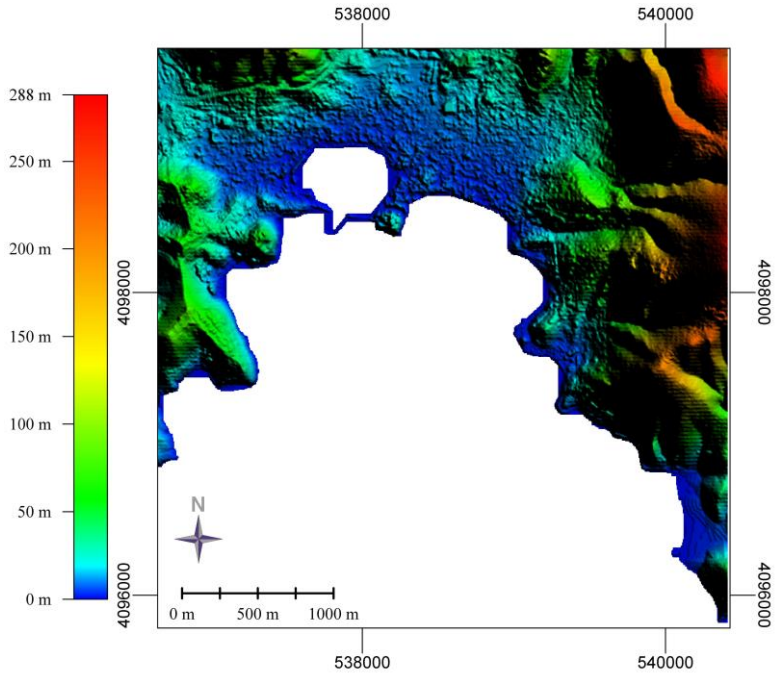

Figure 4.8 Digital elevation model around Central Bodrum region

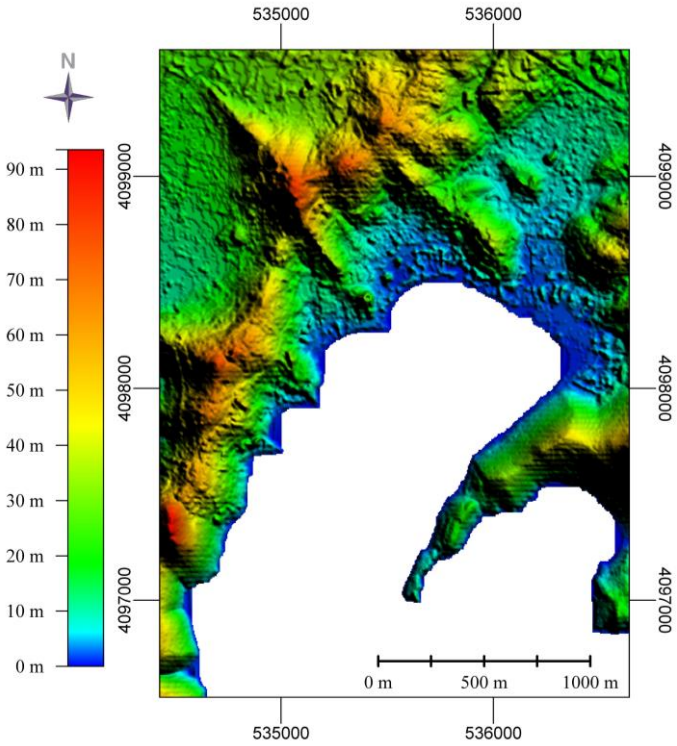

Figure 4.9 Digital elevation model for Gümbet Bay

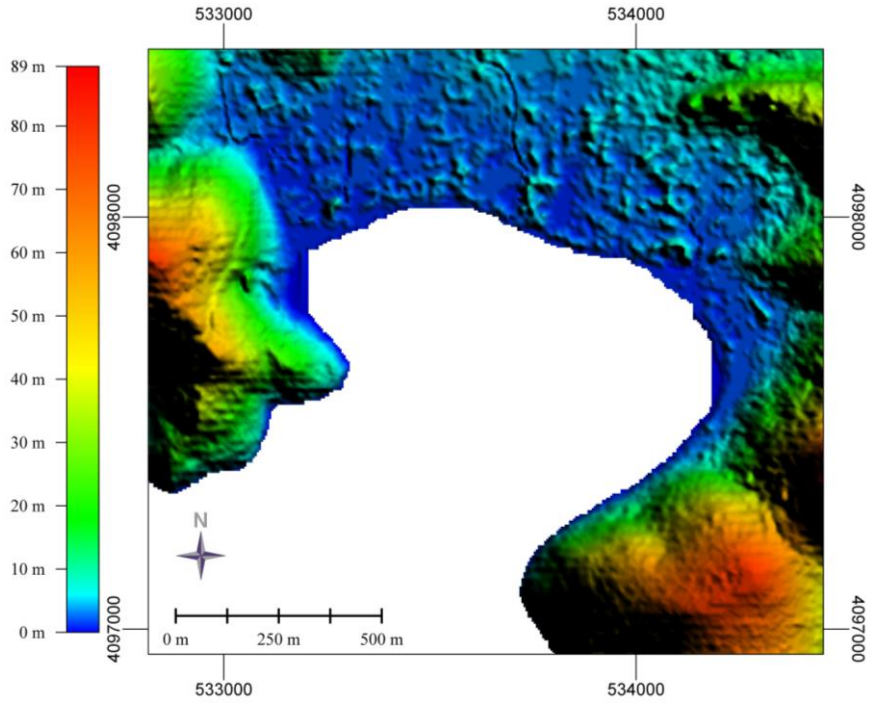

Figure 4.10 Digital elevation model for Bitez Bay

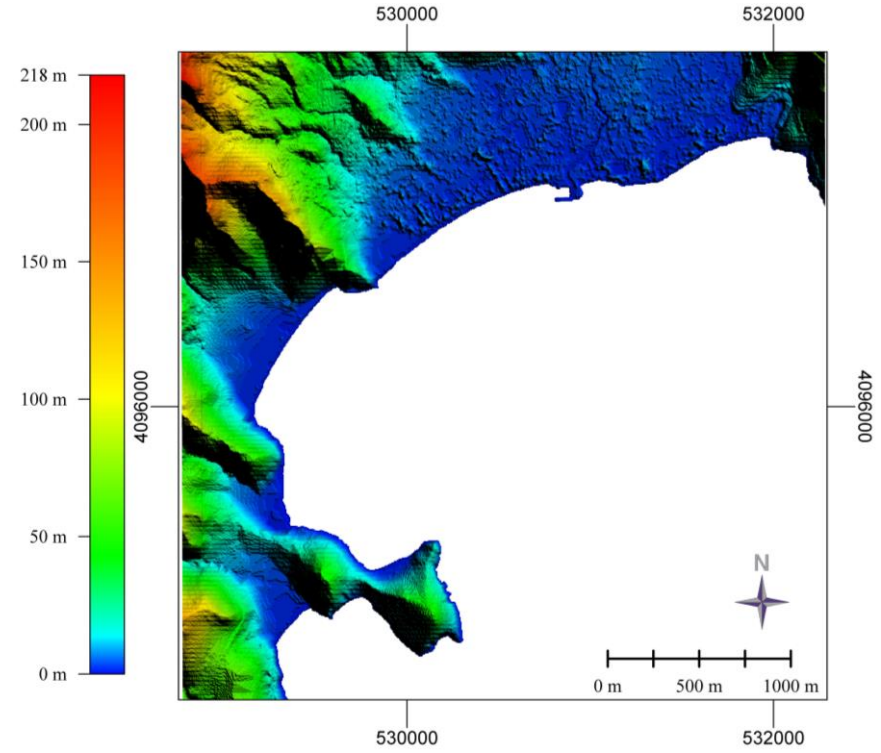

Figure 4.11 Digital elevation model for Yahşi Bay

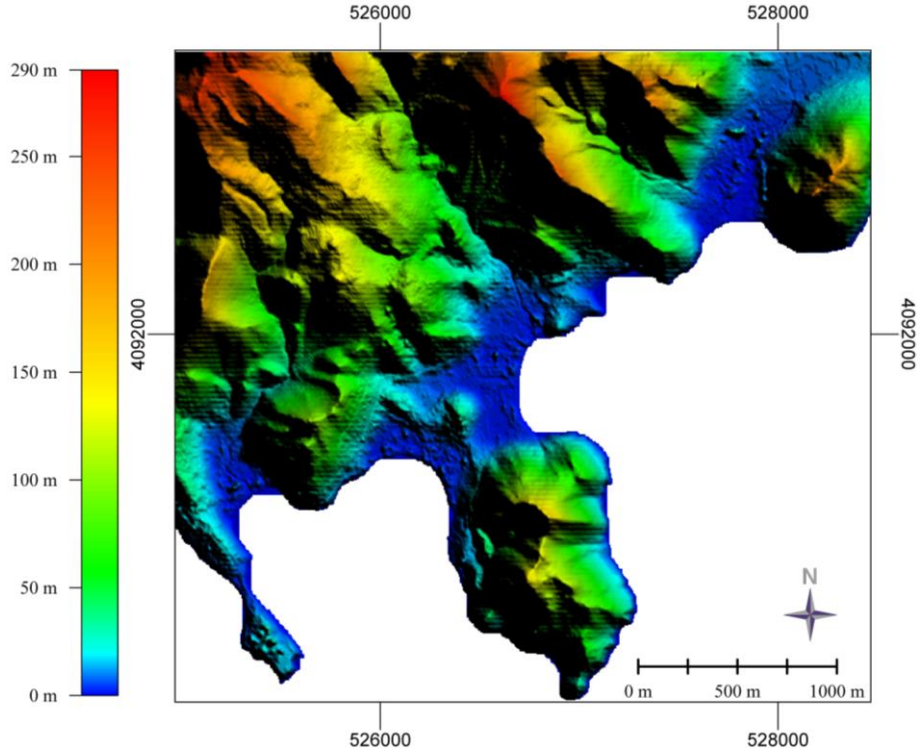

Figure 4.12 Digital elevation model around Akyarlar-Karaincir-Aspat Bays

4.3.2 Land-cover and Land-use Dataset

Land-use/Land-cover is an important issue for pedestrian evacuation from a sudden tsunami disaster. The input data required for this tool are developed areas, bush and cultivated crops, buildings, roads, rivers, and beaches that affect the pedestrian's walking pace. The road data for some of the study areas are gathered from Open Street Map due to the inadequacy of the provided data by Bodrum Municipality. The data is subdivided into the base layer and the ancillary layer to satisfy the Pedestrian Evacuation Analyst Tool's requirements. The base layer is represented as the spatial distribution of observed Earth surface coverage, such as beaches, cultivated lands, bushes, etc. Whereas ancillary layers are any surfaces that can affect the walking pace of the pedestrian during sudden tsunami events such as roads, rivers, any type of barriers, and buildings that are used in order to create more realistic evacuation maps for pedestrians. Energy cost terrain coefficients are determined for certain land-cover types by Soule and Goldman (1972). Then, Wood and Schmidtlein (2012) give "speed conservation value" (SCV) for each type of land-cover/land-use by using the inverse of the energy cost terrain coefficients. The SCV represents the maximum travel speed percentages of each land-cover type. It varies from 0 (no evacuation possibility) to 1 (easiest evacuation is possible). All the data related to land-cover are converted to a single layer named as least-cost-inverse raster by PEAT and used as an input in the creation of path distance surface.

Land-cover data in this study is created by using the latest acquired submeter resolution Google Earth Images at the time of the thesis manually for coastal areas around Central Bodrum, Gümbet Bay, Bitez Bay, Yahşi Bay, and Akyarlar-Karaincir-Aspat Bays (Figure 4.13-17). Speed conservation values of each land-cover type present in the study area are given by utilizing the information provided by Wood and Schmidtlein (2012) (Table 4.1). For the developed-highly populated areas, the maximum value is given to SCV as 0.9091 in the base layer because they are closest to buildings that may provide vertical evacuation for pedestrians easily from tsunami waves. On the other hand, beaches are formed from unconsolidated

sand on which it is very difficult to walk so SCV is given as 0.5556. For cultivated crops and bushes, SCV is assigned as 0.8333 as evacuation is easier than beaches.

Table 4.1 Speed Conservation values of the land-cover types (Wood and Schmidtlein, 2012)

Land-cover Type	Speed Conservation Value (SCV)
Developed- highly populated	0.9091
Cultivated crops	0.8333
Bush	0.8333
Beach	0.5556

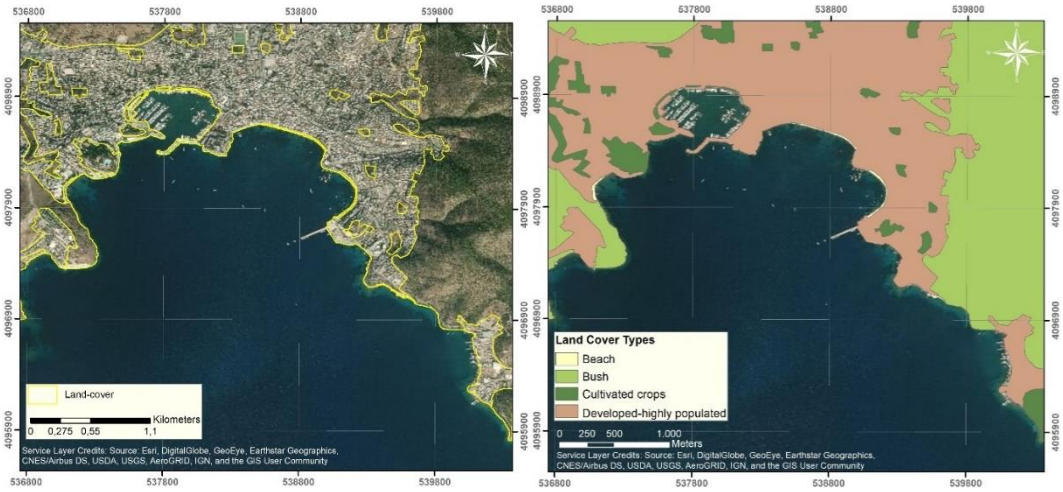

a. **b.**

Figure 4.13 **a.** Google Earth Image of Central Bodrum **b.** Classified land-cover type polygons for Central Bodrum

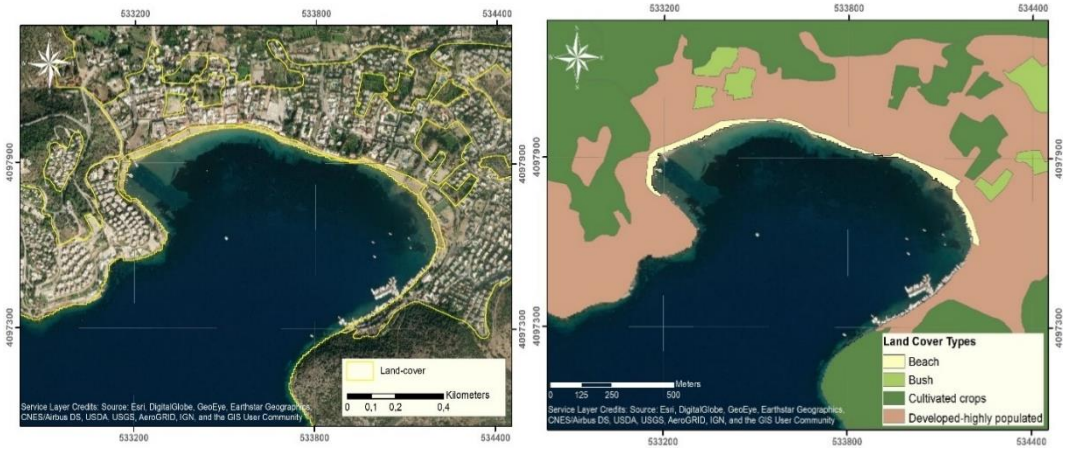

a. **b.**

Figure 4.14 **a.** Google Earth Image of Bitez Bay **b.** Classified land-cover type polygons for Bitez Bay

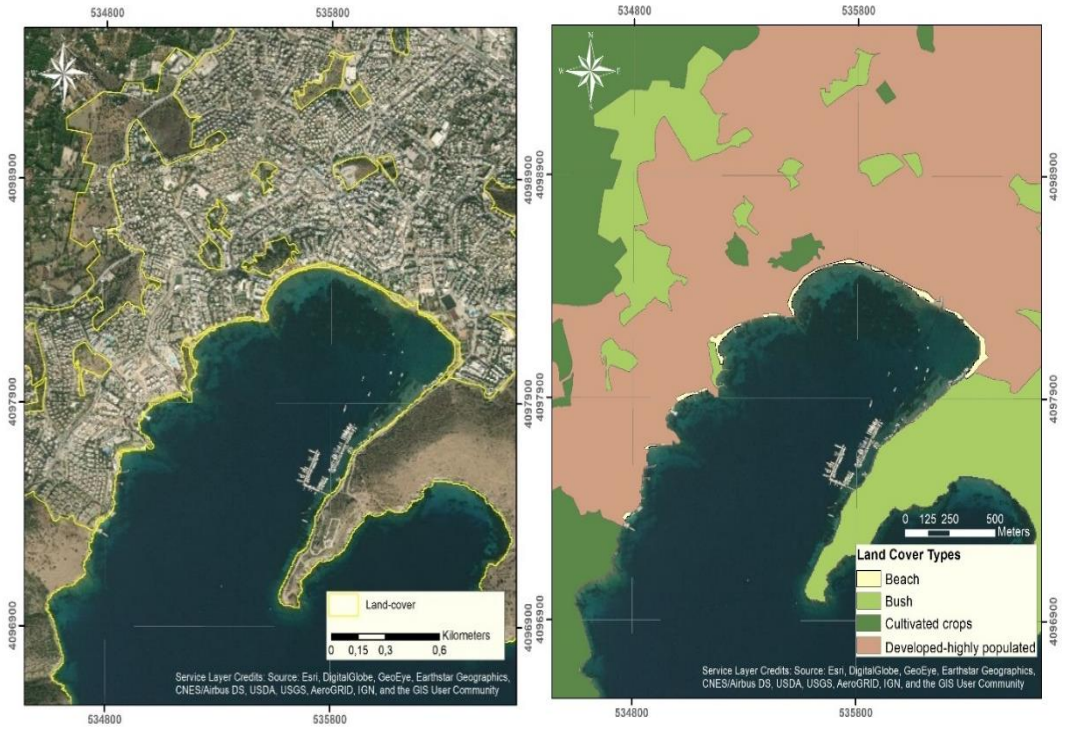

a. **b.**

Figure 4.15 **a.** Google Earth Image of Gümbet Bay **b.** Classified land-cover type polygons for Gümbet Bay

a. **b.**

Figure 4.16 **a.** Google Earth Image of Yahşi Bay **b.** Classified land-cover type polygons for Yahşi Bay

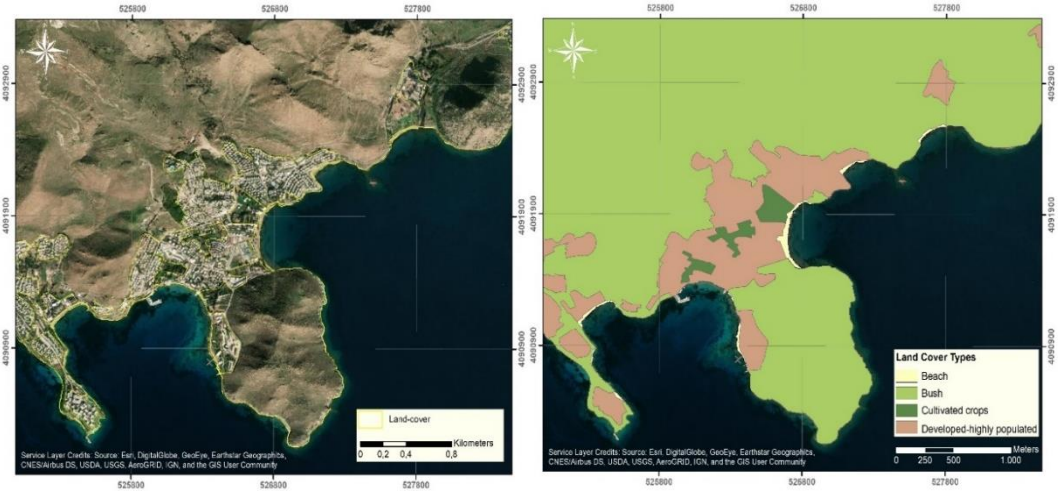

a. **b.**

Figure 4.17 **a.** Google Earth Image of Akyarlar-Karaincir-Aspat Bays **b.** Classified land-cover type polygons for Akyarlar-Karaincir-Aspat Bays

Ancillary layers are composed of existing roads, fences, buildings, water bodies within the study area that affect the pedestrian's evacuation. Roads and rivers are the ancillary layers used in this study. Among all the layers, roads are the most important ancillary layer as they provide pedestrians to evacuate in the easiest way. Except for the data provided by Bodrum Municipality, in some places, Open Street Map is used due to the inadequateness of the provided data. In addition to that, some road data within the hazard zone are added from Google Earth Images since they are thought

as essential for pedestrian evacuation. On the other hand, barrier data are not used in this study since types of barriers are not exactly known from the data (concrete garden separators, metal fences, security walls, etc.). Furthermore, the availability of high-resolution DEM, which already include the building heights removes the necessity to include the building data in ancillary layers.

Bodrum Municipality provided river data used in the study. It is assumed that evacuation is not possible and even dangerous because tsunami waves are propagating fast through rivers. Maximum SCV (1) is given to the road layer as they provide pedestrians to evacuate the fastest and easiest way, while minimum SCV (0) is given to the river layer as they block the pedestrian evacuation, according to Wood and Schmidtlein, (2012). The Pedestrian Evacuation tool gathers base and ancillary layers in the first step, and then, it creates the cost-inverse raster at which the values are showing the inverse of the given SCVs for five study areas (Figure 4.18-22).

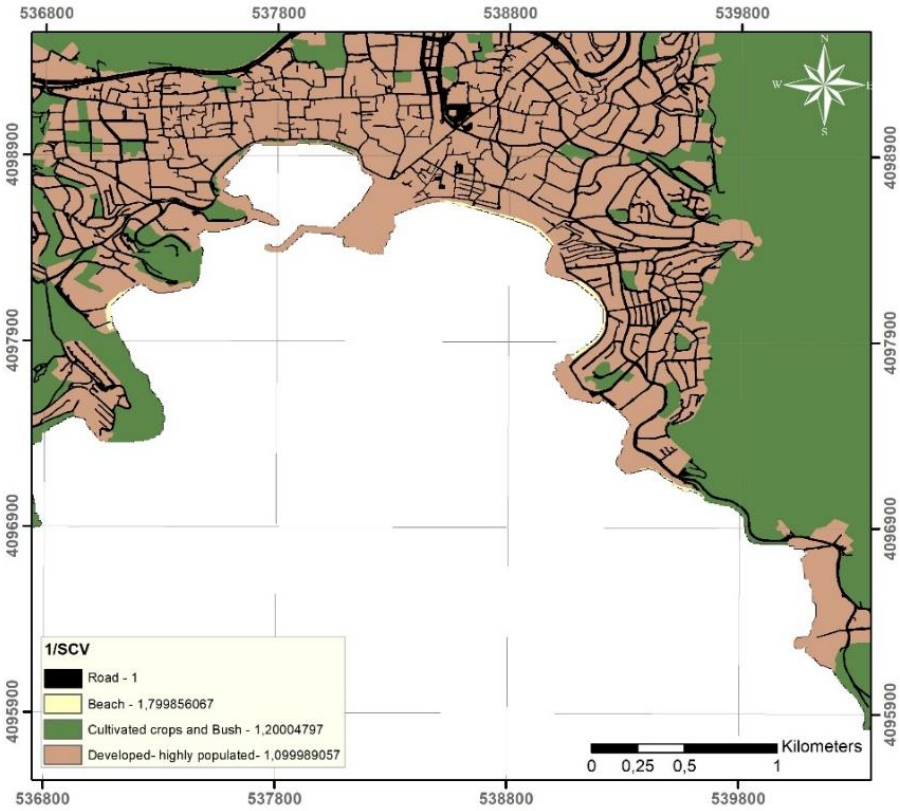

Figure 4.18 Cost-inverse surface around Central Bodrum

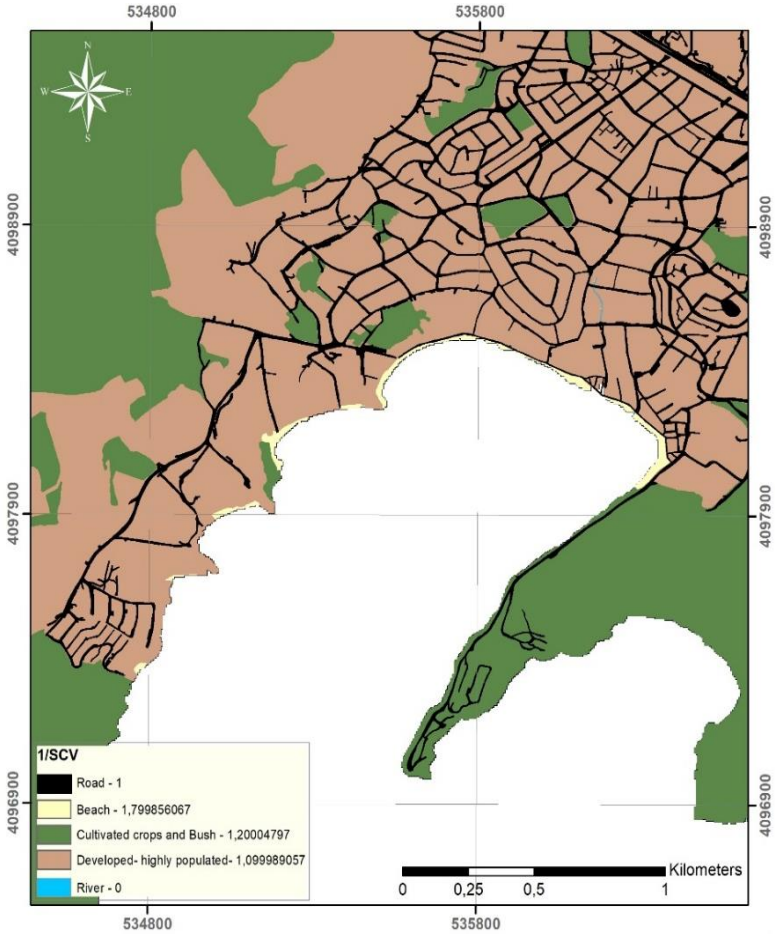

Figure 4.19 Cost-inverse surface for Gümbet Bay

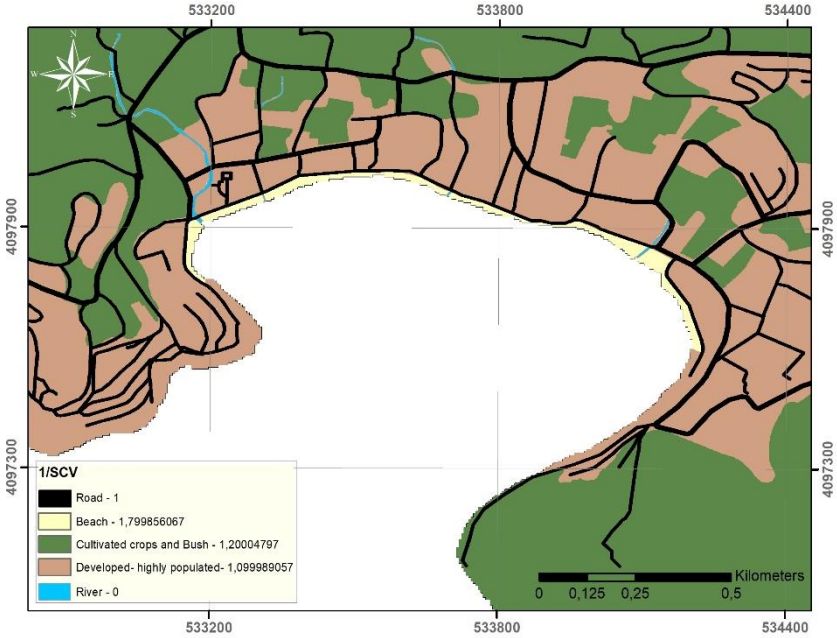

Figure 4.20 Cost-inverse surface for Bitez Bay

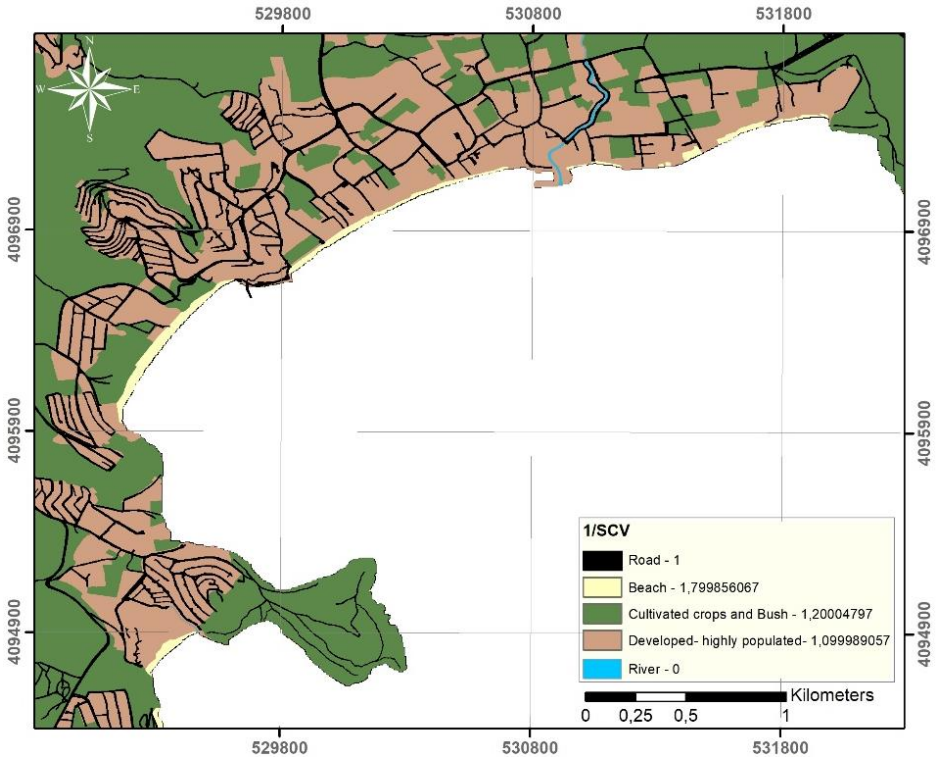

Figure 4.21 Cost-inverse surface for Yahşi Bay

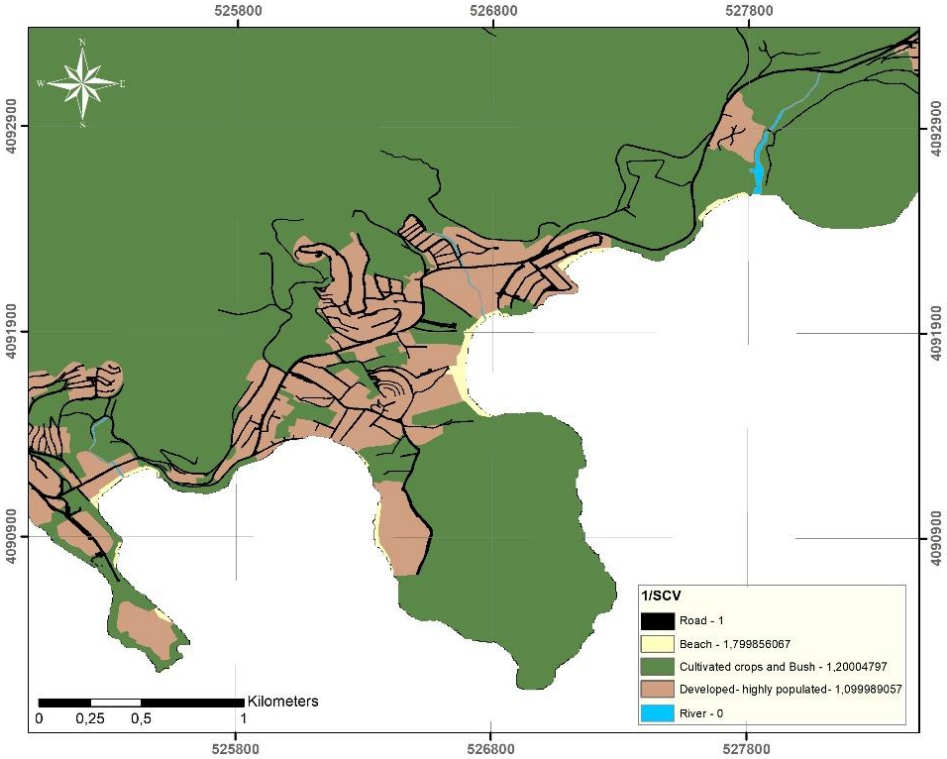

Figure 4.22 Cost-inverse surface for Akyarlar-Karaincir-Aspat Bays

4.3.3 Hazard and Safe Zone

Inundation results of the tsunami modeling simulation are used as hazard zone areas in this study. 1956-Amorgos seismic scenario (i) and Combined Gökova seismic and Gökova North Datça landslide (ii) scenario are the most critical two scenarios which create maximum inundation distances throughout the study area. The resultant raster data showing maximum inundation areas with flow depth values are converted to vector data. This process was performed for five study areas, and a representative Bitez Bay example is shown in Figure 4.23. These polygons are used in the hazard zone preprocessing part of PEAT.

Figure 4.23 **a.** Raster data of maximum flow depth distribution of merged two scenarios for Bitez Bay **b.** Vector data showing hazard zone polygon used as input in PEAT for Bitez Bay

The safe zone is the places within the study area that are out of the hazard zone. Hazard zone polygons are used as input by PEAT in order to create safe zone areas. After safe zone areas are generated by PEAT, validation is needed due to the remaining sliver polygons. Those sliver polygons within the hazard zone are investigated and most of them are found to be due to the existence of buildings or any sudden changes in the DEM. Additionally, any safe island polygons within the inundation zone are removed as they are thought to be unsafe places for pedestrians to evacuate. After the safe zones are reviewed and corrected for five study areas, a quality-assured final safe zone is created that is used in the following processes of PEAT (Figure 4.24).

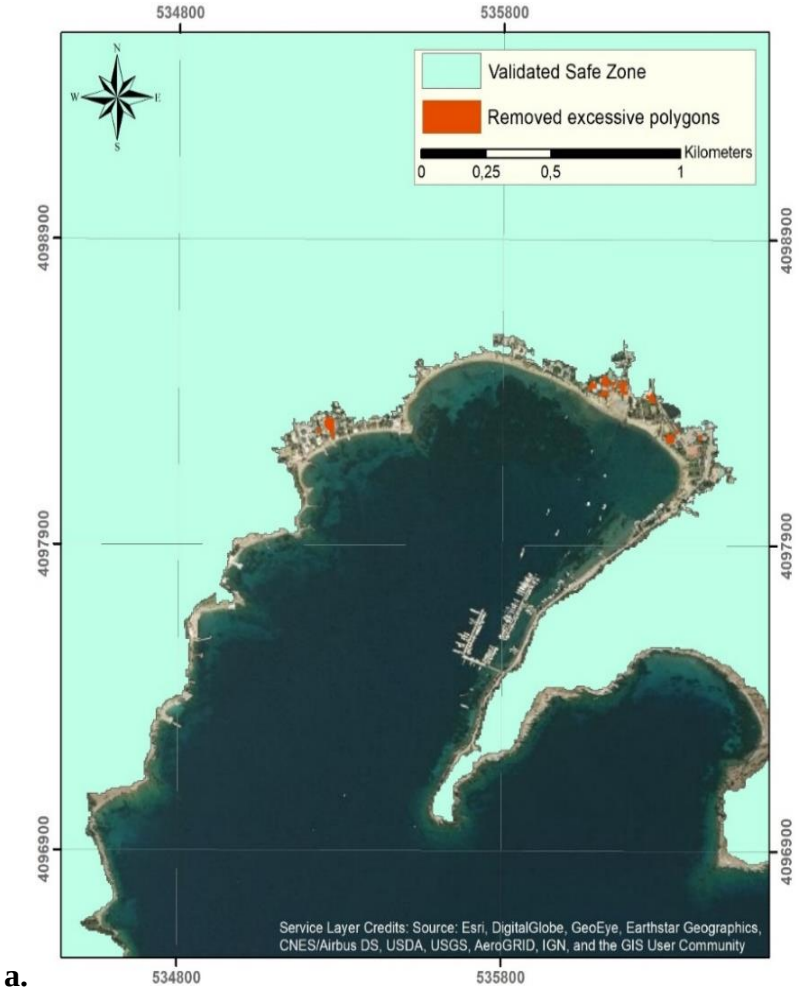

a.

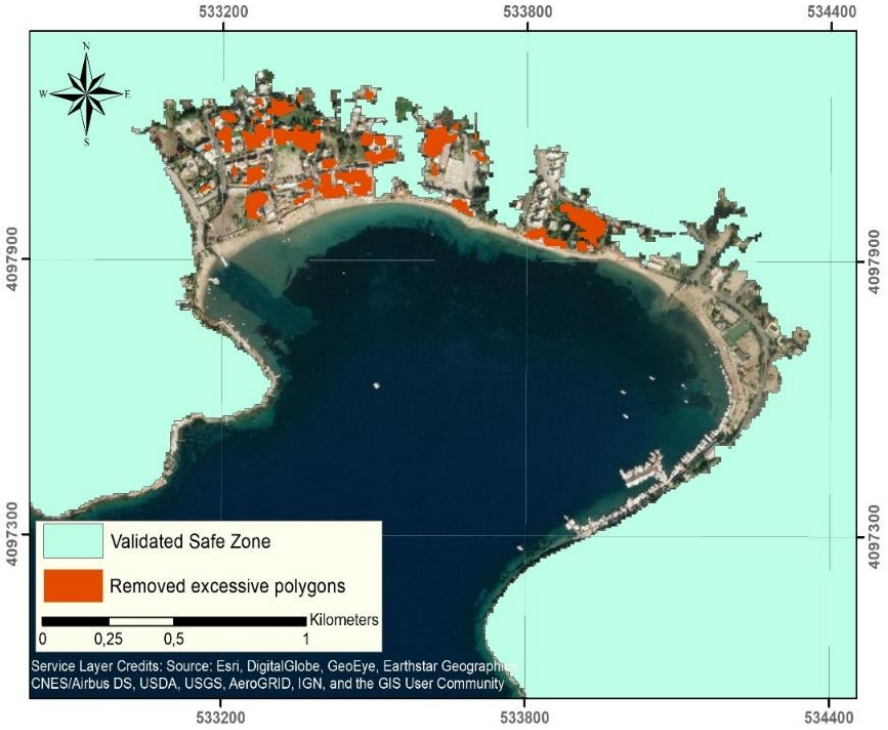
533200
533800
534400
4097900
4097300
N
W
E
S
Validated Safe Zone
Removed excessive polygons
Kilometers
0
0,25
0,5
1
Service Layer Credits: Source: Esri, DigitalGlobe, GeoEye, Earthstar Geographics,
CNES/Airbus DS, USDA, USGS, AeroGRID, IGN, and the GIS User Community

b.

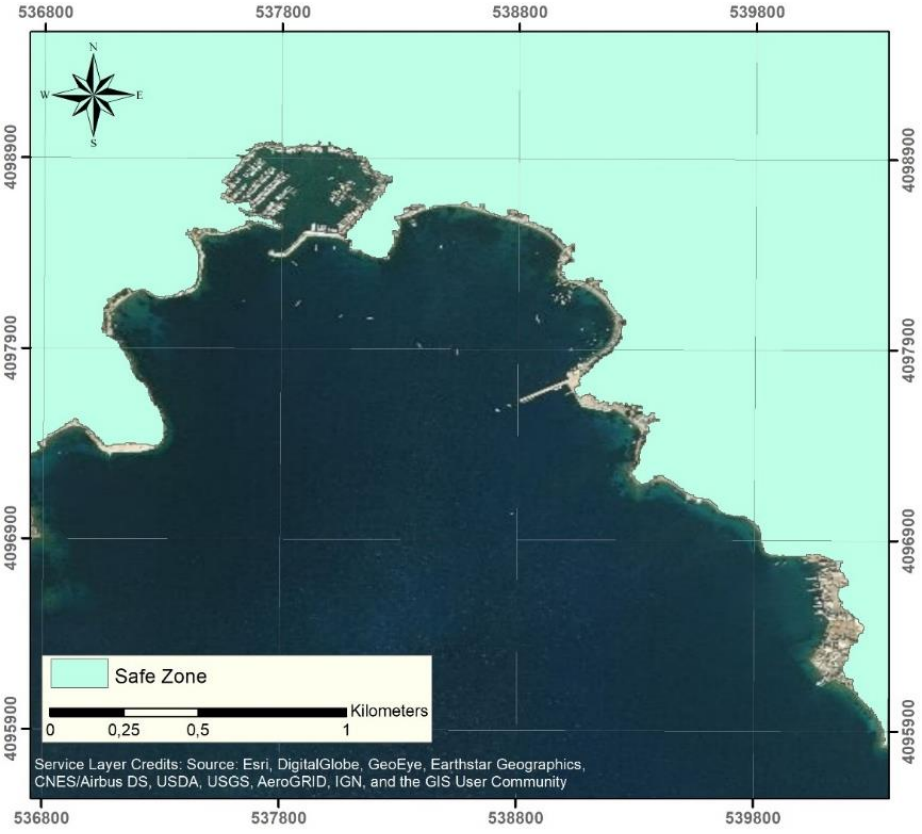
536800
537800
538800
539800
4098900
4097900
4096900
4095900
N
W
E
S
Safe Zone
Kilometers
0
0,25
0,5
1
Service Layer Credits: Source: Esri, DigitalGlobe, GeoEye, Earthstar Geographics,
CNES/Airbus DS, USDA, USGS, AeroGRID, IGN, and the GIS User Community

c.

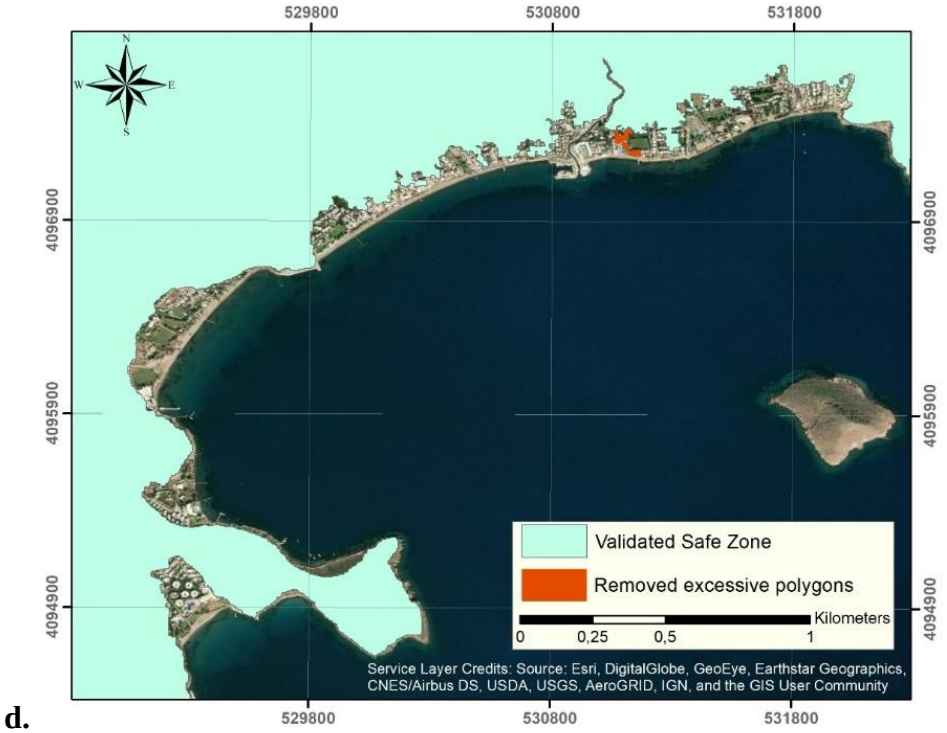

d.

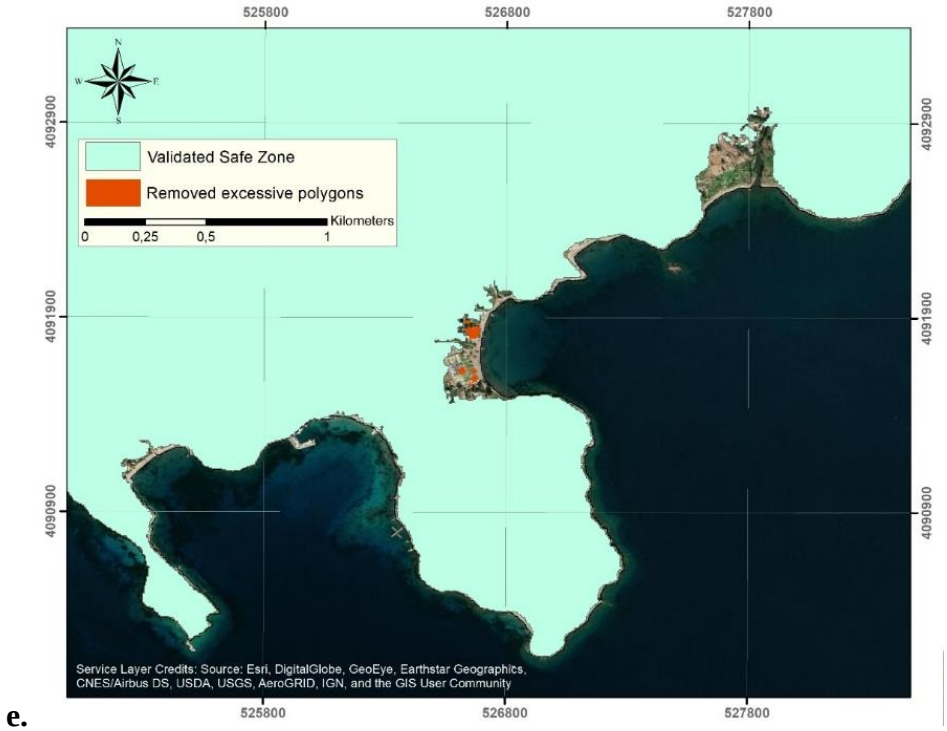

e.

Figure 4.24 Validated safe zone polygons (green color) after manually removal of excessive polygons (orange color) used further analysis for **a.**Central Bodrum, **b.** Gümbet Bay, **c.** Bitez Bay, **d.**Yahşi Bay, **e.**Akyarlar-Karaincir-Aspat Bays

4.4 Resultant Tsunami Evacuation Walk Time Maps

The pedestrian evacuation analyst tool (PEAT) calculates the first path distance surface and then the evacuation surface to create an evacuation time map. Preprocessed DEM, the least-cost-inverse raster and validated safe zone areas are used as input in the Path Distance (PD) surface generation step of PEAT. In this stage, the travel distance from each cell to the nearest safe zone is calculated. After that, the evacuation surface (ES) multiplies the path distance surface with the desired travel speed and calculates travel times to reach the safe zone. According to different travel speeds shown in Table 4.2, users can create different evacuation surfaces using the same path distance surface data. According to the crosswalk walking standards in the United States, a slow walking pace is recommended (Wood and Schmidtlein, 2012). Therefore, in this study slow walking pace (1.1 m/s) is selected as travel speed.

Table 4.2 Categories of Travel speed with their corresponding values used in the Pedestrian Evacuation Analyst Tool. Values are taken from the Federal Highway Administration (2009) and MarathonGuide.com (2011) and modified by Jones et al., 2014.

Travel-speed categories	Travel speed value (m/s)
Slow walk	1.1
Fast walk	1.52
Slow run	1.79
Fast run	3.85

Evacuation time maps are produced by using PEAT for selected five coastal areas: Central Bodrum, Gümbet Bay, Bitez Bay, Yahşi Bay, and Akyarlar-Karaincir-Aspat Bays, and given in Figures 4.25 to 4.29, respectively. Those maps are generated for the areas being highly populated and touristic and have the highest inundation distances resulting from the two critical tsunami scenarios (i) and (ii).

According to the resultant evacuation time maps, the highest travel times for pedestrian to reach the safe zone is calculated by PEAT as 8, 3, 4, 6 and 5 minutes for Central Bodrum, Gümbet, Bitez, Yahşi and Akyarlar-Karaincir-Aspat Bays respectively. In Central Bodrum, the longest value of 8 minutes is resulted by the calculation of the evacuation from the tip of the breakwaters of Bodrum Marina. However, in the case of the absence of breakwaters, the maximum travel time becomes 4 minutes from Aganlar Shipyard & Marina. The tsunami waves propagate mostly through valleys located at Gümbet Beach, so the longest travel time is 3 minutes around those regions in Gümbet Bay. Similarly, in Bitez Bay, the longest pedestrian evacuation times are calculated as 5 minutes around the valley entrance. In Yahşi Bay, the longest travel time is 6 minutes for Camel Beach and Yahşi Marina. The longest travel time value is 5 minutes for Aspat Beach and Karaincir Municipal Beach located Akyarlar-Karaincir-Aspat Bays region.

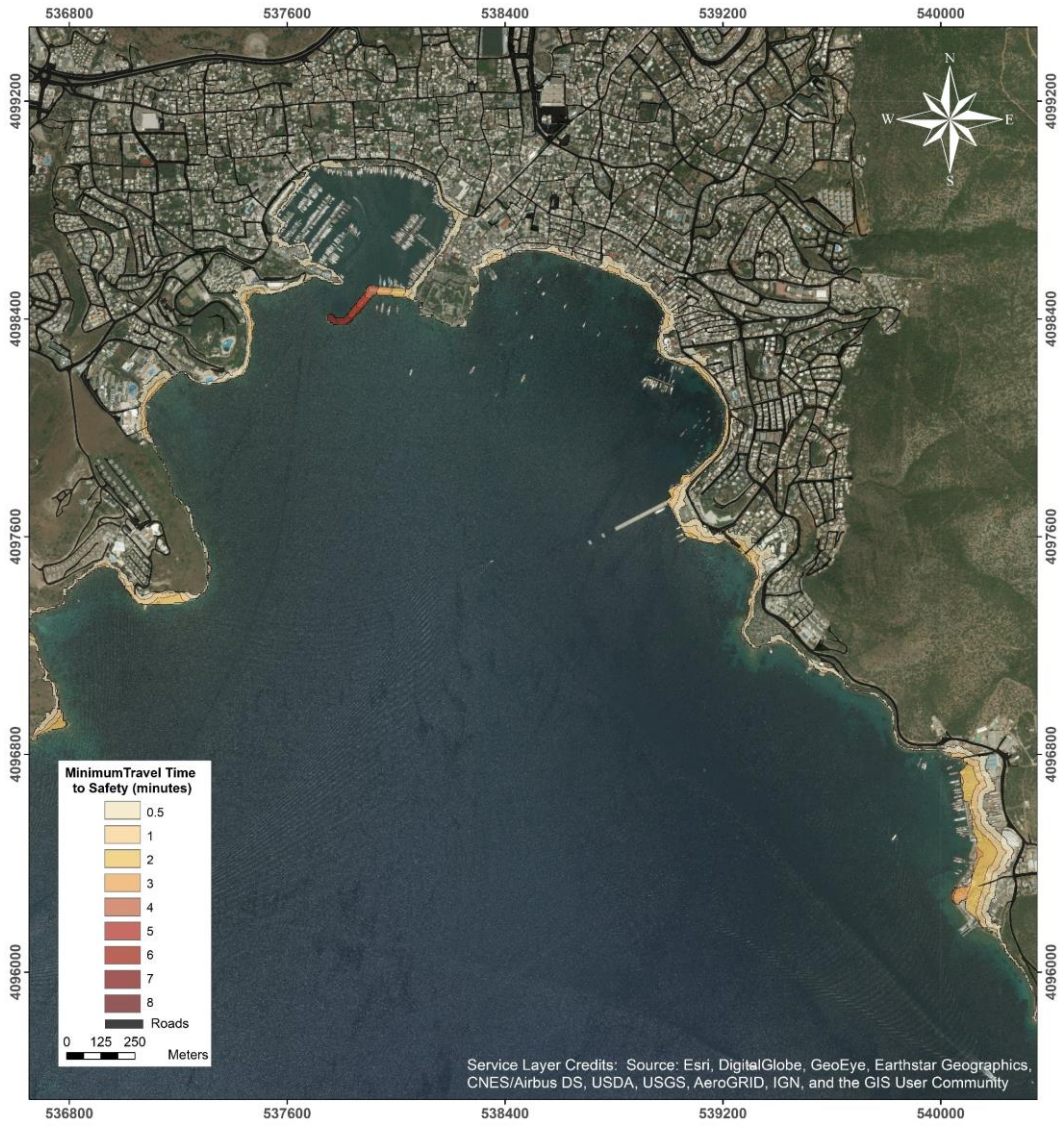

Figure 4.25 Tsunami Evacuation Walk Time Map for the areas around Central Bodrum resulted from Combined Gökova Seismic and Gökova-North-Datça Landslide Scenario(ii)

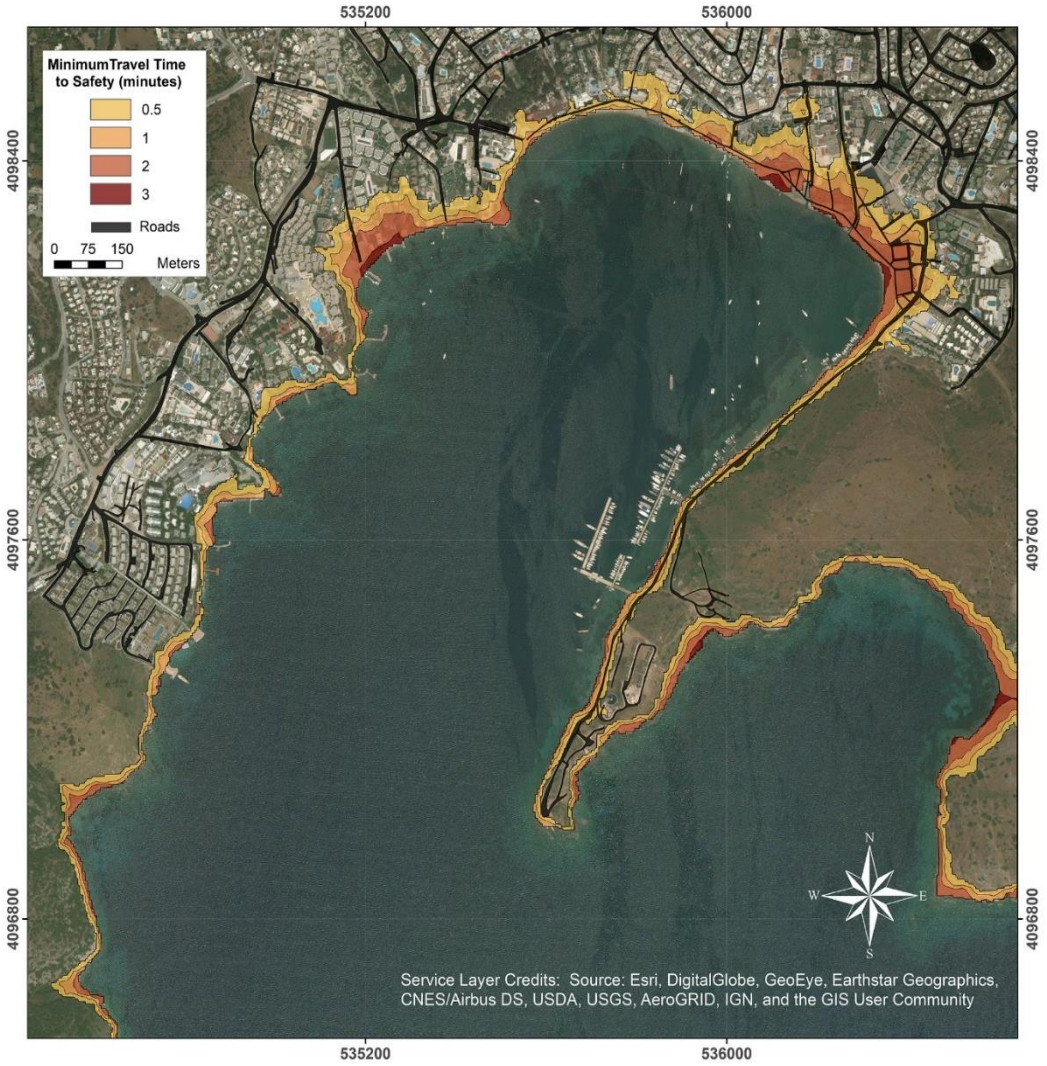

Figure 4.26 Tsunami Evacuation Walk Time Map for the areas around Gümbet Bay resulted from Combined Gökova Seismic and Gökova-North-Datça Landslide Scenario(ii)

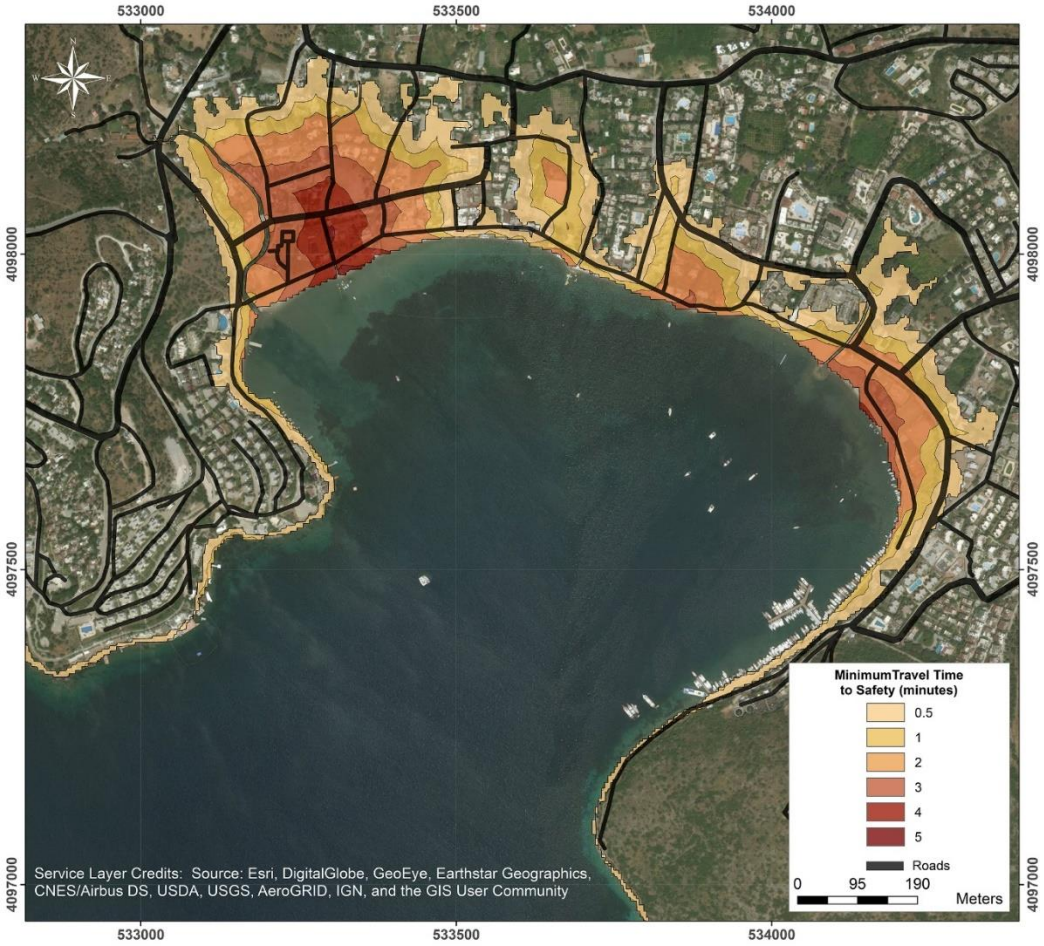

Figure 4.27 Tsunami Evacuation Walk Time Map for the areas around Bitez Bay resulted from two merged scenarios, which are 1956-Amorgos Seismic Scenario(i) and Combined Gökova Seismic and Gökova-North-Datça Landslide Scenario(ii)

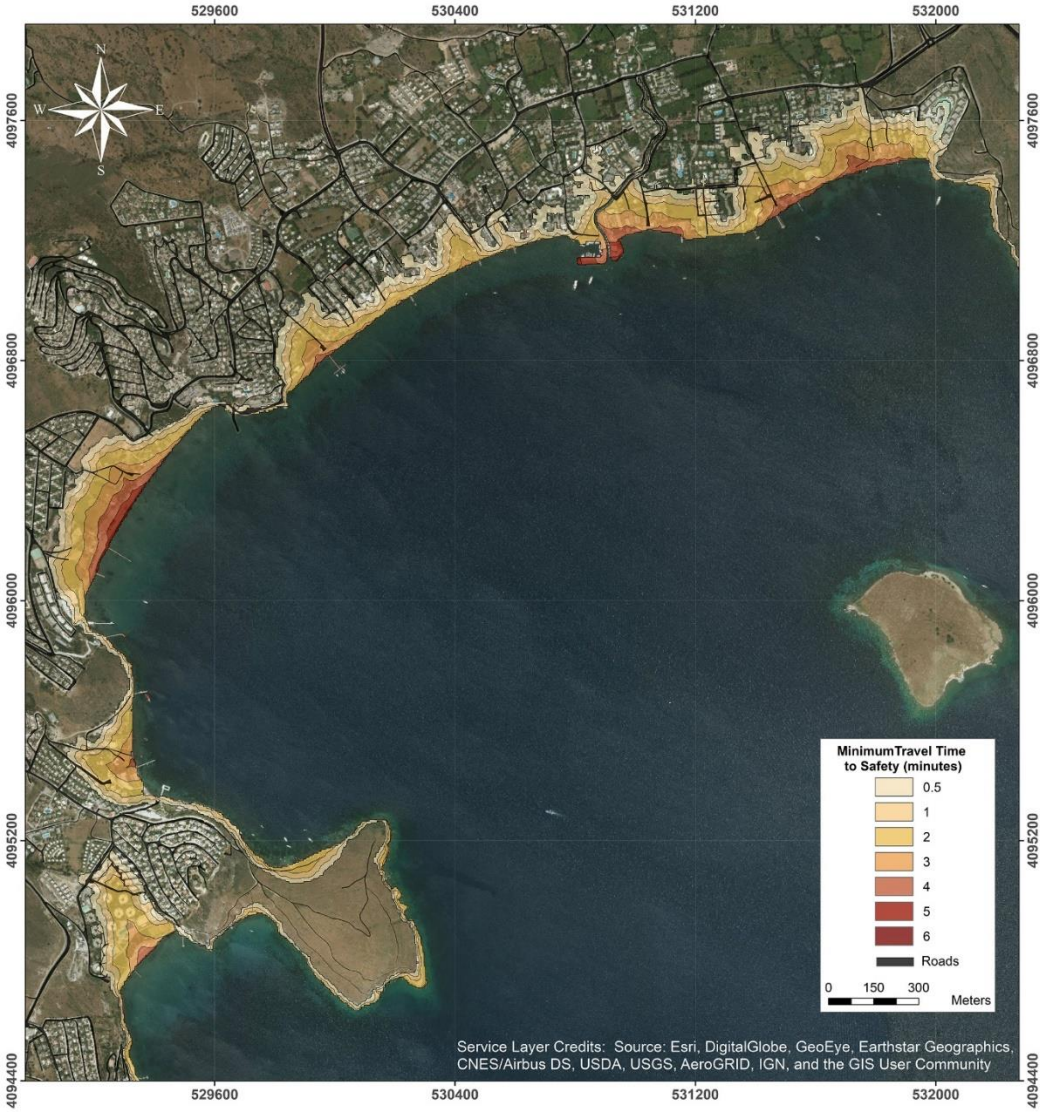

Figure 4.28 Tsunami Evacuation Walk Time Map for the areas around Yahşi Bay resulted from Combined Gökova Seismic and Gökova-North-Datça Landslide Scenario(ii)

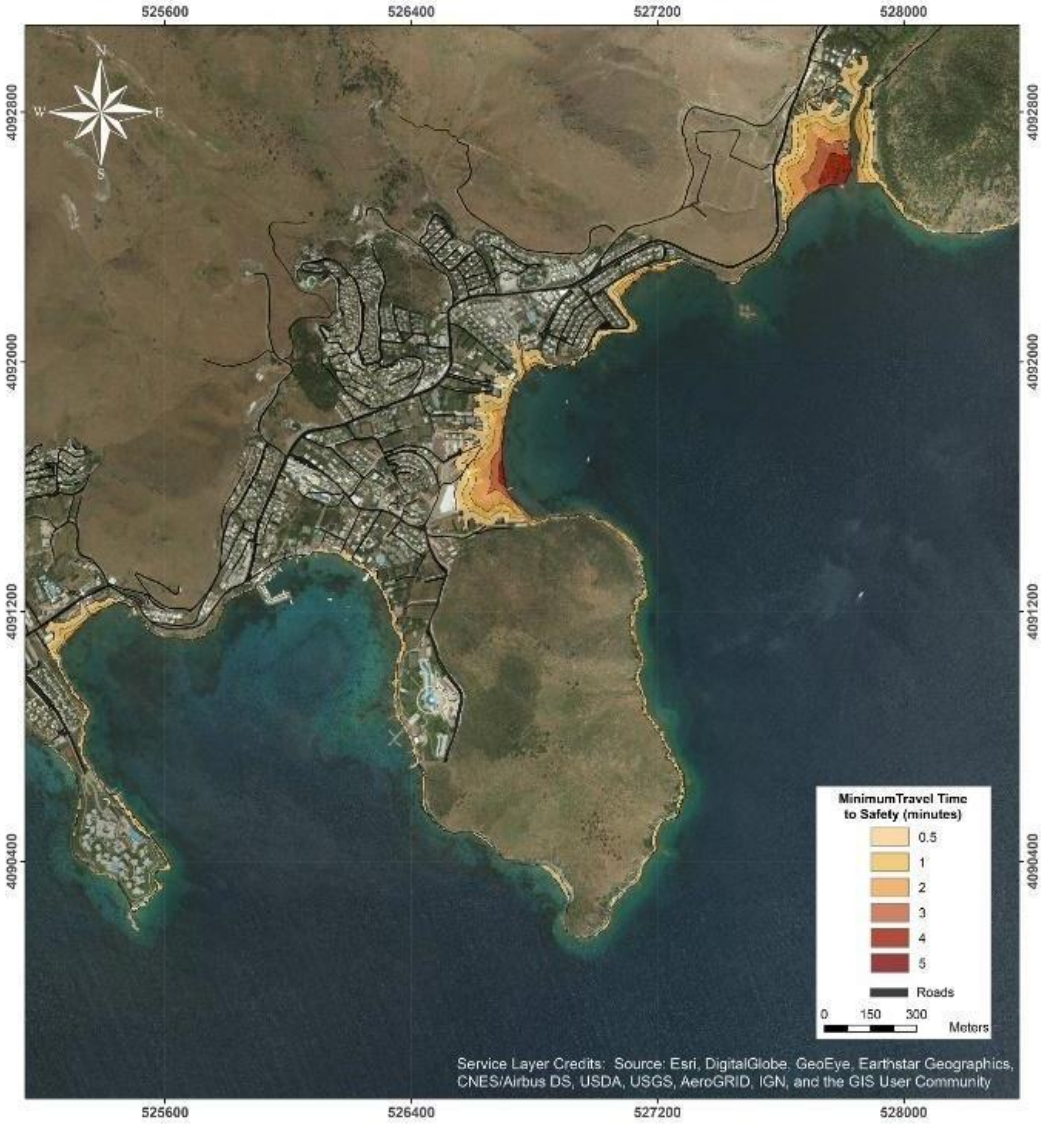

Figure 4.29 Tsunami Evacuation Walk Time Map for the areas around Akyarlar-Karaincir-Aspat Bays resulted from Combined Gökova Seismic and Gökova-North-Datça Landslide Scenario(ii)

4.5 Validation of Tsunami Evacuation Walk Time Maps

The accuracy of the resultant maps is crucial for proper and fast evacuation. Therefore, evacuation time maps should be verified. The maximum evacuation time locations to reach the safe zone from the shortest available path are selected as validation routes in the places where wide and fastest route may be selected easily. Three different selected sites are selected for validation among the five study areas: Gümbet Bay, Bitez Bay, and Yahşi Bay. For this validation, four different routes are selected, located in Gümbet Bay (Figure 4.30), Bitez Bay (Figure 4.31 and Figure 4.32), and Yahşi Bay (Figure 4.33). The validation is performed by a walk at which the time and distance are recorded. It is aimed that the speed constant and not exceeding 1.1m/s (pedestrian speed used in PEAT) during walks. The time in the resultant evacuation time map at the locations where the validation route is starting is compared with the time passed to reach the safe zone during the walk.

According to the measurements taken during the walk and shown in Table 5.1, the measured time to reach the safe zone from selected validation routes is lower than the calculated evacuation time found by PEAT. For those three validation routes, evacuation is possible with a speed about 1 m/s within the time proposed evacuation time by PEAT. However, in the case of Bitez-2 validation route measured time exceeds the calculated evacuation time due to overwalking about 40 meters shown in Figure 4.32. The validation route is right next to the valley at which the inundation distance continues 40 meters longer. This situation had led us to be mistaken during the walk. Such misconceptions may happen to people during the actual evacuation depending mostly on the resolution of the data.

Table 4.3 Measurements during the walk on validation routes

Validation Route	Evacuation Time from PEAT Results(min)	Measured Distance (m)	Measured Time (min)	Average speed (m/s)
Gümbet	3	124	2.32	0,82
Bitez-1	4	171	2.52	0,99
Bitez-2	5	356	5.35	1,06
Yahşi	6	361	5.35	1,08

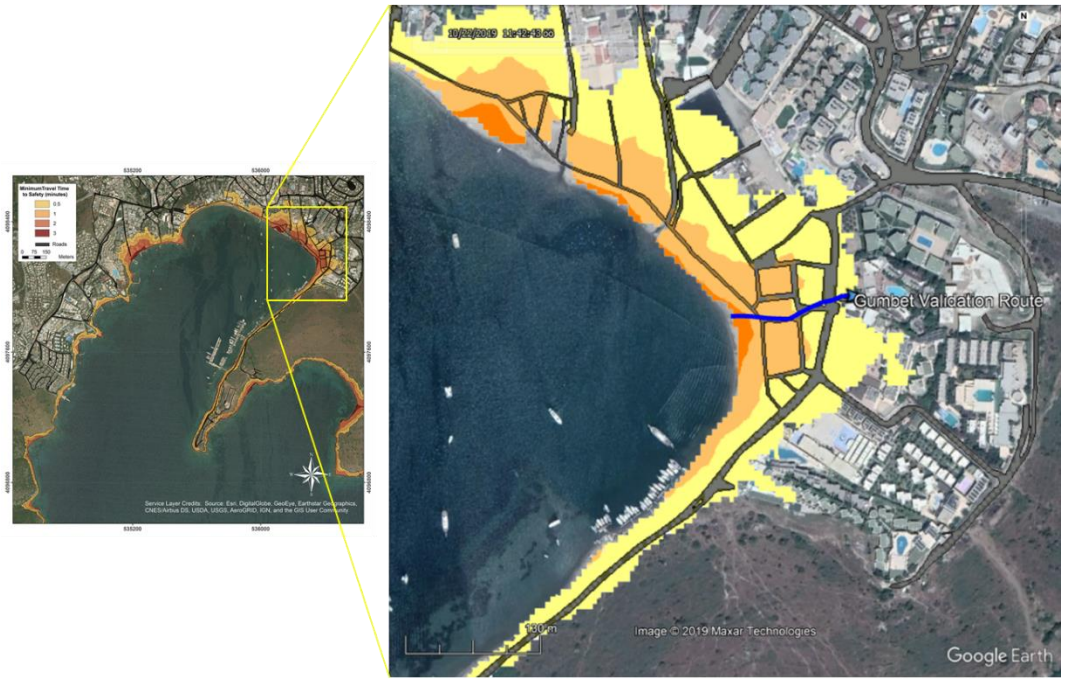

Figure 4.30 Validation Route in Gümbet Bay shown as blue line

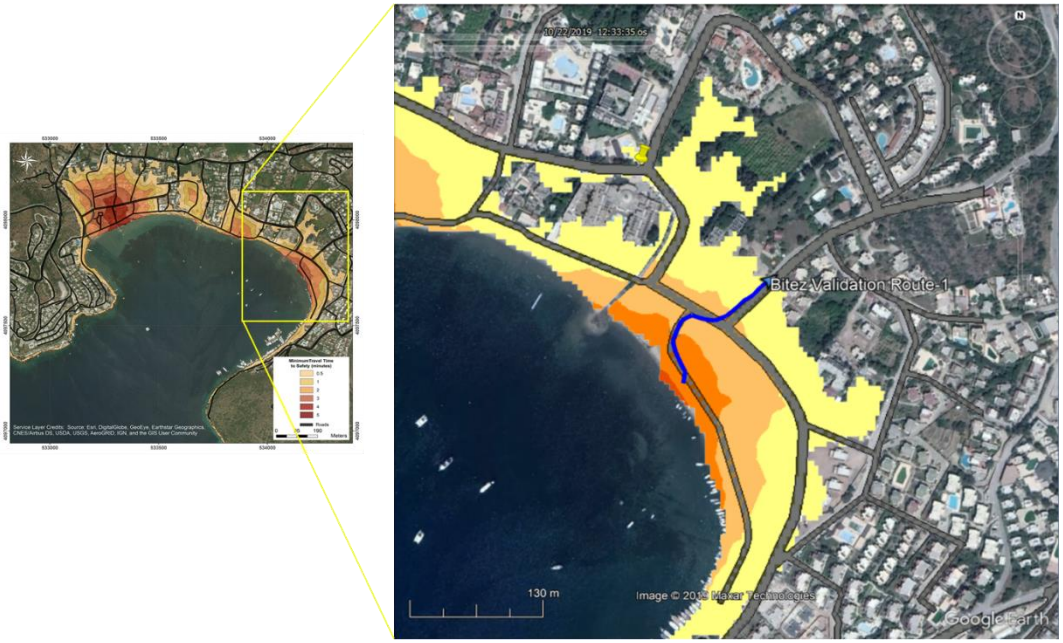

Figure 4.32 Validation Route of Bitez-1 shown as blue line

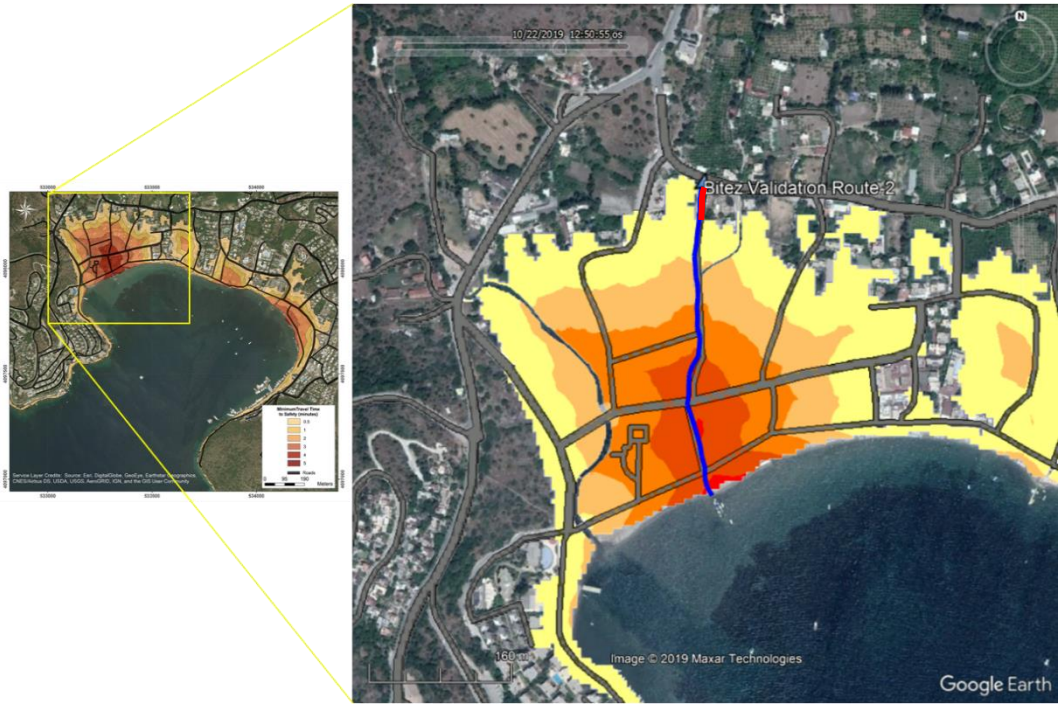

Figure 4.31 Validation Route Bitez-2 shown as blue line, overwalking shown as red line

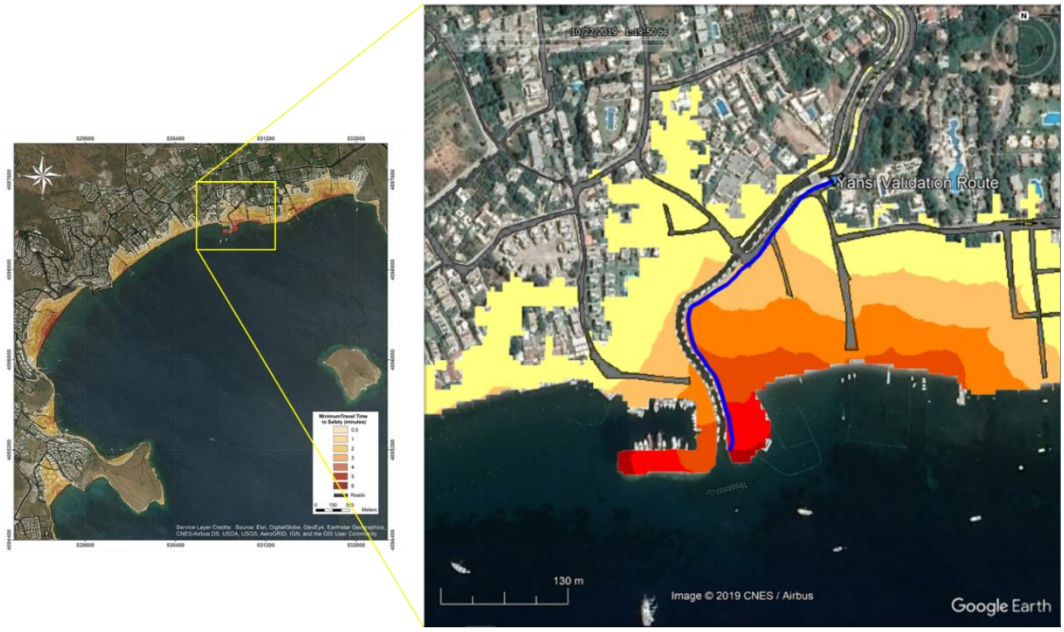

Figure 4.33 Validation Route in Yahşi Bay shown as blue line

CHAPTER 5

DISCUSSIONS

In this study, tsunami evacuation walk time maps are prepared by PEAT for southern coastal regions of Bodrum Peninsula against the selected two worst-case critical tsunami scenarios: (i) and (ii). Here, the least-cost distance model (LCD) is implemented instead of other methods, such as agent-based models (ABM), to understand the spatial distributions of evacuation time within hazard zone. LCD models ignore individual behavior and the interaction between individuals during an evacuation. In contrast, ABMs assess hundreds of individuals' decisions and their interactions based on a set of rules (Wang et al., 2017). During the evacuation, individual decision-making behaviors are a challenging phenomenon that depends on the different levels of awareness of all individuals, such as near experiences and ancestral knowledge of that region (Tufekci et al., 2020). It is assumed in LCD models that all individuals in a community have the same and constant speed of evacuation (no fatigue in time), which does not reflect the real situation and may lead to underestimating the required evacuation time from tsunami hazard (Wood and Schmidtlein, 2012).

PEAT is one of the LCD models that require lots of complex data representing landscape properties that affect pedestrian evacuation pace such as slope, water bodies, any type of barriers and roads etc., within the hazard zone (Wood and Schmidtlein, 2013). In this thesis, some of the available data, either taken from different open-source data such as Google Earth Images and Open Street Maps and/or provided by Bodrum Municipality. The gathered data should be up to date as Bodrum is one of Turkey's important touristic places where the shoreline is constantly changing and developing due to the construction of new coastal facilities such as marinas, renewed buildings, constructions of new buildings like hotels, and roads. Since those changes in the shoreline would directly be related to tsunami

hazards and affect the evacuation, it is crucial to modify the available dataset. Therefore, the data should be updated regularly in order to avoid misleading the pedestrian during evacuation.

Corine land cover (CLC) (EAE, 1995) is not used as a land cover layer in this study since the selected study areas are very small compared to CLC's spatial resolution. Therefore, the land-cover/land-use data are preferred to be produced manually from submeter resolution Google Earth Images. The produced land cover data may change depending on the person who created it and the purpose or priority of the study. Hence it is totally human-dependent. In this stage, some sensitivity analysis could have been done to reduce the human dependency, however, for this thesis both the study areas are too small and the classes are so distinct that it is not implemented. Also, created land-cover data are classified, and SCVs are given to them, according to Wood and Schmidtlein (2012). Pedestrian evacuation maps are sensitive to the assumptions made in changes of land-cover and slope SCVs (Schmidtlein and Wood, 2015). Therefore, any changes in land-cover through time will result in different evacuation time maps. In order to keep the resultant evacuation time map up-to-date the landcover data which might have changed through time should be automatically updated with newer images.

The earthquake impact on buildings, roads, or any infrastructure is ignored, which may slow the evacuation. Moreover, all buildings in Bodrum region are mostly hotels and summer houses with three floors or less, reinforced concrete buildings, assumed to, stay undamaged after the earthquake and during the tsunami. However, in the case of a building collapse to the road after a strong earthquake, important roads for evacuation may be blocked, which creates panic and congestion during an evacuation, leading to the prolonged evacuation. Additionally, roads are assumed as the safest places to evacuate in PEAT; however, a large and strong earthquake may destroy the road network due to liquefaction. In the available road dataset, information of the human capacity does not exist, which is vital knowledge to prevent crowding and congestion situations during the evacuation. Furthermore, roads in Bodrum region mostly consist of narrow streets that are hosted by fairs,

markets, and cafes. This concept is also essential for emergency managers and local decision-makers to offer the shortest evacuation route. Special to Bodrum region, some roads, perpendicular to the sea, intersect with stream valleys, which are the main routes of tsunami waves to propagate through the land. Hence, the road may be flooded by the tsunami waves, which makes evacuation difficult.

The building dataset has already been used as high resolution topographical source for numerical modelling to increase the accuracy and precision of the DEM. This create a topographical barrier to the waves hence conveys the calculated waves to be flowed through only openings. Besides the presence of the building, no information can be produced considering the availability of entrance to that building, hence in this thesis, vertical evacuation is ignored. Furthermore, horizontal evacuation is assumed to be on foot since the use of vehicles may cause congestions in evacuation routes.

Over the past five decades, Bodrum has developed from a small fisher town to Turkey's largest holiday town and become a significant economic activity center around tourism. Although Bodrum population in 2012 is estimated as 152.440, it raises to 2 million people with visitors and tourists in the summer season (Erdogan, 2016). The population's spatial distribution increases significantly for outstanding touristic places like Bodrum due to tourists' migration in the summer seasons. The spatial distribution of the population is also time-dependent because of the variability of human activities and mobility in a daily cycle (Freire et al., 2011). Since tsunamis are time-specific events, spatially detailed demographic datasets that include the population dynamics both in the summer and winter seasons are needed for the touristic regions to create more accurate evacuation planning. However, in this thesis, the spatial distribution of population, based on different evacuation conditions in both day/night and summer/winter, is ignored due to the lack of available data.

Depending on the tsunamigenic source's location, the arrival of a tsunami wave to the land differs in a real case, but it is assumed that all locations are inundated at the same time to get the critical worst-case scenario. Therefore, for some locations where

the tsunami waves come later, there is more time for people to initiate the evacuation. In addition to different arrival times of tsunami through the study area, the reaction time of the tsunami warning system, including the institutional notification and the decision time to notify the people, is also neglected since there is no effectively integrated tsunami warning system such as tsunami sirens in the study area. Even there is no tsunami warning system; earthquakes may act as natural warnings for incoming tsunami waves for people living in coastal regions as they may start evacuation after recognizing the tremor. However, as it is mentioned above, the difference in reaction times of people against tsunami hazard is not included in LCD models.

The routes for validation are selected among the wide and perpendicular routes to the sea. For the regions having several routes side by side with the same properties, it is difficult to suggest the fastest evacuation route for the emergency managers and local decision-makers. Here, factors such as the human capacity of the road, the possibility of buildings collapsing to the road during an earthquake, and the engineering characteristics of the road, gain importance during the decision of the fastest and easiest route for evacuation. During the preparation of emergency response plans, they should also put the tsunami signs along the selected and critical evacuation routes in order to lead evacuees. The people should be aware of these signs and maps before a tsunami event occurs to learn the routes ahead of time for home, work and school.

The tsunami inundated on land assumed to be consist of only water, not the debris material. However, the damage is mostly due to the debris materials such as boats, cars, parts of trees etc., that are carried by the tsunami waves. As observed in the recent Izmir-Samos earthquake and tsunami event, debris materials mostly damage the coastal regions with no engineering structures. Also, simulations are performed according to the present water level, meaning neither at the high tide nor a storm event present.

CHAPTER 6

CONCLUSION

Tsunami evacuation walk time maps are generated for the five selected areas located in Bodrum Peninsula's southern coastline; Central Bodrum, Gümbet Bay, Bitez, Bay, Yahşi Bay and Akyarlar-Karaincir-Aspat Bays. Tsunami generic sources for Bodrum Peninsula were selected and modified to constitute the possible largest earthquakes in the Gulf of Gökova and Eastern Mediterranean. As a result of numerical simulation via NAMI DANCE, two critical worst-case scenarios are selected. Inundation maps of the five selected areas are generated and used for the tsunami evacuation time map.

The data used during the generation of evacuation walk time maps were gathered from different sources. Numerical simulation results were used as hazard zone data. The remaining required spatial datasets were acquired from Bodrum Municipality, Google Earth Images, and Open Street Map. Pedestrian Evacuation Analyst Tool (PEAT), one of the Least-Cost Distance (LCD) models, was used to generate evacuation time maps. It calculates the evacuation time surfaces by considering the speed conservation values for the different spatial distribution of terrain with a defined travel pace. In this study, a slow walk (1.1 m/s) walking speed was selected to generate walk time maps.

The resultant map represents the time needed a person to get out from hazard zone in the fastest way. According to the resultant tsunami evacuation maps, longest evacuation times for pedestrian to get out from hazard zone is 8, 6, 5, 4, and 3 minutes for Central Bodrum, Yahşi, Akyarlar-Karaincir-Aspat Bays, Bitez, and Gümbet bays respectively. The resulting evacuation time maps were validated on-site in selected four different routes by performing walks.

REFERENCES

Acar, S. (2015). Tsunami Hazard Analysis for Güllük Bay, Master dissertation MSc, Middle East Technical University, Turkey

Aktug, B., Kaypak, B., & Çelik, R. N. (2010). Source parameters of 03 February 2002 Çay Earthquake, Mw6.6 and aftershocks from GPS Data, Southwestern Turkey, Journal of Seismology, 14, 445–456.

Aktug, B., Nocquet, J. M., Cingoz, A., Parsons, B., Erkan, Y., England, P. C., Tekgul, A. (2009). Deformation of western Turkey from a combination of permanent and campaign GPS data: Limits to block-like behavior. Journal of Geophysical Research, 114, B10404.

Altinok, Y. (2009). Historical Tsunamis in Eastern Mediterranean. Internal Report of Work Package 1 of TRANSFER Project.

Altinok, Y., Alpar, B., Özer, N., & Aykurt, H. (2011). Revision of the tsunami catalogue affecting Turkish coasts and surrounding regions. Natural Hazards and Earth System Sciences, 11(2), 273-291.

Ambraseys, N. N. (1962). Data for the investigation of the seismic sea-waves in the Eastern Mediterranean. Bulletin of the Seismological Society of America, 52(4), 895-913.

Ambraseys, N., & Synolakis, C. (2010). Tsunami catalogues for the Eastern Mediterranean, revisited. Journal of Earthquake Engineering, 14(3), 309-330.

Arikawa, T,and Oie, T (2015). Study of Evacuation Behavior Characteristic Using Evacuating Simulator Coupled with Numerical Wave Flume. Journal of Japan Society of Civil Engineers, B2 (Coastal Engineering), Vol. 71, No. 2, 2015 pp.I_319- I_324.

Averill, J., Mileti, D., Peacock, R., Kuligowski, E., Groner, N., Proulx, G., Reneke, P., Nelson, H. (2005). Occupant behavior, egress, and emergency communications federal building and fire safety investigation of the world trade center disaster. National Institute of Standards and Technology National Construction Safety Team Act Report 1–7.

Aytore, B., Yalciner, A. C., Zaytsev, A., Cankaya, Z. C., & Suzen, M. L. (2016). Assessment of tsunami resilience of Haydarpaşa Port in the Sea of Marmara by high-resolution numerical modeling. Earth, Planets and Space, 68(1), 139.

Bakillah, M., Klüpfel, H., Lämmel, G., & Walenciak, G. (2013). Multi-agent transport simulation for Regional Evacuation Processes. Pedestrian and Evacuation Dynamics 2012, 1197–1206. https://doi.org/10.1007/978-3-319-02447-9_98

Beisel, S., Chubarov, L., Didenkulova, I., Kit, E., Levin, A., Pelinovsky, E., & Sladkevich, M. (2009). The 1956 Greek tsunami recorded at Yafo, Israel, and its numerical modeling. Journal of Geophysical Research: Oceans, 114(C9).

Cankaya, Z. C., Suzen, M. L., Yalciner, A. C., Kolat, C., Zaytsev, A., & Aytore, B. (2016). A new GIS-based tsunami risk evaluation: MeTHuVA (METU tsunami human vulnerability assessment) at Yenikapı, Istanbul. Earth, Planets and Space, 68(1), 133.

Cheff, I., Nistor, I., Palermo, D. (2018). Pedestrian evacuation modelling of a Canadian West Coast community from a near-field tsunami event. Nat. Hazards. https://doi.org/ 10.1007/s11069-018-3487-5

Chu, J. C., Chen, A. Y., & Lin, Yeh, F. (2017). Variable guidance for pedestrian evacuation considering congestion, hazard, and compliance behavior. Transportation Research Part C: Emerging Technologies, 85, 664–683. https://doi.org/10.1016/j.trc.2017.10.009

CIESM, (2011). Marine geohazards in the Mediterranean. N° 42 in CIESM. Workshop Monographs [F. BRIAND Ed.], 192 pages, Monaco.

Cita, M.B., Rimoldi, B. (1997). Geological and Geophysical Evidence for a Holocene Tsunami Deposit in the Eastern Mediterranean Deep-Sea Record. J. Geodynamics, Vol.24. No:1-7 pp. 293-304.

Cova, T. (1999). GIS in Emergency Management. Geogr. Inf. Syst., 2, 845–858.

Cova, T. J., and Church, R. L. (1997). Modelling community evacuation vulnerability using GIS. International Journal of Geographical Information Science. 11, 763-784.

Dawson, A.G., Lockett, P., Shi S. (2003). Tsunami Hazards in Europe. Environment International, 30 (2004) 577-585.

De Silva, F., Pidd, M., and Eglese, R., (1993). Spatial decision support systems for emergency planning: an operational research/geographical information systems approach to evacuation planning. In Proceedings of the 1993 Simulation Multiconference on the International Emergency Management and Engineering Conference (San Diego: The Society for Computer Simulation), pp.130± 133.

Dewey, J.F., Şengör, A.M.C. (1979) Aegean and surrounding regions. Complex multiplate and continuum tectonics in a convergent zone. Geol. Soc. Am. Bull. 90, 84–92.

Dewi, R. S. (2012). A GIS-based approach of evacuation model for tsunami risk reduction. IDRiM Journal, 2(2), 108-139.

Dilmen, D. I., Kemec, S., Yalciner, A. C., Duzgun, S., & Zaytsev, A. (2015). Development of a tsunami inundation map in detecting tsunami risk in Gulf of Fethiye, Turkey. Pure and Applied Geophysics, 172(3-4), 921-929.

Dogan, G.G., Yalciner, A.C., Yuksel, Y., Ulutaş, E., Polat, O. & Kanoğlu, U. (2021). The 30 October 2020 Aegean Sea Tsunami: Post-Event Field Survey Along Turkish Coast. Pure Appl. Geophys. https://doi.org/10.1007/s00024-021-02693-3

Dogru, A., Gorgun, E., Ozener, H., & Aktug, B. (2014). Geodetic and seismological investigation of crustal deformation near Izmir (Western Anatolia). Journal of Asian Earth Sciences, 82, 21–31.

EEA, (1995). CORINE Land Cover Project, published by Commission of the European Communities

England, P., Howell, A., Jackson, J., & Synolakis, C. (2015). Palaeotsunamis and tsunami hazards in the Eastern Mediterranean. Philosophical Transactions of the Royal Society

Erdogan, G. (2016). Fractal Dimension of Urban Pattern: Bodrum, Turkey. 23rd International Seminar on Urban Form (ISUF)At: Nanjing, China.

ESRI, (2001). ArcGIS (TM) Spatial Analyst: Advanced GIS Spatial Analysis Using Raster and Vector Data., ESRI White Paper, Redlands,1–17.

ESRI, (2009a) Cost distance algorithm. Available viahttp://webhelp.esri.com/arcgisdesktop/9.3/index.cfm?TopicName=Cost_Distance_algorithm.

ESRI, (2009b) Path distance: adding more cost complexity.

Eyidoğan, H., Barka, A. (1996). The 1 October 1995 Dinar earthquake, SW Turkey, Terra Nova, 8, pp. 479-485.

Franzese, O., Sorenson, D. (2004). Fast deployable system for consequence management the emergency evacuation component. Proceedings of the ITS Safety and Security conference, Orlando, FL, 13 p.

Fraser, S., Wood, N., Johnston, D., Leonard, G., Greening, P., Rossetto, T. (2014). Variable population exposure and distributed travel speeds in least-cost tsunami evacuation modelling. Nat. Hazards Earth Syst. Sci. 14 2975–2991

Freire, S., Aubrecht, C., Wegscheider, S. (2011). Spatio-temporal population distribution and evacuation modeling for improving tsunami risk assessment in the Lisbon metropolitan area, Proceedings of 2011 Conference on GeoInformation for Disaster Management, Antalya, Turkey.

Galanopoulos, A. G. (1957). The seismic sea-wave of 9 July 1956. Praktika Academy Athens, 32, 90-101. (in Greek with Engl. abstr.).

Galanopoulos, A. G. (1960). Tsunamis observed on the coasts of Greece from antiquity to present time. Annals of Geophysics, 13(3-4), 369-386.

Görür, N., Şengör, A. M. C., Sakınç, M., Tüysüz, O., Akkük, R., Yiğitbaş, E. (1995). Rift formation in the Gökova region, southwest Anatolia: implications for the opening of the Aegean Sea. Geological Magazine, 132,637–650.

Graehl N. and Dengler L. (2008). Using a GIS to Model Tsunami Evacuation times for the community of Fairhaven CA.

Guidoboni, E., Comastri, A., and Traina, G. (1994). Catalogue of Ancient Earthquakes in the Mediterranean Area up to the 10th Century. Instituto Nazionale di Geofisica, Rome.

Gürer, Ö. F., Sangu, E., Özburan, M., Gürbüz, A., Sarıca-Filoreau, N. (2013). Complex basin evolution in the Gökova Gulf region: implications on the Late Cenozoic tectonics of SW Turkey. International Journal of Earth Sciences. http://dx.doi.org/10.1007/s00531-013-0909-1

Hamacher, H., Tjandra S. (2002). Mathematical modeling of evacuation problems: A state of art, Som D S., Pedestrian and Evacuation Dynamies, Berlin:Springer, p. 227.

Howell, A., Jackson, J., England, P., Higham, T., & Synolakis, C. (2015). Late Holocene uplift of Rhodes, Greece: evidence for a large tsunamigenic earthquake and the implications for the tectonics of the eastern Hellenic Trench System. Geophysical Journal International, 203(1), 459-474.

Iscan, Y., Tur, H., & Gokasan, E. (2013). Morphologic and seismic features of the Gulf of Gökova, SW Anatolia: Evidence of strike slip faulting with compression in the Aegean Extensional Regime. Geo-Marine Letters, 33, 31–48.

Jackson, J., & McKenzie, D. (1984). Active tectonics of the Alpine-Himalayan belt between Western Turkey and Pakistan. Geophysics Journal of Royal Astronomy Society, 77, 185–264.

Jones, J.M., NG, P., Wood, N.J. (2014). The pedestrian evacuation analyst—Geographic information systems software for modeling hazard evacuation potential: U.S. Geological Survey Techniques and Methods, book 11, chap. C9, 25 p. https://dx.doi.org/10.3133/tm11C9

Jonkmann, S., Vrijling, J., Vrouwenvelder, A. (2008). Methods for the estimation of loss of life due to floods: a literature review and a proposal for a new method. Nat Hazards 46:353–389.

Kalafat, D., Horasan G. (2012). A seismological view to Gökova region at southwestern Turkey. International Journal of Physical Sciences, 7(30), 5143-5153.

Karasözen, E., Nissen, E., Büyükakpınar, Cambaz, M.D., Kahraman, M., Ertan, E.K., Abgarmi, B., Bergman, E., Ghods, A., & Özacar, A.A. (2018). The 2017 July 20 Mw 6.6 Bodrum-Kos earthquake illuminates active faulting in the Gulf of Gökova, SW Turkey, Geophysical Journal International, 214, 185–199.

Kian, R., Velioglu, D., Yalciner, A. C., & Zaytsev, A. (2016). Effects of Harbor Shape on the Induced Sedimentation; L-Type Basin. Journal of Marine Science and Engineering, 4(3), 55. http://www.mdpi.com/2077-1312/4/3/55/htm

Kuran, U., Yalciner, A. C. (1993). Crack propagations, earthquakes and tsunamis in the Vicinity of Anatolia, Tsunamis in the World, ed: Stefano Tinti, Advances in Natural and Technological Hazards Research, Springer.

Kurt, H., Demirbag, E., & Kuscu, I. (1999). Investigation of submarine active tectonism in the Gulf of Gökova, southwest Anatolia and SE Aegean Sea, by multi-channel seismic reflection data. Tectonophysics, 305, 477–496.

Laghi, M., and Cavalletti A. (2004). Coastal Risk Analysis of Tsunamis and Environmental Remediation. Evacuation Routes Tools ArcGIS toolbox. Retrieved 1 February 2008, from the following web site: www.adpc.net/v2007/IKM/ONLINE%20DOCUMENTS/Default-DOCUMENTS.asp

Lammel, G., (2011). Escaping the Tsunami: Evacuation Strategies for Large Urban Areas Concepts and Implementation of a Multi-agent Based Approach. Ph.D. Thesis, Universitatsbibliothek.

Lindell, M.K. and Perry, R.W. (2007). Planning and preparedness. In: Tierney KJ and Waugh WF Jr (eds) Emergency Management: Principles and Practice for Local Government, 2nd edn. Washington, DC: International City/County Management Association, 113–141.

Lindell, M.K., Prater, C.S. and Perry, R.W. (2006) Fundamentals of Emergency Management. Emmitsburg, MD: Federal Emergency Management Agency Emergency Management Institute. Available at: hrrc.arch.tamu.edu/publications/books

Liu, P.L.-F., Yeh, H., and Synolakis, C. E. (2008). Advanced Numerical Models for Simulating Tsunami Waves and Runup. Advances in Coastal and Ocean Engineering, 10.

Lorito, S., M. M. Tiberti, R. Basili, A. Piatanesi and G. Valensise. (2008). Earthquake-Generated Tsunamis in the Mediterranean Sea: Scenarios of Potential Threats to Southern Italy, Journal of Geophysical Research, Vol. 113, B01301.

Løvholt, F., Setiadi, N. J., Birkmann, J., Harbitz, C. B., Bach, C., Fernando, N., Kaiser, G., & Nadim, F. (2014). Tsunami risk reduction are we better prepared today than in 2004? International Journal of Disaster Risk Reduction, 10, 127–142. https://doi.org/10.1016/j.ijdrr.2014.07.008

Lynett, P. J., Gately K., Wilson R., Montoya L., Arcas D., Aytore B., Bai Y., Bricker J. D., Castro M. J., Cheung, K. F. David G. C., Dogan G. G., Escalante C., González-Vida J. M., Grilli S. T., Heitmann T. W., Horrillo J., Kânoglu U., Kian R., Kirby J. T., Li W., Macías J., Nicolsky D. J., Ortega S., Pampell-Manis A., Park Y. S., Roeber V., Sharghivand N., Shelby M., Shi F., Tehranirad B., Tolkova E., Thio H. K., Velioglu D., Yalciner A. C., Yamazaki Y., Zaytsev, A., Zhang Y. J. (2017). Inter-model analysis of tsunami-induced coastal currents. Ocean Modelling, 114, 14–32. http://dx.doi.org/10.1016/j.ocemod.2017.04.003

Marrero, J., Garcia, A., Llinares, A., Rodrıguez-Losada, J., Ortiz, R. (2010). The variable scale evacuation model (VSEM) a new tool for simulating massive evacuation processes during volcanic crises. Nat Hazards Earth Syst Sci 10:747–760

Mas, E., Suppasri, A., Imamura, F., & Koshimura, S. (2012). Agent-based Simulation of the 2011 Great East Japan Earthquake/Tsunami Evacuation: An Integrated Model of Tsunami Inundation and Evacuation. Journal of Natural Disaster Science, 34(1), 41-57. doi:10.2328/jnds.34.41

McClusky, S., Balassanian, S., Barka, A., Demir, C., Ergintav, S., Georgiev, I., Gurkan, O., Veis, G. (2000). Global Positioning System constraints on plate kinematics and dynamics in the eastern Mediterranean and Caucasus. Journal of Geophysical Research-Solid Earth, 105, 5695–5719. doi:10.1029/1999jb900351.

McKenzie, D. P. (1972). Active tectonics of the Mediterranean region. Geophysical Journal of the Royal Astronomical Society, 30, 109–185.

Minoura, K., Imamura, Kuran, U., Nakamura, T., Papadopoulos, G., Takahashi, T., Yalçıner, A. C., (2000), Discovery of Minoan Tsunami Deposits. Geology, v. 28, no. 1, pp.: 59-62.

Necmioğlu, Ö. (2014). Tsunami hazard in turkey and surroundings. Doctoral dissertation PhD. Thesis Boğaziçi University Kandilli Observatory and Earthquake Research Institute, Istanbul, Turkey.

Nomikou, P., Papanikolaou, D., Alexandri, M., Sakellariou, D. & Rousakis, G. (2013). Submarine volcanoes along the Aegean volcanic arc, Tectonophysics, 597, 123–146.

NTHMP, (2001) Designing for Tsunami - Seven Principles for Planning and Designing for Tsunami Hazards. National Tsunami Hazard Mitigation

Program. USA, NOAA, USGS, FEMA, NSF, Alaska, California, Hawaii, Oregon, and Washington

Ocakoğlu, N., Nomikou, P., Isçan, Y., Loreto, M.F., Lampridou, D. (2018). Evidence of extensional and strike-slip deformation in the offshore Gökova-Kos area affected by the July 2017 Mw6.6 Bodrum-Kos earthquake, eastern Aegean Sea. Geo-Marine Letters. https://doi.org/10.1007/s00367-017-0532-4

Okal, E.A., Synolakis, C.E., Uslu, B., Kalligeris, N., & Voukouvalas, E. (2009). The 1956 earthquake and tsunami in Amorgos, Greece. Geophysical Journal International, 178(3), 1533-1554.

Ozener, H., Dogru, A., & Acar, M. (2013). Determination of the displacements along the Tuzla fault (Aegean region-Turkey): Preliminary results from GPS and precise leveling techniques. Journal of Geodynamics, 67, 13–20.

Papadopoulos, G. A., & Fokaefs, A. (2005). Strong tsunamis in the Mediterranean Sea: a revaluation. ISET Journal of Earthquake Technology, 42(4), 159-170.

Papadopoulos, G.A. (2016). Historical and Geological Evidence of Tsunamis in Europe and the Mediterranean, in Tsunamis in the European-Mediterranean Region by G.A. Papadopoulos, Hardcover ISBN: 9870124202245, Elsevier.

Papadopoulos, G.A., Minoura K., Imamura F., Kuran U., Yalciner A. C., Fokaefs A., Takahashi T. (2012). Geological evidence of tsunamis and earthquakes at the Eastern Hellenic Arc: correlation with historical seismicity in the eastern Mediterranean Sea, Research in Geophysics 2012 (2), 12, pp: 90-99.

Papadopoulos, G.A., Pavlides, S.B. (1992). The large 1956 earthquake in the South Aegean: Macroseismic field configuration, faulting and neotectonics of Amorgos Island, Earth and Planetary Science Letters, 113, 383-396, Elsevier.

Papazachos, B. C., Dimitriadis, S. T., Panagiotopoulos, D. G., Papazachos, C. B., & Papadimitriou, E. E. (2005). Deep structure and active tectonics of the southern Aegean volcanic arc.Developments in Volcanology,7,47–64. https://doi.org/10.1016/S1871-644X(05)80032-4.

Papazachos, B., C. and Papazachou, C. (1997). The Earthquakes of Greece. Editions ZITI, Thessaloniki.

Papazachos, B.C. and Panagiotopoulos, D.G. (1993). Normal faults associated with volcanic activity and deep rupture zones in the southern Aegean volcanic arc. Tectonophysics, 220, 301-308

Pendyala, R.M., Kitamura, R., Kikuchi, A., Yomamoto, T., Fujii, S. (2005). Florida activity mobility simulator Transp. Res. Rec., 1921, pp. 123-130.

Post, J., Wegscheider, S., Muck, M., Zosseder, K., Kiefl, R., Steinmetz, T., Strunz, G. (2009). Assessment of human immediate response capability related to

tsunami threats in Indonesia at a subnational scale. Nat Hazards Earth Syst Sci, 9,1075–1086.

Reilinger, R., McClusky, S., Vernant, P., Lawrence, S., Ergintav, S., Cakmak, R., Karam, G. (2006). GPS constraints on continental deformation in the Africa-Arabia-Eurasia continental collision zone and implications for the dynamics of plate interactions. Journal of Geophysical Research, 111, B05411.

Rontogianni, S., Konstantinou, K. I., Evangelidis, C., & Melis, N. S. (2011). Investigating potential seismic hazard in the Gulf of Gökova (South-Eastern Aegean Sea) deduced from recent shallow earthquake activity. In AGU Fall Meeting Abstracts.

Şaroğlu, F., Emre, Ö., Kuşçu, İ., Yıldırım, N. (1995). Ekim 1995 Dinar Depremi (ön rapor). MTA Rapor No: 9791, 14 s., Ankara-Turkey (in Turkish).

Sakata, Y., Seki, K. and; Arikawa, T. (2019). Development of evacuation route selection method depending on tsunami level. Journal of Japan Society of Civil Engineers, Ser. B2 (Coastal Engineering), 74(2). https://doi.org/10.2208/kaigan.74.i_397

Scheer, S. J., Varela, V., & Eftychidis, G. (2012). A generic framework for tsunami evacuation planning. Physics and Chemistry of the Earth, Parts A/B/C, 49, 79-91.

Sengor, A. M. C. (1987). Cross-faults and differential stretching of hanging walls in regions of low-angle normal faulting: Examples from western Turkey. In: M. P. Coward, J. F. Dewey, & P. Hancock (Eds.), Continental extensional tectonics (pp. 575–589). London: Geological Society'de. Special Publication, 28.

Shahabi K, Wilson JP (2014) CASPER: intelligent capacity-aware evacuation routing. Comput Environ Urban Syst 46:12–24

Shaw, B., Ambraseys, N. N., England, P. C., Floyd, M. A., Gorman, G. J., Higham, T. F. G., & Piggott, M. D. (2008). Eastern Mediterranean tectonics and tsunami hazard inferred from the AD 365 earthquake. Nature Geoscience, 1(4), 268.

Soule, R.G., and Goldman, R.F. (1972). Terrain coefficients for energy cost prediction. Journal of Applied Physiology, v. 32, no. 5, p. 706–708.

Sözbilir, H., Uzel, B., Sümer, Ö., Eski, S., Softa, M., and Tepe, Ç. (2017). 21 Temmuz 2017 Gökova Körfezi Depremleri ve Bölgenin Depremselliği Raporu. (in Turkish), Dokuz Eylül University Earthquake Research and Application Center Active Fault Research Group, İzmir, Turkey.

Sozdinler, C.O., Yalciner, A.C., Zaytsev, A. (2015). Investigation of tsunami hydrodynamic parameters in inundation zones with different structural layouts. Pure Appl Geophys 172(3):931–952.

Synolakis, C. E. (1991). Tsunami Runup on Steep Slopes: How Good Linear Theory Really Is. Natural Hazards, 4, 221–234.

Synolakis, C. E., Imamura, F., Tinti, S., Tsuji, Y., Matsutomi, H., Cooc, B., and Usman M. (1995). The East Java tsunami of the July 4, 1994. EOS Transactions AGU, 76(26), 257,261-262.

Synolakis, C. E., Okal, E. A. and Bernard, E. N. (2004). Tsunami Science Before and After Boxing Day. Philosophical Transactions of the Royal Society, A364.

Tinti, S. and Maramai, A. (1996), Catalogue of Tsunamis Generated in Italy and in Côte d' Azur, France: A Step towards a Unified Catalogue of Tsunamis in Europe. Annali di Geofisica, Vol. 39, pp. 1253-1299.

Tinti, S., Armigliato, A., Pagnoni, G., and Zaniboni, F. (2005). Scenarios of Giant Tsunamis of Tectonic Origin in the Mediterranean, ISET Journal of Earthquake Technology, 42, 171– 188.

Tinti, S., Maramai, A. and Graziani, L. (2004). The New Catalogue of Italian Tsunamis. Natural Hazards, Vol. 33, No. 3, pp. 439-465.

Tiryakioğlu, B., Aktuğ, C. Ö., Yiğit, H., Yavaşoğlu, H., Sözbilir, H., Özkaymak, Ç., Poyraz, F., Taneli, E. Bulut, F., Doğru, A. & Özener H. (2018). Slip distribution and source parameters of the 20 July 2017 Bodrum-Kos earthquake (Mw6.6) from GPS observations, GeodinamicaActa, 30:1, 1-14. DOI: 10.1080/09853111.2017.1408264

Tiryakioglu, I., Floyd, M., Erdogan, S., Gulal, E., Ergintav, S., McClusky, S., & Reilinger, R. (2013). GPS constraints on active deformation in the Isparta Angle region of SW Turkey. Geophysical Journal International, 195, 1455–1463.

Tobler, W. (1993). Three presentations on geographical analysis and modeling non-isotropic geographic modeling. Speculations on the geometry of geography; and global spatial analysis. UCSB. National Center for Geographic Information and Analysis Technical Report 93-1.

TRANSFER, (2009), Deliverables of EU Funded TRANSFER(Tsunami Risk and Strategies for European Region), http://www.transferproject.eu

Trindade, A., Teves-Costa, P., & Catita, C. (2018). A GIS-based analysis of constraints on pedestrian tsunami evacuation routes: Cascais Case Study (Portugal). Natural Hazards, 93(S1), 169–185. https://doi.org/10.1007/s11069-017-3152-4

Tufekci, D., Suzen, M. L., Yalciner, A. C., and Zaytsev, A. (2018). Revised MeTHuVA method for assessment of tsunami human vulnerability ofBakirkoy district, Istanbul. Nat. Hazards90 (2), 943–974. DOI: 10.1007/s11069-017-3082-1

Tufekci-Enginar, D., Suzen, M.L., & Yalciner, A.C. (2020). The evaluation of public awareness and community preparedness parameter in GIS-based spatial tsunami human vulnerability assessment (MeTHuVA). Natural Hazards. doi:10.1007/s11069-020-04416-8

TUIK, (2020). Turkish Statistical Institute. http://www.tuik.gov.tr

Tur, H., Yaltırak, C., Elitez, İ., &Sarıkavak, K. T. (2015). Pliocene–Quaternary tectonic evolution of the Gulf of Gökova, southwest Turkey. Tectonophysics, 638, 158-176.

Ulug, A., Duman, M., Ersoy, S., Ozel, E., & Avci, M. (2005). Late Quaternary sea-level change, sedimentation and neotectonics of the Gulf of Gökova: Southeastern Aegean Sea. Marine Geology, 221, 381–395.

UNESCO-IOC, (2009). Tsunami Risk Assessment and Mitigation for the Indian Ocean, knowing your Tsunami Risk and What to do About It. UNESCO Intergovernmental Oceanographic Commission (IOC), Manuals and Guides#52, 2009.

Velioglu, D. (2017). Advanced Two- and Three-Dimensional Tsunami Models: Benchmarking and Validation. Ph.D. Thesis. Middle East Technical University, Ankara.

Wang, H., Mostafizi, A., Cramer, L.A., Cox, D., & Park, H. (2017). An agent-based model of a multimodal near-field tsunami evacuation: Decision-making and life safety. Transportation Research Part C: Emerging Technologies, 64, 86-100. doi:10.1016/j.trc.2015.11.010

Wilensky, U., (1999). NetLogo Itself: Center for Connected Learning and Computer-Based Modeling, Northwestern University, Evanston, IL.

Wood, N. J., Schmidtlein, M. C., & Peters, J. (2015). Changes in population evacuation potential for tsunami hazards in Seward, Alaska, since the 1964 good Friday earthquake. Natural Hazards, 70(2), 1031–1053. https://doi.org/10.1007/s11069-013-0859-8

Wood, N.J., & Peters, J. (2014). Variations in population vulnerability to tectonic and Landslide-related tsunami hazards in Alaska. Natural Hazards, 75(2), 1811-1831. doi:10.1007/s11069-014-1399-6

Wood, N.J., & Schmidtlein, M.C. (2013). Community variations in population exposure to near-field tsunami hazards as a function of pedestrian travel time to safety. Natural Hazards, 65(3), 1603-1628. doi:10.1007/s11069-012-0434-8

Wood, N.J., and Schmidtlein, M.C. (2012). Anisotropic path modeling to assess pedestrian evacuation potential from Cascadia related tsunamis in the US Pacific Northwest. Natural Hazards, v. 62, no. 2, p. 275–300. doi 10.1007/ s11069-011-9994-2

Yalciner, A. C., Dilmen, I. D., Insel I. (2008). An Investigation on the Tsunami Risk Map of Turkey. Report of the Project METU. 06-03-03-2-02-05, for Ministry of Transport Turkey.

Yalciner, A.C., Kuran, U., Akyarli, A., Imamura, F. (1995) An Investigation on the Propagation of Tsunamis in the Aegean Sea by Mathematical Modeling. In: Tsuchiya Y., Shuto N. (eds) Tsunami: Progress in Prediction, Disaster Prevention and Warning. Advances in Natural and Technological Hazards Research, vol 4. Springer, Dordrecht. https://doi.org/10.1007/978-94-015-8565-1_4

Yalcıner, B., Yalçıner, A. C., & Zaytsev, A. (2017). Accelerated Solutions in Tsunami Simulation and Visualization with Case Studies. itsbali2017.com

Yalciner, B., Zaytsev, A., (2017). Assessment of efficiency and performance of tsunami numerical modeling with GPU. Abstract EGU2017–1246 Presented in European Geoscience Union, EGU April 2017, https://meetingorganizer.copernicus.org/EGU2017/EGU2017-1246.pdf

Yeh, H., Fiez, T., Karon, J. (2009). A comprehensive tsunami simulator for long beach peninsula phase-1 framework development final report. State of Washington Military Department Emergency Management Division.

Yolsal, S., Taymaz, T. and Yalciner, A.C. (2007). Understanding tsunamis, potential source regions and tsunami-prone mechanisms in the Eastern Mediterranean Geological Society, London, Special Publications; v. 291; p. 201-230.

Yolsal-Çevikbilen, S., Taymaz, T. and Helvacı, C. (2014). Earthquake Mechanisms'in the Gulfs of Gökova, Sığacık, Kuşadası, and the Simav Region (western Turkey): Neotectonics, seismotectonics and geodynamic implications. Tectonophysics, 635, 100-124.

Zaytsev, A., Kostenko I., Kurkin A., Pelinovsky E., Yalciner A. C. (2016). The depth effect of earthquakes on tsunami heights in the Sea of Okhotsk, Turkish J Earth Sci, 25: 289-299, TÜBİTAK. doi:10.3906/yer-1509-6

Zheng, H., Son, Y., Chiu, Y., Head, L., Feng, Y., Xi, H., Kim, S., Hickman, M. (2013). A Primer for Agent-Based Simulation and Modeling in Transportation Applications, fhwa-hrt-13-054. Tech. rep., FHWA.

APPENDICES

APPENDIX A

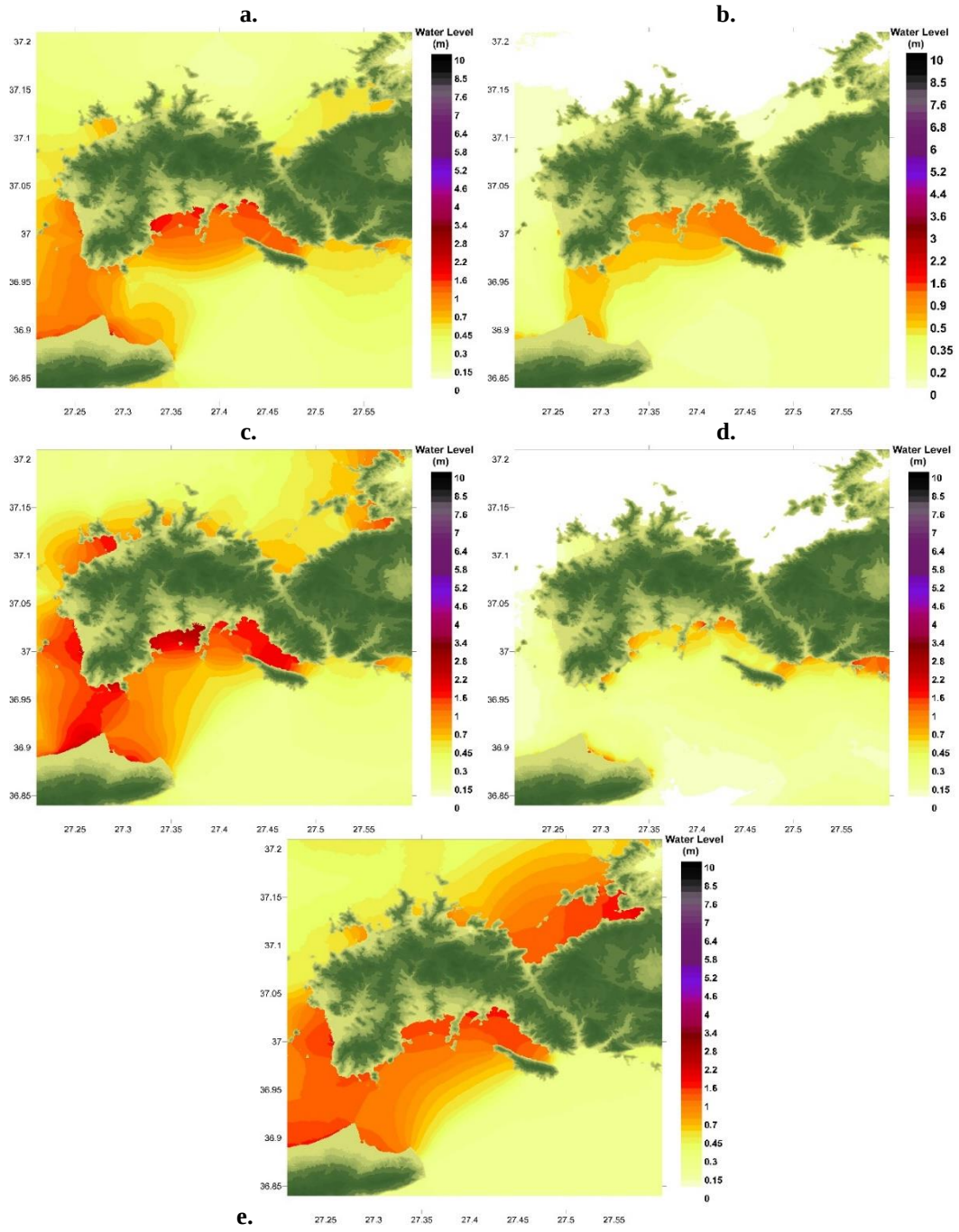

Figure A.1 Distributions of maximum water for seismic scenarios of **a.**365-Crete **b.**1303-Eastern Mediterranean **c.**1956-Amorgos **d.**Gökova **e.**Güllük Bay

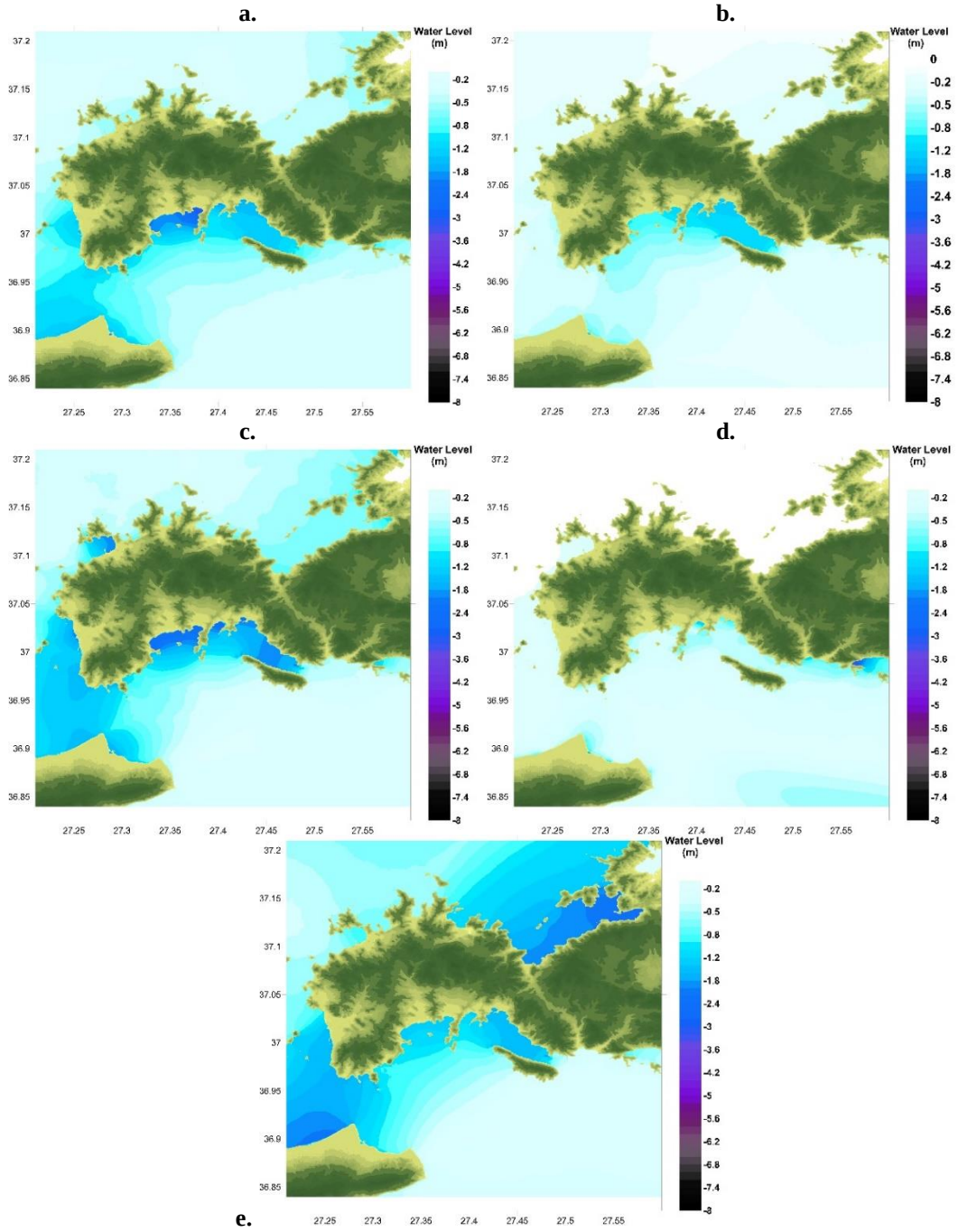

Figure A.2 Minimum water level distribution of seismic tsunami scenarios of **a.** 365-Crete **b.** 1303-Eastern Mediterranean **c.** 1956-Amorgos **d.** Gökova **e.** Güllük Bay

APPENDIX B

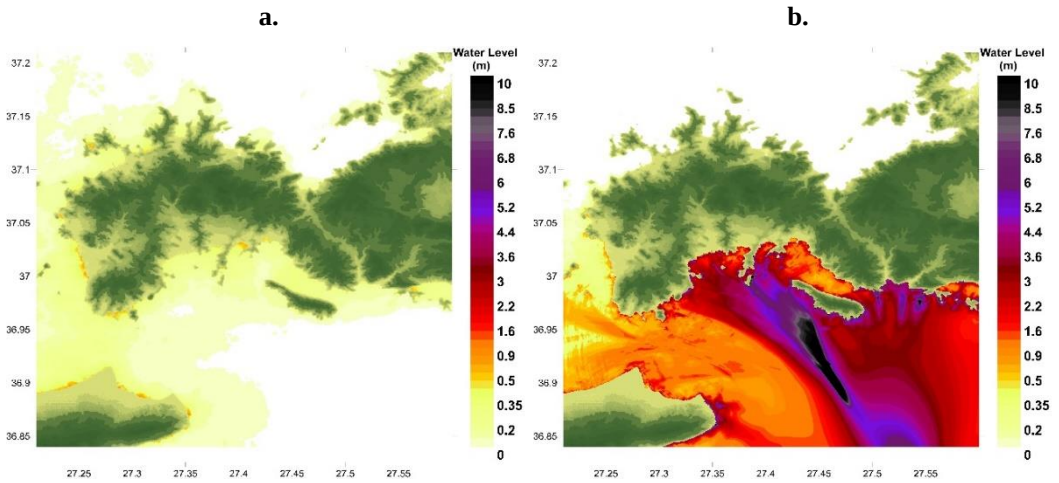

Figure B.1 Distribution of Maximum water levels in Domain D for **a.** Amorgos Landslide **b.** Gökova-North-Datça Landslide

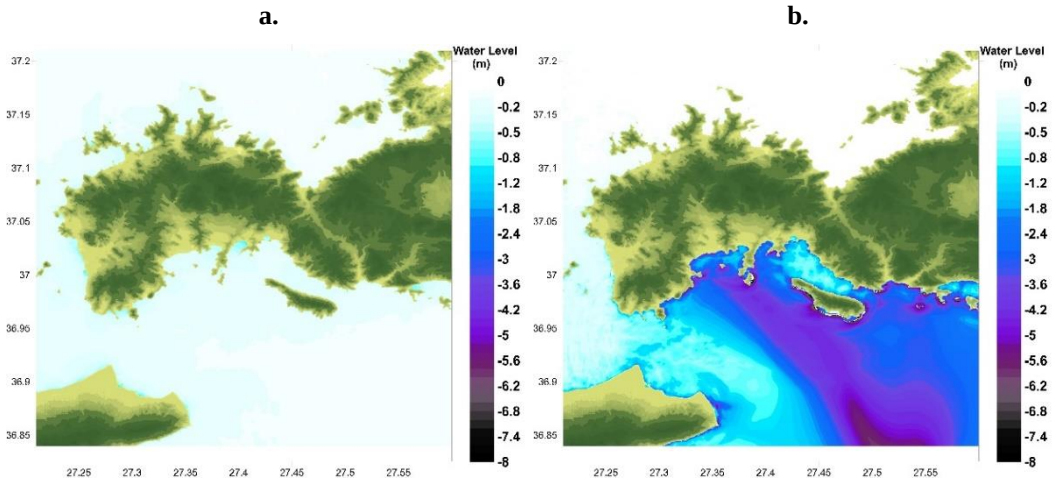

Figure B.2 Distribution of Minimum water levels in Domain D for **a.** Amorgos Landslide **b.** Gökova-North-Datça Landslide

APPENDIX C

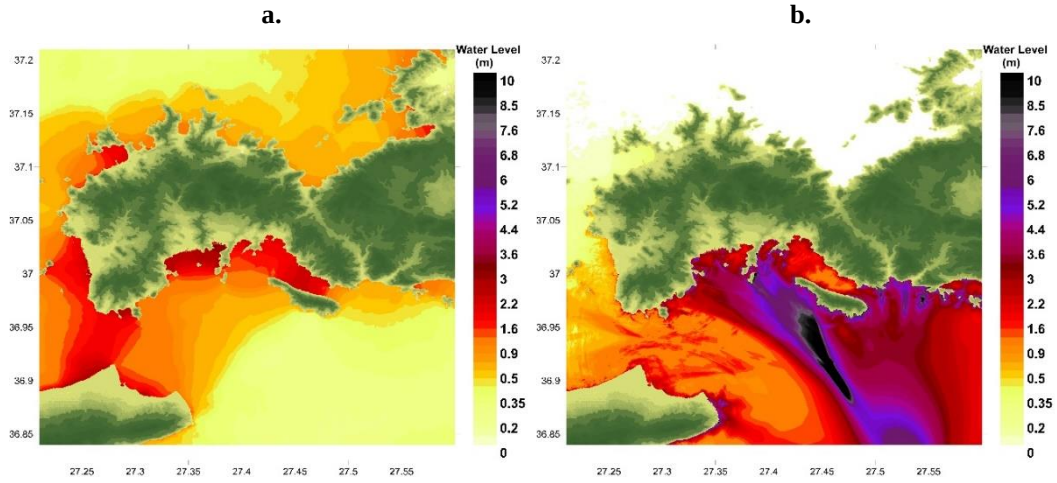

Figure C.1 Distribution of Maximum water levels in Domain D for **a.** Combined 1956-Amorgos Seismic + Amorgos Landslide Scenario **b.** Combined Gökova Seismic + Gökova-North-Datça Landslide Scenario

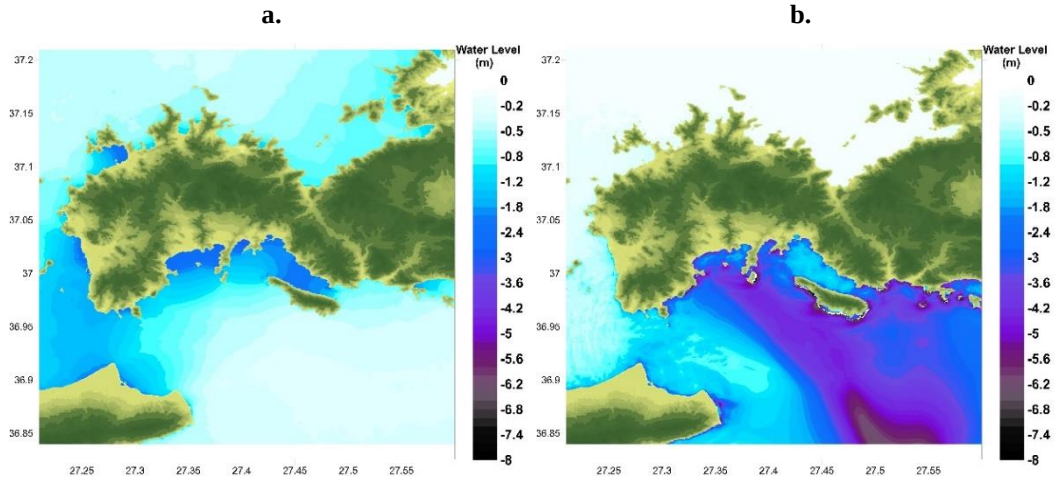

Figure C.2 Distribution of Minimum water levels in Domain D for **a.** Combined 1956-Amorgos Seismic + Amorgos Landslide Scenario **b.** Combined Gökova Seismic + Gökova-North-Datça Landslide Scenario

APPENDIX D

Table D.1 Maximum flow depth values at all gauge points according to selected seismic, landslide, and seismic/landslide combined sources (units in m)

Scenario	IDSL	IDSL*	Bodrum-TG	Gümbet	Bitez	Karaincir	Kos Port
365-Crete	1.51	1.54	1.56	1.81	1.88	0.80	2.17
1303-Eastern Mediterranean	1.24	1.26	1.26	1.08	1.26	0.72	1.01
1956-Amorgos	1.70	1.74	1.78	1.86	2.84	1.03	1.89
Gökova	0.77	0.85	0.86	1.55	0.70	0.93	1.48
Güllük Bay	1.60	1.65	1.62	1.70	1.57	1.27	1.50
Amorgos Landslide	0.23	0.26	0.25	0.72	0.44	0.45	0.83
Gökova North Datça Landslide	1.33	2.31	2.65	2.43	2.91	2.20	0.92
Combined 1956-Amorgos and Amorgos Landslide	1.70	1.55	1.75	2.25	2.80	1.2	2.25
Combined Gökova and North Datça Landslide	1.54	2.50	2.98	2.70	3.20	2.30	1.70

Table D.2 Maximum inundation distances (m) according to selected seismic, landslide, and seismic/landslide combined sources

Scenario/Arrival Time	Bodrum Center	Gümbet Bay	Bitez Bay	Yahşi Bay	Akyarlar-Karaincir-Aspat Bays
365-Crete	75	200	300	140	30
1303-Eastern Mediterranean	70	80	225	25	20
1956-Amorgos	100	210	350	210	115
Gökova	60	190	110	25	20
Güllük Bay	90	195	300	140	265
Amorgos Landslide	30	15	12	15	25
Gökova Datça North Landslide	65	225	240	310	410
Combined 1956-Amorgos and Amorgos Landslide	100	220	350	200	100
Combined Gökova and North Datça Landslide	90	270	320	325	300

Table D.3 First tsunami wave arrival times (min) according to selected seismic, landslide, and seismic/landslide combined sources

Scenario	IDSL	IDSL*	Bodrum-TG	Gümbet	Bitez	Karaincir	Kos Port
365-Crete	90.2	90.5	90.2	89.8	89.3	88.6	88.1
1303-Eastern Mediterranean	65.2	65.3	65.2	66.6	63.0	64.7	57.1
1956-Amorgos	43.0	43.4	43.1	41.3	42.8	41.0	40.5
Gökova	9.6	10.1	20.8	9.9	21.8	15.9	13.4
Güllük Bay	34.8	35.1	33.8	32.1	32.3	29.0	27.2
1956-Amorgos Landslide	90.7	91.2	90.9	64.3	59.2	62.1	61.8
Gökova North Datça Landslide	14.0	15.0	14.4	16.9	16.5	15.2	14.5
Combined 1956-Amorgos and Amorgos Landslide	43.0	43.4	43.1	41.3	42.8	41.0	40.5
Combined Gökova and North Datça Landslide	9.6	10.1	14.4	9.9	16.5	15.2	13.4

Table D.4 Arrival times of maximum wave (min) for the simulated scenarios

Scenario	IDSL	IDSL*	Bodrum-TG	Gümbet	Bitez	Karaincir	Kos Port
365-Crete	135.9	136.9	135.9	128.5	173.1	137.4	166.1
1303-Eastern Mediterranean	86.7	87.1	86.2	87.9	127.2	125.6	121.8
1956-Amorgos	129.1	129.2	128.7	159.5	94.5	63.9	64.2
Gökova	55.5	57.5	56.0	24.2	87.4	22.7	40.9
Güllük Bay	82.7	82.8	82.3	82.1	80.4	76.7	74.9
1956-Amorgos Landslide	209.2	158.2	158.6	210.5	172.2	174.7	143.8
Gökova North Datça Landslide	19.0	21.1	21.7	19.0	26.6	26.9	21.4
Combined 1956-Amorgos and Amorgos Landslide	126.0	98.0	128.0	101.0	94.0	64.0	67.0
Combined Gökova and North Datça Landslide	27.0	29.0	22.0	24.0	28.0	21.0	20.0